LA-13960-MS

Approved for public release;
distribution is unlimited.

Geology of the Western Part of Los Alamos National Laboratory (TA-3 to TA-16), Rio Grande Rift, New Mexico

Los Alamos
NATIONAL LABORATORY

This work was funded by the Office of Infrastructure, Facilities, and Construction of the Los Alamos National Laboratory Operations Directorate.

Edited by Roger Eckhardt

Cover Photos:

Views of a gas pipeline trench through LANL Technical Area 9 graben (see Plate 1).

Top left photo: Cleaning and logging trench walls.

Bottom right photo: Fractured and possibly faulted Bandelier Tuff (Tshirege Member Unit 4 upper) overlain by thin colluvial cover.

LA-13960-MS

Issued: December 2002

Geology of the Western Part of Los Alamos National Laboratory (TA-3 to TA-16), Rio Grande Rift, New Mexico

Claudia J. Lewis

Alexis Lavine

Steven L. Reneau

Jamie N. Gardner

Ryan Channell

C. William Criswell

Los Alamos
NATIONAL LABORATORY

TABLE OF CONTENTS

Page

TABLE OF CONTENTS v
LIST OF FIGURES AND PLATES vii
LIST OF TABLES viii

ABSTRACT 1

I. INTRODUCTION 3

II. PREVIOUS WORK 5

III. METHODS 8
A. Geologic Mapping 8
B. Geochemistry 9
C. Examination of Cores from Boreholes 9
D. Structural Analysis 11
E. Trench Logging 11
F. Notes on Units of Measure and Terminology 11

IV. GEOLOGY 12
A. Stratigraphy 12
1. Bedrock units of the Bandelier Tuff 12
a. Tshirege Member of the Bandelier Tuff (Qbt) 13
2. Surficial geologic units 16
a. Older mesa-top alluvial deposits (Qoal) 16
b. Older alluvial fan deposits (Qfo) 17
c. Intermediate-age alluvial fan deposits (Qfi) 17
d. El Cajete pumice (Qec) 17
e. Younger alluvial fan deposits (Qfy) 19
f. Stream terraces (Qt) 19
g. Young alluvium along stream channels (Qal) 19
h. Colluvium (Qc) 19
i. Artificial fill 20
B. Geochemistry of Bedrock Units 20
C. Structural Geology 22
1. Subsidiary faults of the Pajarito fault zone 22
2. North-striking structures in the eastern part of the Pajarito fault zone 22
3. Fractures and minor faults at Material Disposal Area P 29
4. Faults and folds in the easternmost part of the study area 32

V. DISCUSSION 33
A. Tshirege Member Stratigraphic Units 33
B. Surficial Geologic Units 35
C. Structural Geology 36

TABLE OF CONTENTS CONTINUED

Page

1. Origin of fracturing at Material Disposal Area P 36
2. Structural setting of the study area 40
3. Comparison of structure to previous studies 41
4. Ages of faulting and related deformation 43

D. Recommendations 44

VI. ACKNOWLEDGMENTS 44

VII. REFERENCES 45

APPENDIX A. WHOLE ROCK GEOCHEMISTRY 53

APPENDIX B. STRUCTURAL ANALYSIS 56

APPENDIX C. TOTAL STATION SURVEY DATA 77

LIST OF FIGURES AND PLATES

Page

FIGURES

1. Map of the Rio Grande Rift in Northern New Mexico 3
2. The Pajarito Fault System 4
3. Generalized Bandelier Tuff Stratigraphy 6
4. Bedrock Contacts, Boreholes, Traverses, and Fractures at MDA P 10
5. Bandelier Tuff Stratigraphy in the Study Area 14
6. Western Part of the TA-9 Trench 18
7. Silica and Titania Variation in Bandelier Tuff 21
8a. Pajarito Canyon Profile 24
8b. Cañon de Valle Profile 25
9a. Contoured Upper Surface of Unit 3T 26
9b. Contoured Upper Surface of Unit 3 27
10. Profile of the TA-9 Trench Showing Surveyed Data 28
11. Point Density Plots of Poles to Fracture Planes Measured at MDA P 30
12. Rose Diagrams of Strikes of Fracture Data from MDA P 31
13. Fracture Aperture Distributions 33
14. Apertures along Traverse 5 34

PLATES

1. Geologic Map of the Western Part of Los Alamos National Laboratory . . . . . .inside rear cover
2. Cross Sections A-A' and B-B' . . . . . .inside rear cover

LIST OF TABLES

Page

1. Mean Values of Some Major Oxides in Tshirege Member Units 20
2. Fracture Density Along MDA P Traverses 32
3. Elevation of Tshirege Member Contacts in Boreholes at Building TA-16-260 Outfall Area, Cañon de Valle 35
4. Comparison of Results from Selected Pajarito Plateau Fracture Studies 37

A-1. Locations of Bandelier Tuff Samples 53
A-2. Major and Trace Element Geochemistry of Bandelier Tuff 54–55

B-1. MDA P Fracture Data 58–75
B-2. Eigenvectors and Uncertainties for MDA P Fracture Data 76

C-1. TA-9 Trench Total Station Survey Data 77–94
C-2. MDA P Total Station Survey Data 95–98

GEOLOGY OF THE WESTERN PART OF LOS ALAMOS NATIONAL LABORATORY (TA-3 TO TA-16), RIO GRANDE RIFT, NEW MEXICO

by

Claudia J. Lewis, Alexis Lavine, Steven L. Reneau, Jamie N. Gardner,
Ryan Channell, and C. William Criswell

ABSTRACT

We present data that elucidate the stratigraphy, geomorphology, and structure in the western part of Los Alamos National Laboratory between Technical Areas 3 and 16 (TA-3 and TA-16). Data include those gathered by geologic mapping of surficial, post-Bandelier Tuff strata, conventional and high-precision geologic mapping and geochemical analysis of cooling units within the Bandelier Tuff, logging of boreholes and a gas pipeline trench, and structural analysis using profiles, cross sections, structure contour maps, and stereographic projections. This work contributes to an improved understanding of the paleoseismic and geomorphic history of the area, which will aid in future seismic hazard evaluations and other investigations.

The study area lies at the base of the main, 120-m (400-ft) high escarpment formed by the Pajarito fault, an active fault of the Rio Grande rift that bounds Los Alamos National Laboratory on the west. Subsidiary fracturing, faulting, and folding associated with the Pajarito fault zone extends at least 1,500 m (5,000 ft) to the east of the main Pajarito fault escarpment. Stratigraphic units in the study area include upper units of the Tshirege Member of the early Pleistocene Bandelier Tuff, early Pleistocene alluvial fan deposits that predate incision of canyons on this part of the Pajarito Plateau, and younger Pleistocene and Holocene alluvium and colluvium that postdate drainage incision.

We discriminate four sets of structures in the area between TA-3 and TA-16: a) north-striking faults and folds that mark the main zone of deformation, including a graben in the central part of the study area; b) north-northwest-striking fractures and rare faults that bound the eastern side of the principal zone of deformation and may be the surface expression of deep-seated faulting; c) rare northeast-striking structures near the northern limit of the area associated with the southern end of the Rendija Canyon fault; and d) several small east-west-striking faults. We consider all structures to be Quaternary in that they postdate the Tshirege Member (1.22 million years old) of the Bandelier Tuff. Older mesa-top alluvial deposits (Qoal), which may have a large age range but are probably in part about 1.13 million years old, are clearly faulted or deformed by many structures. At two localities, younger alluvial units (Qfo and Qfi) appear to be truncated by faults, but field relations are obscure, and we cannot confirm the presence of fault contacts. The youngest known faulting in the study area occurred in Holocene time on a down-to-the-west fault, recently trenched at the site of a new LANL Emergency Operations Center (Reneau et al. 2002).

I. INTRODUCTION

Los Alamos National Laboratory (LANL) lies within the Española basin of the Rio Grande rift, a tectonically active zone of east-west crustal extension (Fig. 1; e.g., Kelley 1979; Manley 1979; Golombek et al. 1983; Chapin and Cather 1994; Kelson and Olig 1995). The Rio Grande rift is a major tectonic feature of the North American continent and exhibits a long history of faulting, volcanism, and seismicity (e.g., Riecker 1979; Baldridge et al. 1984; Keller 1986). Abundant data indicate that the rift continues to be tectonically and magmatically active (e.g., Sanford et al. 1991; Baldridge et al. 1995; Wolff and Gardner 1995; Machette et al. 1998; Steck et al. 1998). In the vicinity of Los Alamos, the western margin of the rift is locally defined by the Pajarito fault system, which comprises the potentially seismogenic Pajarito, Rendija Canyon, and Guaje Mountain faults (Fig. 2). Paleoseismic studies indicate that each of these faults has generated multiple prehistoric earthquakes of approximate magnitude 7 (Gardner et al. 1990; Wong et al. 1995; Kelson et al. 1996; McCalpin 1998, 1999). The frequency and future likelihood of these large earthquakes are topics being addressed by the Laboratory's Seismic Hazards Program.

The LANL Seismic Hazards Program is focused in part on evaluating specific areas for seismic surface rupture potential through detailed studies to identify faults and gain understanding of the area's structural geology (Olig et al. 1996; Gardner et al. 1998a, 1999, 2001; Krier et al. 1998a, 1998b; Reneau et al. 2002). Previous studies focused on the stratigraphy, geomorphology, and structure in and around TA-55, TA-3, and TA-16 (Fig. 2) in relation to siting of new facilities or evaluation of existing facilities, particularly those that handle hazardous or radioac-

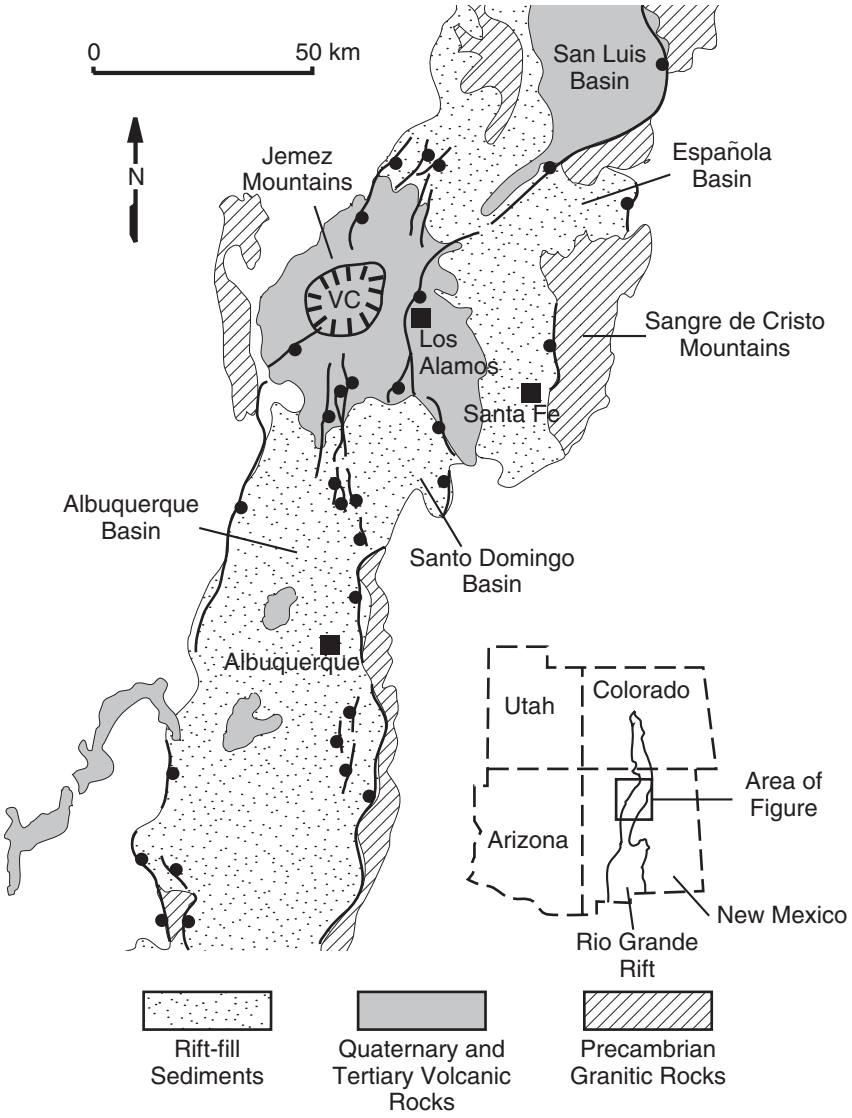

Figure 1. Map of the Rio Grande Rift in Northern New Mexico. Major fault systems are shown schematically (ball on downthrown side). VC is the Valles-Toledo caldera complex, the source of the Bandelier Tuff (modified from Gardner and Goff 1984).

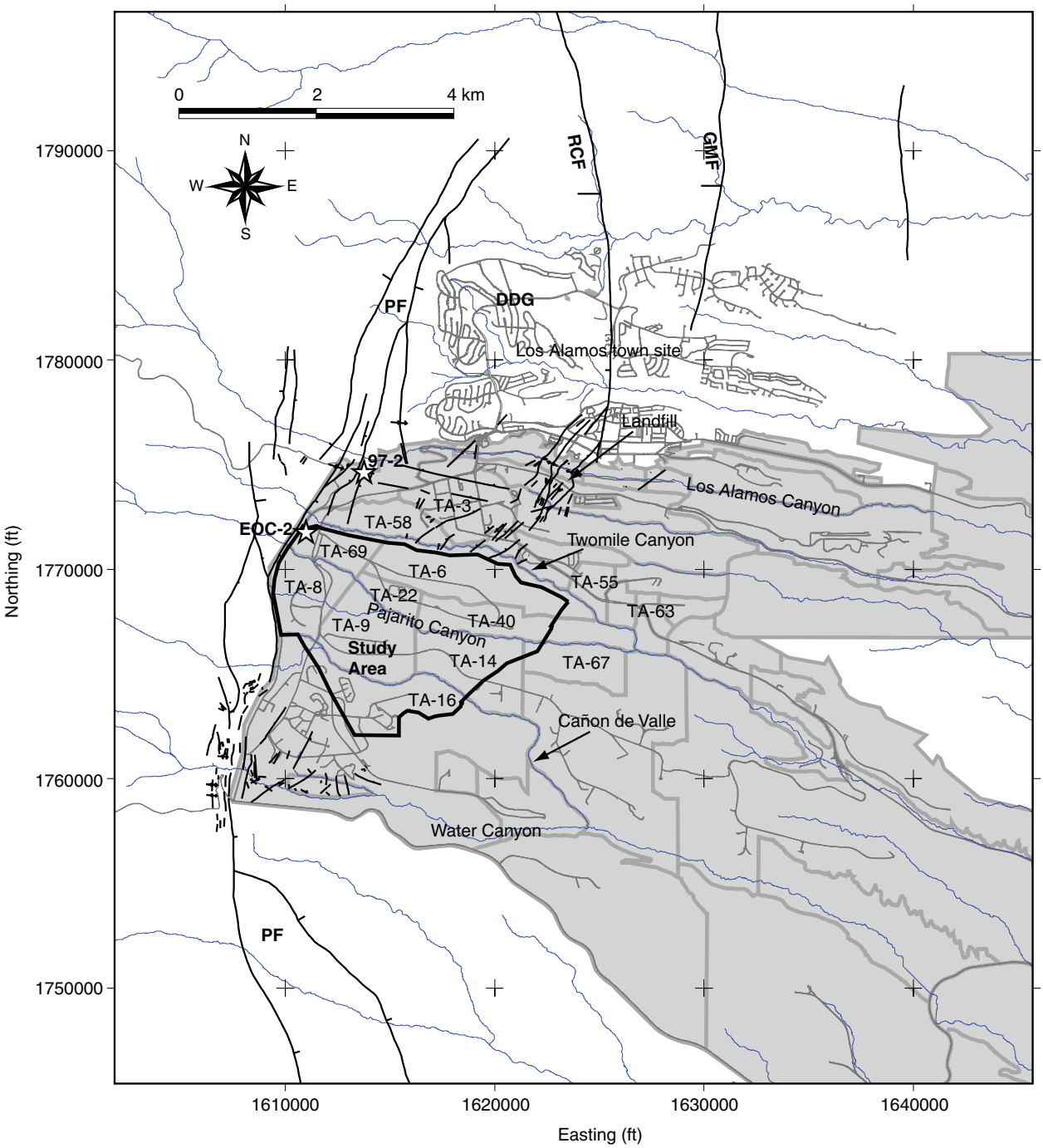

Figure 2. The Pajarito Fault System. The map shows the study area and the faults and folds of the Pajarito fault system (bold black lines) in the vicinity of Los Alamos National Laboratory. LANL is shaded light gray. Fine, dark-gray lines are roads; broad, medium-gray lines are technical area boundaries. Blue lines are stream channels. Abbreviations: DDG, Diamond Drive graben; GMF, Guaje Mountain fault; PF, Pajarito fault; RCF, Rendija Canyon fault. Stars indicate sites of paleoseismic trench investigations in the Pajarito fault zone (McCalpin 1998; Reneau et al. 2002). The structure in the northwest portion of LANL is from Gardner et al. (1999) and that in the southwest portion of LANL is from Gardner et al. (2001). Coordinates are northing and easting in State Plane Coordinate System, New Mexico Central Zone, 1983 North American Datum.

tive materials and have a need for maintaining containment integrity. Difficulties in correlation of geologic units among these areas and interpretation of structure in the western area of the Laboratory have arisen due to the absence of continuous, consistent, and detailed geologic mapping in the area east of the Pajarito fault escarpment between TA-3 and TA-16. This area contains active facilities that handle hazardous and radioactive materials, material disposal areas (MDAs), and sites of ongoing LANL Environmental Restoration (ER) Project activities. This area also contains outcrops that are key to understanding the Quaternary geologic evolution of this part of the Pajarito Plateau.

The study area for this report (Fig. 2) covers about 8 km^2 (3 mi^2) contained within a large number of technical areas: TA-6, -8, -9, -14, -16 (also known as S-Site), -22, -40, -67, and -69. The main emphasis of this study is the geology of the area that lies between TA-3 and TA-16, including the northern part of TA-16 (Plate 1). The study area is delimited on the north by Twomile Canyon, on the west by West Jemez Road (NM 501), on the southeast by an arbitrary, northeast-striking boundary east of MDA P, and on the southwest by a northwest-striking boundary south of buildings TA-16-260 and TA-16-340 on the south side of Cañon de Valle (Plate 1). Bedrock and surficial geologic mapping cover the entire study area. In addition, we have integrated bedrock data from a number of boreholes that lie south of Cañon de Valle in the vicinity of MDA P and building TA-16-260. In this report, we present data on the stratigraphy, geomorphology, and structure of the western part of the Laboratory.

II. PREVIOUS WORK

The most obvious part of the Pajarito fault zone in the vicinity of the study area is the > 120-m (400-ft) high escarpment west of the Laboratory. Significant advances in understanding the nature and style of deformation in the Pajarito fault zone were provided by McCalpin (1997) with his recognition that much of the prominent portion of the Pajarito fault west of the Laboratory is expressed at the surface as a large, north-trending, faulted monocline. Along strike, the surface expression of the Pajarito fault varies from a simple normal fault to broad zones of small faults to faulted monoclines and largely unfaulted monoclines (e.g., McCalpin 1997, 1998; Gardner et al. 1999). These varied styles of deformation are all considered expressions of deep-seated normal faulting. The work of McCalpin (1997), building on unpublished mapping by S. Reneau and J. Gardner, also showed that much of the main escarpment was extensively modified by mass wasting. Landslides in this area are cut by pronounced aerial photographic lineaments and other linear features that cannot be identified as faults with certainty.

Geochemical correlations of Bandelier Tuff units (see Fig. 3 for generalized stratigraphy of Bandelier Tuff) across the main escarpment of the Pajarito fault zone near Water Canyon (south of the map area, Fig. 2) indicate that stratigraphic separation on the tuff exceeds 120 m (400 ft) down to the east (Gardner et al. 2001). Where the fault zone crosses upper Pajarito Canyon (west of the map area, Fig. 2), stratigraphic separation on the Tshirege Member of the Bandelier Tuff is about 79 m (260 ft) down to the east across the main escarpment [Gardner et al. 2001; shown as ~ 155 m (~ 510 ft) by Olig et al. (1996)].

TA-3 to TA-55. Gardner et al. (1999) evaluated the structure of the western part of the Los Alamos town site and the northwestern part of LANL between and including TA-3 and TA-55. North of LANL and within the Los Alamos town site, this area includes two major potentially active normal faults, the generally north-striking Pajarito and Rendija Canyon faults, which bound the Diamond Drive graben (Fig. 2). Near the south side of the Los Alamos town site, the Rendija Canyon fault splays to the southwest into a broad zone of deformation (Gardner et al. 1999). The fault zone widens from about 610 m (2,000 ft) where it crosses Los Alamos Canyon and passes through the Los

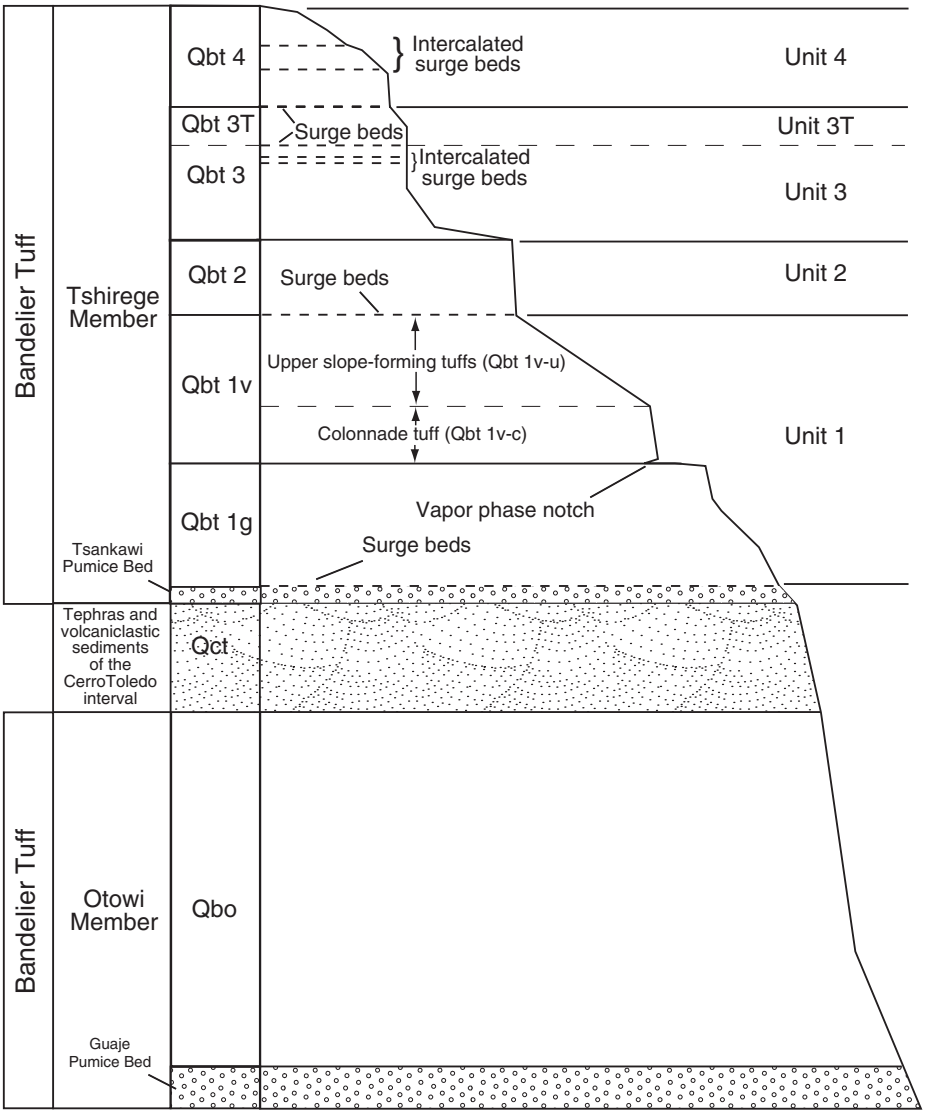

Figure 3. Generalized Bandelier Tuff Stratigraphy. The figure shows the stratigraphy of the Bandelier Tuff and associated deposits (modified from Broxton and Reneau 1995).

Alamos County landfill to about 1,500 m (5,000 ft) in Twomile Canyon. The fault zone appears to die out just south of Twomile Canyon. In TA-3, the Rendija Canyon fault is a zone of distributed deformation consisting largely of northeast-striking normal faults with < 3 m (10 ft) of dip slip, monoclines, and faulted monoclines with < 15 m (50 ft) of vertical deformation on Bandelier Tuff. This zone of distributed deformation, including gentle northward tilts of structural blocks, forms part of the approximate southern boundary of the Diamond Drive graben (Fig. 2). At Twomile Canyon, net down-to-the-west displacement is about 10 m (30 ft) on Bandelier Tuff.

Near the southern edge of Los Alamos Canyon, McCalpin (1998) found evidence for five to seven displacement events in a trench across one of several visible fault scarps of the Pajarito fault zone (trench 97-2, Fig. 2). None of these events could be dated precisely. All events postdate deposition of alluvium estimated to be several hundred thousand years old (thousand years old = ka). All events predate formation of a soil horizon that is at

least 40 ka. Downward tapering wedges of colluvium fill what may be Holocene fissures associated with faulting. This down-to-the-east fault can be traced some 1,000 m (3,000 ft) to the south, nearly to the edge of the present study area.

TA-16. In the vicinity of TA-16, deformation associated with the Pajarito fault extends at least 1,500 m (5,000 ft) to the east of the Pajarito fault escarpment (Gardner et al. 2001). Numerous north- and northeast-striking faults and monoclines with small amounts of dip slip, as well as monoclinal folding of originally east-dipping stratigraphy to horizontal or westward dips, represent a zone of distributed faulting and folding that is likely deformation of the hanging wall of the Pajarito fault. East of West Jemez Road and about 150 to 500 m (500–1,500 ft) east of the base of the main Pajarito fault escarpment, several down-to-the-west faults form the eastern side of a graben. A relatively broad zone of deformation is associated with the eastern margin of this graben. Net down-to-the-west deformation across these faults, together with contributions from monoclinal folding, is likely greater than 30 m (100 ft) on Bandelier Tuff. The eastern margin of the graben can be traced northwards some 1,000 m (3,000 ft) by an abrupt disappearance of exposed bedrock at the surface, a substantial thickness of post-Bandelier sediments, and a topographic anomaly. Gardner et al. (2001) also identified a prominent north-northeast-trending fissured lineament that extends for about 760 m (2,500 ft) through TA-16. The northern part of the fissured lineament may have about 2 m (7 ft) of net down-to-the-west separation on Bandelier Tuff. The fissured lineament is parallel to the local trend of the Pajarito fault escarpment and may locally mark an eastern margin of the zone of young deformation associated with the Pajarito fault.

Stratigraphy and structure logged in boreholes at the Weapons Engineering Tritium Facility (WETF) at TA-16 indicated the presence of at least two normal faults and two fissures, all of which intersect boreholes and strike north-northeast (Gardner et al. 2001). Stratigraphic and structural relations in one borehole (WETF-2C) indicated that a fissure-opening rupture or ruptures occurred sometime prior to 8,000 radiocarbon years before present [8 ^{14}C ka, or ca. 8.7–9.2 calibrated ^{14}C ka (cal ka)]. Subsequently, fissure-fill sediments were faulted in a paleoseismic event or events either sometime before deposition of the dated part of the sequence [prior to ca. 8 ^{14}C ka (ca. 8.7–9.2 cal ka)], after deposition of the entire sequence [since ca. 6 ^{14}C ka (ca. 7.1–7.4 cal ka)], or during deposition of the dated sequence [ca. 6–8 ^{14}C ka (ca. 7.1–9.2 cal ka)].

In recent years, a great deal of geoscientific work has been done in the vicinity of MDA P and the building TA-16-260 outfall area (Plate 1) in support of LANL ER Project efforts (e.g., Broxton et al. 1996, 2002; Warren et al. 1997; LANL ER Project 1998). LANL ER Project (1998) reported results from 16 boreholes drilled near Cañon de Valle. The cores from the boreholes provided new data important to characterizing units in the upper part of the Tshirege Member of the Bandelier Tuff. Specifically, Warren et al. (1997) subdivided Unit 4 (see below) into a number of petrologic subunits, but others have not been successful in applying these subunits consistently in the field (e.g., Gardner et al. 2001). By correlating borehole logs, LANL ER Project (1998) constructed a three-dimensional subsurface model of the stratigraphy for the building TA-16-260 outfall area. Subsequently, Broxton et al. (2002) drilled the 592-m (1,942-ft) deep characterization well R-25 (Plate 1) on the mesa top south of Cañon de Valle. The R-25 well log provides subsurface data on elevations of contacts within the Tshirege Member as well as underlying rock units.

Budding and Purtymun (1976) show a normal fault, which they termed "the Water Canyon fault," skirting the eastern side of TA-16; they state that the fault exhibits about 9 m (30 ft) of down-to-the-east separation on an unspecified datum in the north wall of Water Canyon. Additionally, Reynolds [no date; reported and discussed in Dransfield and Gardner (1985)] ran a seismic reflection line along the portion of State Road 4 at

the southern boundary of TA-16 and reported about 15 m (50 ft) of down-to-the-east separation on the base of the Bandelier Tuff in this area. However, mapping of Gardner et al. (2001) does not indicate the existence of such a fault in Water Canyon. Brown et al. (1988) reported results from a series of shallow drill holes around MDA P, in the northeastern corner of TA-16, and interpreted that "the Water Canyon fault" displaces the Bandelier Tuff 3 to 5 m (10–15 ft) down to the east about 150 m (500 ft) east of MDA P. The existence of this fault has not been confirmed.

Area between TA-3 and TA-16. A number of small-scale geologic maps encompass the study area (e.g., Griggs 1964; Smith et al. 1970; Gardner and House 1987). Previous geologic mapping in or near the study area of sufficient detail for identification of geologic structures with respect to specific facilities was done by Rogers (1995) and Reneau et al. (1995). Rogers (1995) identified some of the structures that we document, but for many structures, we differ from Rogers (1995) in their placement and interpretation of their style of deformation (see "Origin of fracturing at Material Disposal Area P" below, page 36). In addition, Rogers (1995) did not recognize some of the structural features that we have identified by combining bedrock and geomorphic mapping, examination of core from boreholes, and detailed structural analysis.

Reneau et al. (1995) identified a fault zone in early Pleistocene alluvium and Bandelier Tuff at Pajarito Mesa, east of our study area. They documented 1.2-m (4-ft) down-to-the-west offset in a 20-m (66-ft) wide zone. In addition, they recognized 7–9-m (23–30-ft) down-to-the-west dip separation across a 100–200-m (330–660-ft) wide zone at a contact within the Tshirege Member. They also found a number of additional faults farther west on Pajarito Mesa and Twomile Mesa [up to 4 m (13 ft) separation], at the extreme eastern end of our study area (Plate 1). The majority of these faults display a down-to-the-west sense of displacement. The most recent faulting in this area occurred prior to 50 to 60 ka. The largest offset faults are east of our study area.

Trenching at the proposed site of a new LANL Emergency Operations Center in the northwest corner of the study area (Plate 1) characterized the stratigraphy and structure of the east side of a graben at the base of the Pajarito fault escarpment (Reneau et al. 2002). The main zone of faulting in the trench, with evidence for both normal and strike-slip displacement, displayed down-to-the-west stratigraphic separation and forms the eastern edge of an approximately 160-m (525-ft) wide graben at the base of the east-facing Pajarito fault escarpment. Net vertical separation of 2.0 to 2.5 m (7–8 ft) on post-Bandelier Tuff strata was estimated across the main fault zone in the trench although samples from boreholes indicate a structural depth for the graben of at least 8 m (24 ft). The additional vertical deformation may be accommodated by offset on relatively old faults that were not exposed in the trench, by westward tectonic tilting, or by a combination of both. The trench exposures provided evidence for a minimum of six surface-rupturing events in the last 1.22 million years, demonstrating the recurring nature of surface faulting at the site. The most recent event occurred sometime within the last 10,500 years.

III. METHODS

A. Geologic Mapping

We mapped bedrock and surficial geologic units in the field at a scale of 1:1200, using topographic maps with 2-ft contours derived from the LANL 1991 digital elevation model (DEM). We then generated base maps from databases of the LANL Geographic Information Systems Laboratory and the LANL Seismic Hazards Program.

The geologic map (Plate 1) was created using ArcView (© ESRI) and ArcMap (© ESRI). Field geologic maps were digitized using ArcMap. Lines representing geologic features and contacts were converted to points for which northing and easting

coordinates were calculated. Elevations of these points were then obtained from the 1991 DEM. Some geologic contacts were surveyed using a total station at MDA P in Cañon de Valle and a 1999 gas pipeline trench north of Cañon de Valle at TA-9 [Plate 1; techniques described by Lavine et al. (1997, 1998) and Gardner et al. (1998a, 1999, 2001)]. Coordinates of points from digitized geologic maps were then integrated and examined with the surveyed data. We performed detailed computer-aided and field analyses of anomalies in point elevations on certain geologic surfaces. Field data were analyzed in profiles, geologic cross sections, three-dimensional surface diagrams, and maps constructed with a variety of software packages. The different software packages are capable of generating images of the same data at different scales and from varied perspectives, enabling exaggeration and identification of subtle elevation anomalies.

The basic soil-stratigraphic framework used in the surficial mapping is partially derived from previous investigations that included soil pits and trenches on the western Pajarito Plateau, including sites both inside and outside the map area (e.g., Kolbe et al. 1994, 1995; Reneau et al. 1995, 1996a, 1996b, 2002; Wong et al. 1995; Longmire et al. 1996; McDonald et al. 1996; Reneau and McDonald 1996; McCalpin 1998, 1999; Phillips et al. 1998; Gardner et al. 2001). Large parts of the map area have been disturbed by human activities, partially obscuring original geologic relations. In addition, there are extensive soil-covered areas of low relief without natural or artificial exposures. Unit designations in these areas were in part inferred based on the lithology of any clasts in the soil combined with evidence from adjacent areas. An improved map in these areas would require subsurface exploration using soil pits, trenches, and/or drilling.

B. Geochemistry

We collected samples of Bandelier Tuff for whole-rock x-ray fluorescence (XRF) analysis to further support unit identification and stratigraphic correlations (see, for example, Krier et al. 1998b; Gardner et al. 1999, 2001). We sampled one measured section on the north side of Cañon de Valle (Plate 1), taking a total of ten samples from an outcrop depth of 5 to 10 cm (2–4 in) to avoid obvious weathering rinds. We also collected samples of core from boreholes at MDA P (Fig. 4), on the south side of Cañon de Valle, which were drilled by the LANL ER Project in September 2001. The two deepest boreholes were sampled. Eight samples were collected from borehole 273 and 10 from borehole 257. Sample locations are tabulated in Appendix A, Table A-1.

Major and trace elements were analyzed in 28 bulk samples using an automated Rigaku wavelength-dispersive XRF spectrometer. Results are compiled in Appendix A. Samples were first crushed and homogenized in 15–20-gram portions in a tungsten-carbide shatterbox in accordance with Yucca Mountain Project procedure LANL-EES-DP-130—Geologic Sample Preparation. Sample splits were dehydrated at 110°C for 4 hours and then allowed to equilibrate with ambient atmosphere for 12 hours. One-gram splits were fused at 1100°C with 9 grams of lithium tetraborate flux to obtain fusion disks. Additional one-gram splits were heated at 1000°C to obtain the loss-on-ignition (LOI) measurements. Elemental concentrations were calculated by comparing x-ray intensities for the samples to those for 21 standards of known composition, after correcting for absorption. The XRF method employed calculates the concentrations of ten major oxides (SiO_2, TiO_2, Al_2O_3, Fe_2O_3, MnO, MgO, CaO, Na_2O, K_2O, and P_2O_5), ten trace elements (V, Cr, Ni, Zn, Rb, Sr, Y, Zr, Nb, and Ba), and LOI (Appendix A, Table A-2). Elemental concentrations of V, Cr, and Ni in the Bandelier Tuff are generally below detection limits and therefore are not reported in Appendix A.

C. Examination of Cores from Boreholes

Borehole data from previous and parallel studies in the vicinity have been integrated with our results (LANL ER Project 1998; Criswell et al., in prepa-

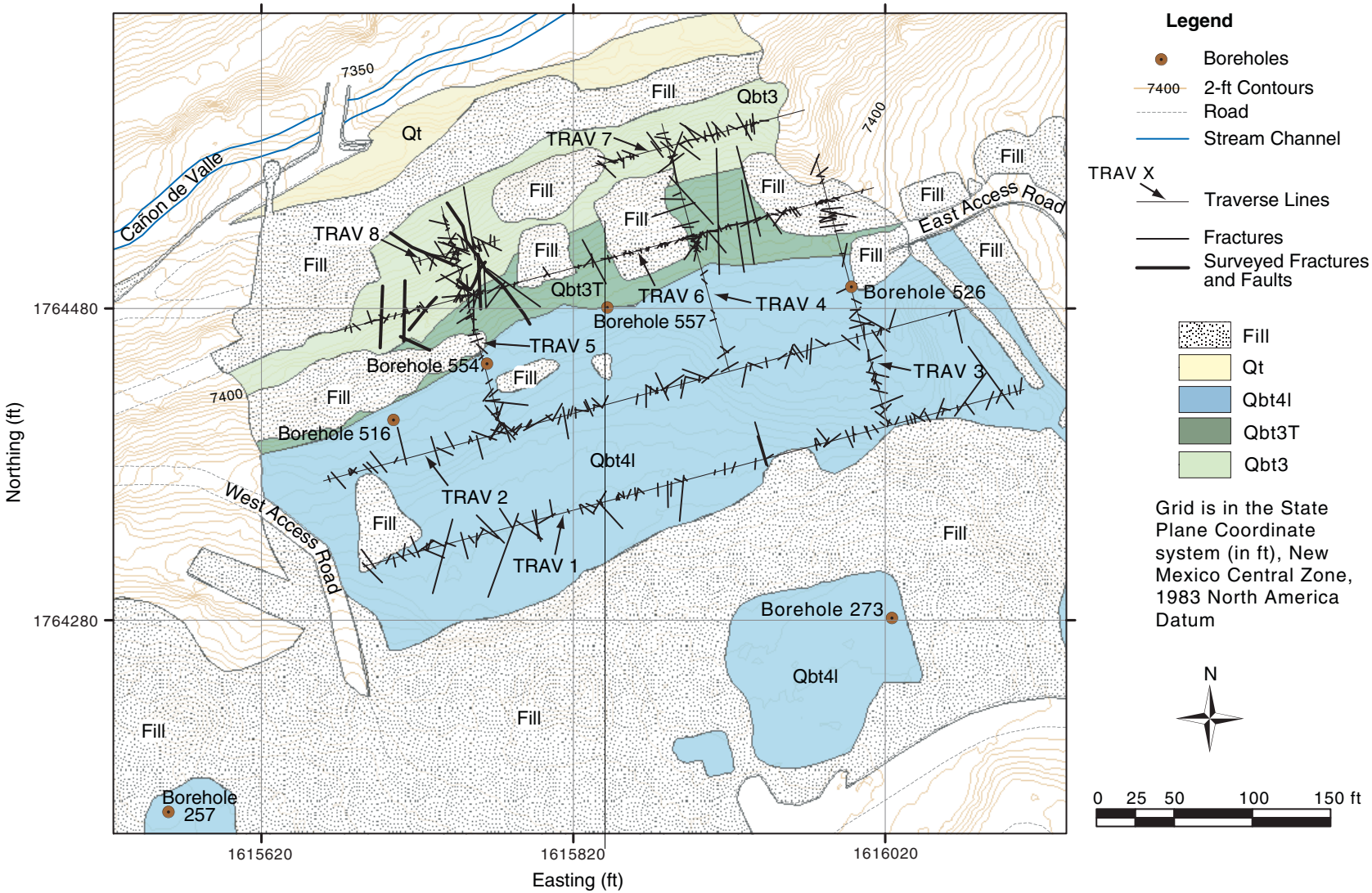

Figure 4. Bedrock Contacts, Boreholes, Traverses, and Fractures at MDA P. Each fracture shown is a schematic representation, showing the total length accurately but not the shape of the fracture. Fractures measured with a tape are located with an accuracy of better than ± 1.5 m (5 ft). Uncertainty includes errors in surveyed grid points, measurement error, and digitizing error. Fractures and faults indicated with heavy black lines were surveyed with a total station; accuracy is ± 1 cm. Abbreviation: TRAV, traverse. Stratigraphic units are as shown on Plate 1. Topography is from Carey and Cole (2002).

ration). Locations and stratigraphic data have been taken from LANL ER Project documents. After re-examination of core from boreholes at the building TA-16-260 outfall area, we have modified the stratigraphy of LANL ER Project (1998) based on petrographic and geochemical comparisons with our field units (see "Discussion," page 33).

D. Structural Analysis

Across the study area, and much of the Pajarito Plateau, exposure of bedrock is excellent on south-facing cliffs in densely welded tuffs. By contrast, bedrock exposure is poor on north-facing, colluvium-covered, and vegetated slopes and on mesa tops extensively modified by Laboratory operations. Mapping of surficial deposits in relation to topography aids greatly in identification of possible faults. To further improve recognition of faults and related structures, we complement bedrock and geomorphic mapping with geometric analysis of profiles, cross sections, and structure contour maps.

Data obtained by conventional geologic mapping were prepared for structural analysis by conversion of lines on the geologic map to points, followed by calculation of *x*-*y*-*z* coordinates for these points using the 1991 DEM. Inaccuracies in the DEM and the process of digitizing results in small uncertainties in point elevations. Profiles were created by projecting points along a given mesa rim into the orientation of profile lines shown on Plate 1. Ground-surface elevations were added to these profiles by projecting topography from the crown, or high part, of the mesa. This technique may result in inaccuracies in the profiles but allows us to project into the profiles the contact between Bandelier Tuff and post-Bandelier strata where it exists. It also allows us to show the maximum preserved thickness of post-Bandelier Tuff strata, highlighting thickness variations and, therefore, possible structure. Three-dimensional surface models of selected geologic surfaces were interpolated using kriging (a linear regression technique for minimizing variance of unsampled values between points; Deutsch and Journel 1998) and were then contoured to examine anomalies and trends in surfaces.

Rigorous geometric analysis of faults and fractures was possible only at MDA P (Plate 1; Fig. 4) where the LANL ER Project removed 40,000 cubic meters (52,000 cubic yards) of contaminated fill, Bandelier Tuff, and post-Bandelier strata from the south side of Cañon de Valle. Restoration of the site provided exceptional exposures of the bedrock stratigraphy and the faults and fractures that cut it. The excellent exposure at MDA P afforded an opportunity to measure a large number of fractures in three different geologic units in a three-dimensional bedrock exposure (see Appendix B for details on methods; data compiled in Table B-1). With the fracture data, we performed a statistical analysis of preferred directions, fracture density, and apertures of fractures. The results can be compared to fracture analyses done in other parts of the Laboratory (e.g., Kolbe et al. 1994, 1995; Reneau et al. 1995; Wohletz 1995; Vaniman and Chipera 1995).

E. Trench Logging

A shallow [~ 1.2-m (4-ft) deep] trench, excavated in 1999 for a gas pipeline on the mesa top just north of Cañon de Valle in the southern part of TA-9 (cover photos; Plate 1; Fig. 2), exposed Unit 4 of the Tshirege Member of the Bandelier Tuff and post-Bandelier tuff stratigraphic units. The surface of the trench, the contact between alluvium/colluvium and the upper surface of the Bandelier Tuff, several post-Bandelier Tuff stratigraphic units, and fractures and possible small faults were surveyed using a total station (data compiled in Appendix C).

F. Notes on Units of Measure and Terminology

We use a mixture of English and metric units in this report. For maps and other georeferenced figures, we employ English units because the three-dimensional reference framework for this area (the

State Plane Coordinate System, New Mexico Central Zone, 1983 North American Datum) is in feet, as are most of the LANL engineering databases. In all other cases, we use the metric system following general scientific practice. For length measurements at the centimeter scale or greater, we provide English units in parentheses adjacent to the metric length.

We use several specialized geologic terms that we define here (Bates and Jackson 1980) for optimal understanding of the structural interpretations.

- *slip*—the relative displacement of formerly adjacent points on opposite sides of a fault, measured in the fault surface. Synonym: total displacement.
- *throw*—the vertical component of the net slip.
- *separation*—the distance between any two parts of an index plane (e.g., bed, dike) disrupted by a fault.
- *stratigraphic separation*—the thickness of strata that originally separated two beds brought into contact at a fault.
- *vertical separation*—in a fault, the distance measured vertically between two parts of a displaced marker (e.g., bed).

Where the orientation of a fault plane through strata and the slip vector can be measured, the term slip may be used. However, in an area such as this of dominantly normal faulting, finding piercing points (e.g., two points along a faulted stream channel or a dike displaced by a fault) is a rare occurrence. In some cases, we apply the term apparent slip where we assume, for example, dip slip. Where we can see that strata are faulted but cannot measure the orientation of the fault, we use throw or separation, either stratigraphic or vertical. We use displacement in the general case or where we wish to convey the effects of faulting but the specifics on the magnitude or direction of slip are unknown.

We also use the following terms:

- *fracture*—a general term for any break in a rock, whether or not it causes displacement, due to mechanical failure by stress; the term fractures includes fissures, joints, and faults.
- *fissure*—a fracture along which there is distinct horizontal opening.
- *joint*—a surface of fracture or parting in a rock, without displacement. Note that this term is often applied to fractures in ash-flow tuffs produced by thermal contraction during cooling, thus the term cooling joints.
- *fault*—a fracture or fractures along which there has been displacement of the sides relative to one another parallel to the fracture.
- *fold*—a curve or bend of a planar structure, such as rock strata, bedding planes, or foliation. A fold is usually a product of deformation, although its definition is descriptive and not genetic and may include primary structures.
- *monocline*—a local steepening in otherwise uniformly dipping strata.

IV. GEOLOGY

A. Stratigraphy

The oldest exposed and most widespread unit in the study area is the Pleistocene Bandelier Tuff, which forms the local, near-surface bedrock. Overlying the Bandelier Tuff is a variety of mostly volcaniclastic surficial units, including the 50 to 60 ka El Cajete tephra deposits.

1. Bedrock units of the Bandelier Tuff

The Bandelier Tuff consists of two members that were erupted as a series of ash flows during enormous, caldera-forming volcanic events at about

1.61 Ma and 1.22 Ma [age from Izett and Obradovich (1994)]. Figure 3 shows a generalized stratigraphy of the Bandelier Tuff and associated deposits. The younger member of the Bandelier Tuff, the Tshirege Member, is exposed in the study area, whereas the older member, the Otowi, has been encountered in one relatively deep hydrologic monitoring well in the study area (well R-25, south side of Cañon de Valle; Plate 1). Beneath the Otowi Member in well R-25 are sands and coarse gravels of the Puye Formation (Broxton et al. 2002), which ranges in age from about 7 Ma to about 1.6 Ma (Bailey et al. 1969; Gardner et al. 1986).

a. Tshirege Member of the Bandelier Tuff (Qbt)

The stratigraphy for the Tshirege Member that we employ is largely based on that first presented by Broxton and Reneau (1995) and later modified by Gardner et al. (1999, 2001). The stratigraphy of Broxton and Reneau (1995) is based on cooling units in the central and eastern parts of the Laboratory and was modified from earlier work of Vaniman and Wohletz (1990). Mapping westwards from central portions of the Laboratory (e.g., Gardner et al. 1999, 2001) has identified a number of other mappable Tshirege units not included in the stratigraphy of Broxton and Reneau (1995). Furthermore, with increasing proximity to the caldera source of the ignimbrites, the cooling-unit stratigraphy is increasingly difficult to apply as cooling breaks become less distinct. Where possible, we employ the Broxton and Reneau (1995) stratigraphy with modifications and additions based on petrographic variations in the sequence (Fig. 3). Subdivisions of the Tshirege Member have been used in our bedrock mapping and in analysis of boreholes at MDA P (Plate 1; Figs. 4 and 5). In limited areas on Plate 1, Qbt represents undivided Tshirege Member of the Bandelier Tuff. These areas are mainly on mesa tops or on steep slopes where exposure was too poor to distinguish units. Tshirege Member stratigraphic units exposed in the study area are Unit 3, Unit 3T, and Unit 4, which includes two principal subunits. Stratigraphic thickness was determined from MDA P boreholes, a measured section north of MDA P in Cañon de Valle, and map patterns (Figs. 4 and 5; Plate 1). Below are descriptions of Tshirege Member units exposed in the study area.

Unit 3: 21 to 34 m (70–110 ft) thick. The basal part of Unit 3 and its contact with the underlying Unit 2 is exposed just beyond the northeastern-most part of the study area. Unit 3 in that location is about 50 m (150 ft) thick. In the MDA P boreholes [where Unit 3 is at least 34 m (110 ft) thick], a lower, nonwelded portion of Unit 3 exists. Drilling beyond this zone resulted in no recovery of core, likely due to the nonwelded and crystal-rich aspect of the tuff in this part of the section. The top of Unit 3 is marked locally by a crystal-rich surge deposit. In a few locations, we have mapped surges within Unit 3. The surge deposits are commonly crystal-rich (up to 90%), ash-poor, and composed of sand-sized grains of crystals and both cognate and accidental lithic fragments. In outcrop, and even in core, these deposits can exhibit sedimentary structures that include planar beds and low-angle crossbeds. The top of Unit 3 is locally characterized by gas escape pipes that reach diameters of more than 10 cm. Unit 3 is pumice-rich (about 30%) compared to the underlying Unit 2 and contains relatively abundant (locally up to 5%) accidental lithic fragments, most of which are around 5 cm in diameter. In contrast to other units, Unit 3 is more porphyritic, with at least 30% phenocrysts. Quartz and sanidine occur in subequal amounts, but fairly distinctive of the phenocryst population of Unit 3 is the relatively coarse crystal size, with most phenocrysts 4 to 6 mm across. Phenocrysts are most commonly euhedra of single crystals or single-crystal fragments.

Unit 3T: 0 to 20 m (0–65 ft) thick. Unit 3T (Gardner et al. 1999) pinches out between Units 3 and 4 in the eastern part of the study area and thickens progressively to the west. The pinchout of Unit 3T occurs along a fairly straight north-south line (except for rare lenses farther

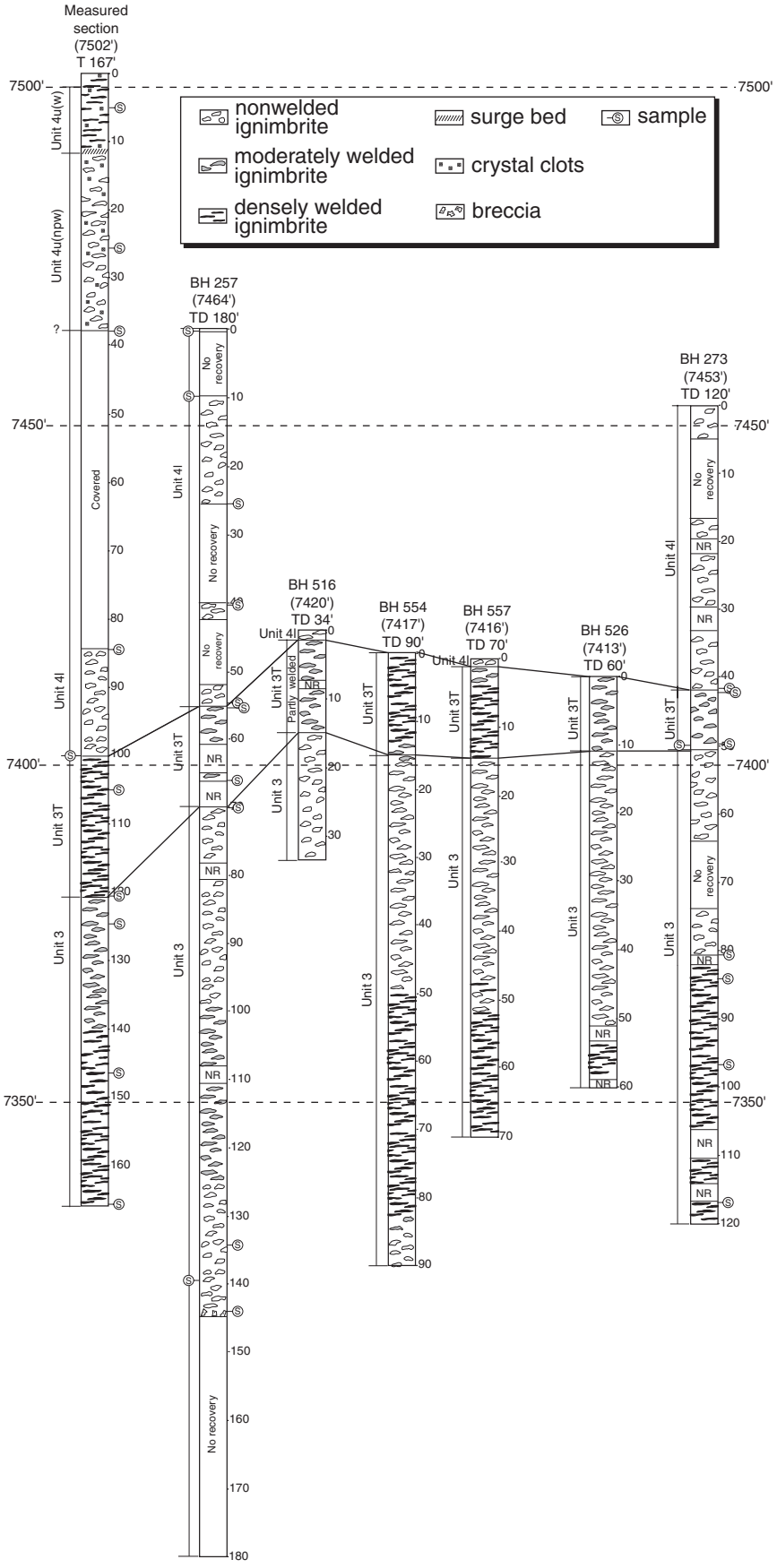

Figure 5. Bandelier Tuff Stratigraphy in the Study Area. This schematic of stratigraphic sections shows units of the Bandelier Tuff and sampling locations in a measured section and boreholes at MDA P. Measured section and boreholes are projected into an east-west line and are aligned vertically by elevation where the borehole penetrated the ground surface. Depth scales are in feet. Units labeled 3, 3T, 4l, 4u(npw), and 4u(w) are within the Tshirege Member (see text for discussion). Abbreviations: BH, borehole; S, geochemistry sample; T, thickness of stratigraphic section; TD, total depth of borehole; NR, no recovery. There is no horizontal scale. Borehole locations are indicated on Fig. 4 and the measured section on Plate 1.

east) that runs from the Van de Graff Accelerator near the intersection of Diamond Drive and Pajarito Road in TA-3 to the eastern edge of MDA P (Cross-section A-A', Plate 2, and map pattern on Plate 1). In several places near the eastern pinch-out, Unit 3T crops out in thin lenses before pinching out entirely (Cross-section A-A'). In the vicinity of MDA P, Unit 3T is around 2 to 7 m (7–20 ft) thick in six boreholes and in our measured section on the north slope of Cañon de Valle (Fig. 5). Unit 3T is commonly moderately to densely welded to its top and bottom contacts. Locally, crystal-rich pyroclastic surges occur within Unit 3T as well as at the contact with overlying Unit 4; however, none of these surges is as continuous, as widespread, or as traceable as those associated with the unit in the TA-3 area to the north (Gardner et al. 1999). Unit 3T is moderately porphyritic with about 20 to 25% phenocrysts, but the phenocryst population includes both large (4–6 mm) and small (2–3 mm) crystals. The contact between Unit 3T and the underlying Unit 3 is generally sharp where the top of Unit 3 is partially or moderately welded or where the contact is marked by surge deposits (i.e., Pajarito Canyon). However, in outcrop near MDA P, Unit 3 is moderately to densely welded, making identification of the Unit 3/3T contact quite difficult without careful examination of the phenocryst, accidental lithic, and pumice content and/or geochemical analysis.

Unit 4: ~ 0 to 34 m (~ 0–110 ft) thick. We include a number of distinctive packages of cooling units in Unit 4. In the south-central part of the study area, in the vicinity of Cañon de Valle, Unit 4 includes two principal subunits. The lower subunit, termed Unit 4l (l = lower) in this report, consists of poorly to moderately welded, crystal-poor ignimbrites, correlative to Unit 4 mapped by Gardner et al. (1998a, 1999) at TA-3 and TA-55. The upper subunit, termed Unit 4u (u = upper) in this report, consists of nonwelded to partially welded ignimbrites [Unit 4u(npw)] with conspicuous agglomerates of quartz and feldspar crystals (referred to herein as "clots") and densely welded ignimbrites [Unit 4u(w)] with conspicuous crystal clots. Unit 4u locally has a nonwelded top preserved. Units 4u(npw) and 4u(w) are correlative to clot-rich Unit 4 mapped by Gardner et al. (2001) at TA-16. Some of these subunits have been divided out locally in the bedrock mapping, but some could not be mapped consistently throughout the study area because they are nonwelded slope formers and tend to be covered with colluvium and vegetation. Where nonwelded Units 4l and 4u(npw) are co-extensive, for example, it is difficult to map the contact between them. In such areas on Plate 1, we have left these units undivided and map them as Unit 4.

Unit 4l, the basal part of Unit 4, is relatively pumice poor (less than 5% pumice) and crystal poor (10–15% phenocrysts of mostly quartz and feldspar 2–3 mm across) with rare accidental lithic fragments. Petrographically, this ignimbrite strongly resembles Unit 4 as mapped by Gardner et al. (1999) in the TA-3 area. In addition, mapping from this study connected this part of Unit 4 with that mapped by Gardner et al. (2001). The basal ignimbrite in this series is the most widespread part of Unit 4 in the study area, although poor exposure prevented us from differentiating it from the overlying ignimbrite where both occur together. The thickness of Unit 4l varies from around 5 to 22 m (15–72 ft), generally thickening to the east but with notably thick sections in the building TA-16-260 area (Cross-sections A-A' and B-B', Plate 2; also see below). Crystal-rich and ashy surge deposits typically, but not everywhere, mark the contact between Unit 4l and the overlying clot-rich Unit 4u.

The central part of Unit 4 [Unit 4u(npw)] in the study area comprises nonwelded to partially welded ignimbrites [0 to 20 m (0–65 ft) thick] with conspicuous crystal clots. Maximum thickness occurs on the north side of Cañon de

Valle near MDA P. The crystal clots are relatively large, up to 2 cm, and consist of intergrown feldspar and quartz with minor amphibole and pyroxene. Thin sections reveal that these clots are commonly cored with plagioclase (Gardner et al. 2001).

Unit 4u(npw) is overlain by the most distinctive part of Unit 4. Unit 4u(w) consists of moderately to very densely welded ignimbrites that contain large vitrophyric fiamme commonly 15 to 20 cm in length as well as abundant crystal clots as found in the underlying nonwelded to partially welded Unit 4u(npw). Unit 4u(w) can be up to 14 m (45 ft) thick and forms the "caprock" on mesas in the south-central part of the study area. This three-part sequence [Units 4l, 4u(npw), and 4u(w)] strongly resembles the sequence exposed at the east end of Campground Mesa, above the sharp curves on State Road 4 (Gardner et al. 2001). A thin surge sequence [less than 60 cm (2 ft) thick] typically, but not everywhere, separates the principal clot-rich parts of Unit 4 [Units 4u(npw) and 4u(w)]. Within the study area, Unit 4u pinches out to the north and the east (Cross-section B-B', Plate 2, and map pattern on Plate 1). The most northerly exposures are located on the south side of Pajarito Canyon. Near the pinch-out, the upper part is only partially welded.

In the south-central part of the map area, one additional pyroclastic flow marks the welding break at the base of Unit 4u(w). In western Cañon de Valle and the canyon north of building TA-16-340 (Plate 1), the surge sequence between Units 4u(npw) and 4u(w) includes a thin ignimbrite that thickens to the west. Welding in this ignimbrite also increases to the west, towards the source, such that the cooling break in Unit 4u lies above this thin ignimbrite to the east and below this ignimbrite to the west.

In a few localities, an upper nonwelded part of Unit 4 is preserved on mesa tops on top of Unit 4u(w). This subunit crops out, for example, in the vicinity of well R-25 (Plate 1). We did not map this part of Unit 4 as a distinct unit.

2. Surficial geologic units

Surficial geologic units in the study area that postdate the Bandelier Tuff include a variety of alluvial fan deposits (Qoal, Qf), the El Cajete pumice (Qec), fluvial (Qt, Qal) and colluvial (Qc) deposits, as well as materials disturbed or added by anthropogenic works (e.g., fill). Qt and Qal represent alluvial deposits along the modern stream channels.

a. Older mesa-top alluvial deposits (Qoal)

Unit Qoal consists of dacite-rich alluvium commonly found on drainage divides between the present-day watersheds, topographically higher than the top of the Bandelier Tuff. Qoal also includes some gravel deposits within shallow tributary canyons that presently head on the Pajarito Plateau. Qoal varies greatly in thickness and has an estimated maximum thickness of greater than 6 m (20 ft) north and south of Cañon de Valle (Gardner et al. 2001) and similar thicknesses north and south of Pajarito Canyon (this study). At the other extreme, Qoal locally consists of discontinuous lag deposits of dacite gravels. Old, post-Bandelier Tuff pumice beds, partially reworked, are present within the mesa-top alluvial deposits at several sites on the Pajarito Plateau, including the study area. The high-percentage of pumice in these layers, along with their thickness and wide geographic distribution, indicates that they were probably deposited relatively soon after eruption of the pumice. Geochemical fingerprinting of the pumice indicates that the primary source is the Cerro del Medio dome complex in the Valles caldera (e.g., Appendix D of Reneau et al. 2002). Cerro del Medio lavas have yielded $^{40}Ar/^{39}Ar$ ages of 1.21 to 1.10 Ma [Spell and Harrison 1993; Izett and Obradovich 1994; Spell and Harrison (1993) argue that the most "reliable age" is 1.13 Ma], indicating an early Pleistocene age for the mesa-top alluvium associated with these pumice beds. Elsewhere, these gravels may be younger, but they are no younger than the ca. 50 to 60 ka El Cajete pumice (see Qfi below). The base of Qoal has a gradient

that is gentler than the modern stream channels in Cañon de Valle and Water Canyon (Gardner et al. 2001) and in Pajarito Canyon (this study), apparently roughly parallel to the original upper surface of the Tshirege Member of the Bandelier Tuff. Along Cañon de Valle near MDA P, a unit Qoal2 is distinguished that is topographically lower than other nearby gravels to the west and represents a younger inset deposit. Similarly, Qoal along Pajarito Canyon in the western part of the study area is subdivided into three adjacent units of different elevations (oldest to youngest: Qoal1, Qoal2, Qoal3).

b. Older alluvial fan deposits (Qfo)

Unit Qfo consists of relatively old dacite-rich alluvial deposits that are typically inset below the top of the Tshirege Member of the Bandelier Tuff along major canyons in the western Pajarito Plateau; thus, these deposits postdate initial canyon incision. Stratigraphic relations indicate that these deposits are younger than nearby deposits of Qoal and older than intermediate-age fan deposits (Qfi); however, the age range of Qfo is unknown, and these deposits may overlap in age with Qoal and Qfi. In the study area, Qfo occurs as several distinct fan segments near Cañon de Valle, inset about 6 m (20 ft) below the top of Qoal, with an apparent gradient roughly parallel to Qoal (Gardner et al. 2001). Qfo has an estimated maximum thickness in the study area of greater than 3 m (10 ft).

c. Intermediate-age alluvial fan deposits (Qfi)

Unit Qfi consists of intermediate-age alluvial fan deposits that predate the ca. 50 to 60 ka El Cajete pumice (Qec). Qfi includes abundant dacite gravel along the main drainages that head in the Sierra de los Valles west of the study area but largely contains Bandelier Tuff clasts along smaller drainages. Qfi is locally buried beneath younger alluvial fans (Qfy) or colluvium (Qc) [e.g., trench EOC-2, Reneau et al. (2002), and soil pit WJR-4, Reneau and McDonald (1996), pp. 94–96], as well as Qec. Qfi probably includes deposits with a wide range in age. Where exposed in a 1999 gas pipeline trench in TA-9 north of Cañon de Valle (Plate 1; Fig. 6), the youngest Qfi deposits are apparently only slightly older than the El Cajete pumice because there was only weak soil development in the Qfi alluvium that directly underlay Qec. The maximum age of Qfi is uncertain. The distinction between Qfi and Qfo is based on local topographic relations and is only consistently reliable within a given drainage. Near Cañon de Valle, Qfi includes multiple distinct fan lobes, some of which appear to have gradients roughly parallel to Qfy (see below) and others that appear to have gradients roughly parallel to Qfo, supporting the inference that Qfi may span a considerable period of time (Gardner et al. 2001).

d. El Cajete pumice (Qec)

Unit Qec consists of the El Cajete pumice, derived from the youngest major eruptions from the Valles caldera and dated at ca. 50 to 60 ka [age from Toyoda et al. (1995) and Reneau et al. (1996b)]. In the formal stratigraphy of the Jemez volcanic field, this unit is the El Cajete Member of the Valles Rhyolite (Bailey et al. 1969; Gardner et al. 1986). Commonly, Qec consists of primary fallout deposits of dominantly pumice lapilli that directly overlie the pre-eruption soil, but some locations on the main escarpment of the Pajarito fault provide evidence for local reworking. Trench exposures in nearby areas (Kolbe et al. 1994; Reneau et al. 1995) have shown that deposits of undisturbed pumice can be quite discontinuous and that the pumice is often highly disrupted by burrowing animals and other forms of bioturbation. The pumice beds are also typically overlain by colluvial, alluvial, or eolian deposits (Kolbe et al. 1994; Reneau et al. 1995, 1996a, 1996b; Wong et al. 1995; Reneau and McDonald 1996; Gardner et al. 2001). In the map area, the existence of Qec below the surface soil can often be inferred from the presence of abundant pumice in mounds adjacent to animal burrows. We generally made no attempt on Plate 1 to separate Qec from overlying colluvium and eolian deposits. Instead, a composite "Qc/Qec" map unit is employed that indicates that Qec is at least locally present in the shallow subsurface.

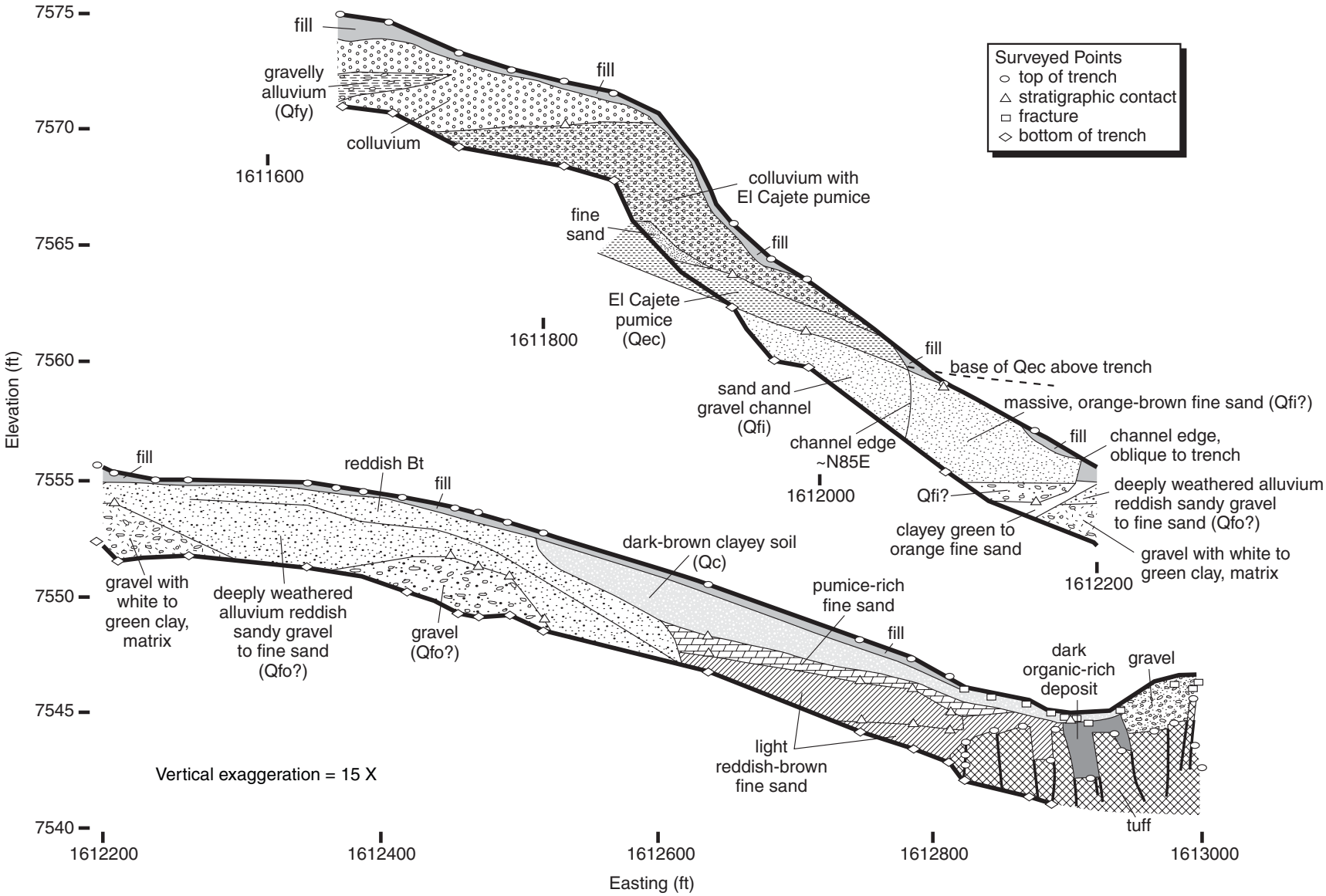

Figure 6. Western Part of the TA-9 Trench. The sketch of the western 300 m (1,000 ft) of the TA-9 trench shows generalized stratigraphy and fractures. The easternmost 60 m (200 ft) are part of zone A (see Fig. 10). Abbreviation: Bt, soil horizon with silicate clay either formed in situ or translocated within or into the horizon. Unit designations are as in Plate 1.

Importantly, previous trench studies (Kolbe et al. 1994; Reneau et al. 1995) have shown that even where no undisturbed pumice remains, the top of the pre-El Cajete soil can generally still be recognized in such areas and used as a key stratigraphic horizon in paleoseismic studies. Maximum observed thickness of primary fallout El Cajete pumice at LANL is about 2.0 m (6.5 ft) along a northern tributary to Water Canyon and about 2.1 m (7 ft) on Frijoles Mesa about 4.8 km (3 mi) southeast of the study area (Reneau and McDonald 1996, pp. 73–75; Gardner et al. 2001).

e. Younger alluvial fan deposits (Qfy)

Unit Qfy consists of relatively young alluvial fan deposits that postdate the El Cajete pumice. In some areas where there is no age control, the distinction between Qfy and Qfi is arbitrary and will probably require revision. Qfy includes stream terraces along some drainages, as the distinction between fan and terrace remnants is also often arbitrary. The thickness of Qfy is unknown in most areas. Radiocarbon dates on detrital charcoal from the upper part of a 6-m (20-ft) thick section north of Water Canyon are ca. 9.3 to 9.6 ^{14}C ka (ca. 10.3–10.9 cal ka) and probably closely constrain the end of fan deposition at that site (Gardner et al. 2001). Soils exposed in a pit in Qfy along Cañon de Valle (soil WJR-6, Reneau and McDonald 1996, pp. 93–95) suggest a similar age for that fan unit. A Qfy stream terrace along Water Canyon that was trenched by Wong et al. (1995) may be of similar age (see also Reneau and McDonald 1996, p. 82). Qfy deposits are as young as 4.7 to 9.4 ^{14}C ka (5.5–10.7 cal ka) at trench EOC-2 in the western part of the study area (Reneau et al. 2002). In contrast, at a soil pit on the south fork of Pajarito Canyon, the youngest Qfy depositional event is estimated at ca. 20 to 40 ka where Qfy overlies pre-El Cajete (Qfi) fan deposits (soil WJR-4, Reneau and McDonald 1996, pp. 94–96). Qfy occurs on the modern channel divide between the Cañon de Valle and Pajarito Canyon watersheds at TA-9 (Fig. 6), indicating that the Cañon de Valle fan overtopped the drainage divide sometime within the past 50 to 60 ka. Along Cañon de Valle, Qfy has a gradient that is slightly steeper than the modern stream channel, being about 6 m (20 ft) higher than the channel at the base of the Pajarito fault escarpment but converging with the channel about 915 m (3,000 ft) to the east (Gardner et al. 2001).

f. Stream terraces (Qt)

Unit Qt consists of stream terraces along the modern drainages. Texturally, this unit includes coarse sand and gravel that represent bed-load sediment deposits, medium sand to silt that represents overbank sediment deposits, and some colluvium derived from adjacent slopes. Based on work in other canyons on the Pajarito Plateau (e.g., McDonald et al. 1996; Reneau and McDonald 1996; Reneau et al. 1996a; Reneau 2000), Qt has a probable age range from late Pleistocene to late Holocene. In many areas, Qt was not broken out separately from Qal. The thickness of Qt has not been determined in the map area but could range from < 1 m to > 10 m (~ 3–33 ft).

g. Young alluvium along stream channels (Qal)

Unit Qal consists of relatively young alluvium along stream channels and includes presently active channels and adjacent floodplains, low terraces, and associated colluvium. Qal also includes active channels with little or no alluvium in some areas. Radiocarbon dates indicate a middle Holocene age for a buried Qal terrace in one area in Cañon de Valle near MDA P (Gardner et al. 2001).

h. Colluvium (Qc)

Unit Qc includes deposits with a wide range in texture, origin, and age that were not practical to subdivide in this investigation. The term "colluvium" is used in this report to include both deposits on steep slopes that record primarily gravity-driven transport and deposits on gentle slopes that record deposition by surface runoff. As used in this context, the distinction between colluvium and alluvium is somewhat arbitrary and is made solely for convenience in mapping. In addition, Qc includes fine-grained deposits that are probably dominated by eolian sediment, although this eolian sediment may be locally reworked by surface runoff and/or

mixed with other material by bioturbation. Qc also locally includes dark organic-rich deposits, as exposed in the 1999 gas pipeline trench at TA-9 (Fig. 6). Qc includes deposits that range in age from > 50 to 60 ka (pre-Qec) to present. Evidence for the eolian origin of some early Holocene and late Holocene deposits on Pajarito Mesa, east of the map area, is presented in Reneau et al. (1995, 1996a), and eolian deposits of similar age may be widespread in the study area. On Plate 1, Qc is in many places included in other map units and not broken out separately. Where possible, the unit directly underlying Qc is noted in the map designation to aid in interpreting the distribution of different units; for example, "Qc/Qbt" indicates that thin colluvium overlies tuff.

i. Artificial fill

Artificial fill and anthropogenic disturbances are widespread in the map area. On Plate 1, this unit locally includes highly disturbed areas such as roads, parking lots, and borrow pits. Many areas that include patchy or thin fill were mapped instead as the underlying stratigraphic unit.

B. Geochemisty of Bedrock Units

Geochemical compositions of samples obtained in this study are similar to compositions of Tshirege Member samples from previous studies on the Pajarito Plateau (Table 1; Appendix A). Silica (SiO_2), titania (TiO_2), zirconium (Zr), strontium (Sr), rubidium (Rb), and barium (Ba) concentrations are each strongly zoned with respect to stratigraphy and have been shown to effectively differentiate among units within the Tshirege Member of the Bandelier Tuff (Broxton et al. 1996; Warren et al. 1997; Gardner et al. 1998a, 1999, 2001; Krier et al. 1998a, 1998b; Stimac et al. 1998). As demonstrated in previous work, Tshirege Member samples show systematic variations from higher silica to slightly lower silica and from lower titania to higher titania toward the top of the section. Titania is the single most useful major-element oxide used for unit identification throughout most of the Tshirege Member sequence. The variation in SiO_2 and TiO_2 in the measured section and cores from MDA P show geochemical trends similar to those observed in areas to the north, west, and south of the present study area (Gardner et al. 1999, 2001; Fig. 7; Table 1). Table 1 shows trends towards lower SiO_2 and higher TiO_2 upsection in the upper units of the Tshirege Member. The geochemical results in all cases confirmed field petrographic calls.

The geochemical data reveal an unusual component of Unit 4 in MDA P boreholes 257 and 273 (Figs. 4 and 7), identified previously in Water Canyon on the adjacent Pajarito fault escarpment, and in the bedded-ash and surge sequence at the base of Unit 4 in most of the WETF boreholes (Gardner et al. 2001). The lowermost three samples of Unit 4 in MDA P borehole 257 and the single sample of Unit 4 in borehole 273 have distinctively high TiO_2 (> 0.35 wt %), high Ba concentrations (490–600 ppm), and moderately high SiO_2 (70–72 wt %). Basal portions of Unit 4 within the study area therefore exhibit the high Ba and high TiO_2 but not the low SiO_2 whole-rock chemistry of basal portions of Unit 4 observed in nearby areas (Gardner et al. 2001). Some of the samples from MDA P boreholes could have artificially high Ba concentrations due to contamination from waste

Table 1. Mean Values of Some Major Oxides in Tshirege Member Units*

Unit	Number of analyses	Weight % SiO_2	Weight % TiO_2
Gardner et al. (2001):			
4	71	71.96 ± 2.44	0.28 ± 0.08
3T	41	74.49 ± 1.15	0.20 ± 0.04
3	15	76.55 ± 1.27	0.14 ± 0.01
This study:			
4	10	72.01 ± 1.44	0.28 ± 0.06
3T	5	75.27 ± 0.44	0.15 ± 0.01
3	4	75.58 ± 0.91	0.14 ± 0.01

*Mean of analyses with 2σ standard deviation.

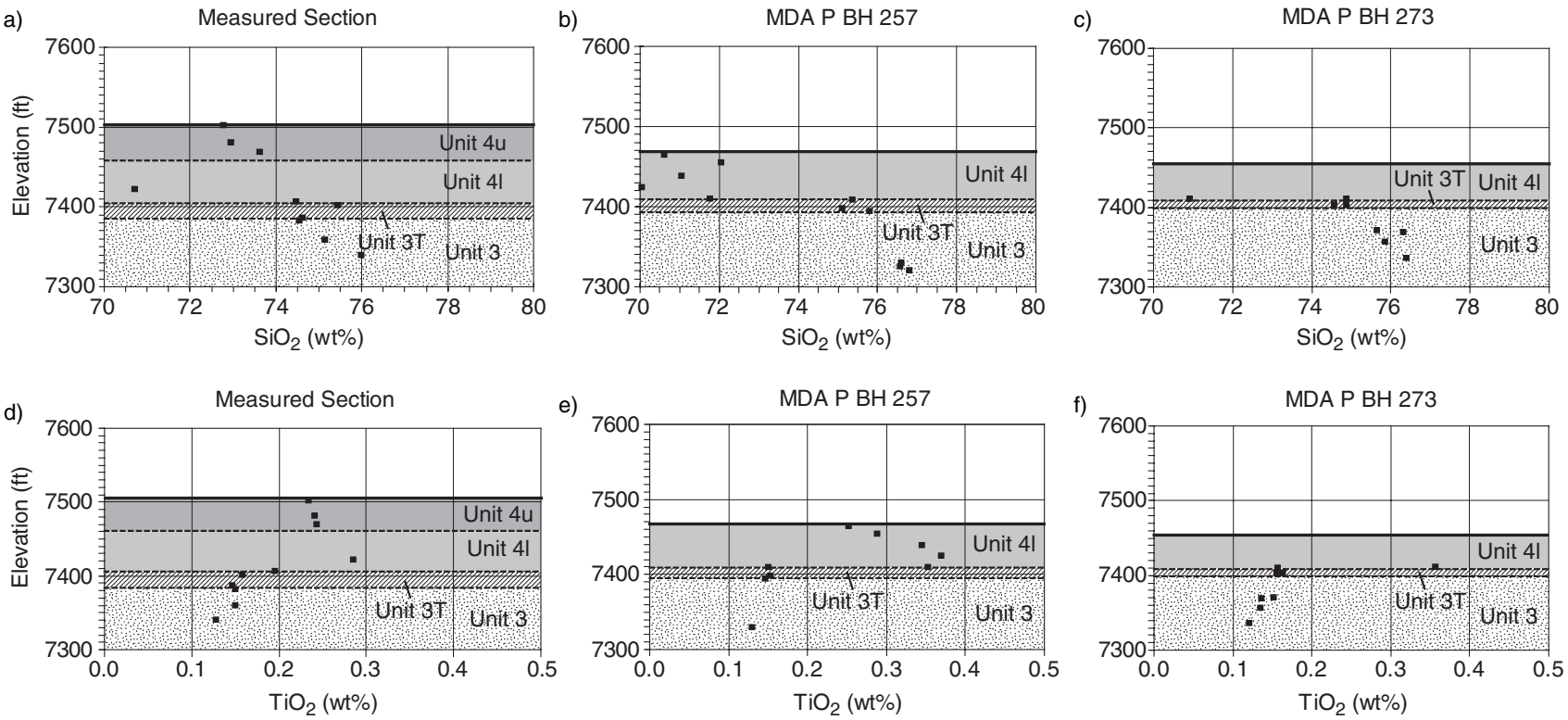

Figure 7. Silica and Titania Variation in Bandelier Tuff. Panels a) through c) show the variation in SiO_2 with respect to elevation for samples from the measured section and boreholes (BH) at MDA P. Panels d) through f) show the variation in TiO_2 for samples from the same sites. Borehole locations are indicated on Fig. 4, and the location of the measured section is shown on Plate 1.

left over from high-explosives machining and stockpiled at MDA P (William Criswell, personal communication).

C. Structural Geology

1. Subsidiary faults of the Pajarito fault zone

The northwestern corner of the study area encompasses part of a 160-m (525-ft) wide graben at the base of the Pajarito fault escarpment (G1, Plate 1). Part of this graben and its eastern bounding fault (F1, Plate 1) were trenched prior to construction of the new LANL Emergency Operations Center (Reneau et al. 2002; see "Previous Work," page 8). Trench exposures provided evidence for Holocene faulting on fault F1.

Along its southern continuation, fault F1 has ~ 6 m (20 ft) of throw on Bandelier Tuff contacts and the base of Qoal (Plate 1). The footwall of this fault is the east-dipping, steep limb of a monocline with as much as 23 m (75 ft) down-to-the-east displacement; the axis of this monocline appears to parallel Anchor Ranch Road (M1, Plate 1). Folding apparently occurred after deposition of Qoal, based on parallelism between the base of Qoal and the Unit 3T/4 contact and the higher-than-usual dip of the base of Qoal (~ 4° compared to ~ 2° elsewhere). A profile of stratigraphic contacts along the north side of Pajarito Canyon shows both the fault and the monocline (Fig. 8a), whereas a structure contour map on the top surface of Unit 3T shows the monocline (Fig. 9a).

2. North-striking structures in the eastern part of the Pajarito fault zone

TA-9 Graben. The largest structure in the study area is a north-trending graben (here named the TA-9 graben, G2, Plate 1) whose western bounding fault is located about 1,200 m (4,000 ft) east of the Pajarito escarpment. The graben is about 610 m (2,000 ft) wide at its southern mapped end between building TA-16-260 and MDA P, narrowing to about 305 m (1,000 ft) wide at its northernmost mapped extremity in Pajarito Canyon west of building TA-22-52. The total length of this structure appears to be about 1,200 m (4,000 ft), but the mapped trace is discontinuous and must therefore be inferred along part of its length. Structural displacements along graben bounding faults can be measured readily at the well-exposed welding break in Unit 4u. The fairly continuous surge deposits at that contact provide an outstanding structural marker. The TA-9 trench also provided excellent exposure of this graben (see below).

At Cañon de Valle, the eastern boundary of the graben is a pair of north-northwesterly-striking faults with a total of ~ 3 m (10–11 ft) down-to-the-west apparent dip slip at the welding break between Unit 4u(npw) and Unit 4u(w) (F2, Plate 1; Cross-section A-A', Plate 2; Fig. 8b). These two faults intersect near the north rim of Cañon de Valle and run northwards across the mesa top, forming a prominent break in slope in Qoal; they appear to link with the eastern boundary of a graben identified in the TA-9 trench (see below). Beyond the trace of the TA-9 trench, the eastern bounding fault can be traced another 150 m (500 ft) to the north. Aligned faults farther north, though not mapped as continuous through the area, may connect fault F2 to a zone of faulting on the north side of Pajarito Canyon that has about 3 m (10 ft) of down-to-the-west vertical separation on the Unit 3T/4 contact (F3, Plate 1).

The western bounding fault of the TA-9 graben (G2) has 1.5 m (5 ft) of down-to-the-east vertical separation on the welding break between Unit 4u(npw) and Unit 4u(w) (F4, Plate 1). Like the eastern fault, the western fault can be traced northwards across the mesa top, where it forms a prominent topographic step in Qoal, and through the trace of the TA-9 trench, where it appears to form the western bounding fault of the graben identified in the trench. The northward continuation of fault F4 beyond the TA-9 trench can only be inferred due to abundant fill and anthropogenic works. The fault may connect with a mapped fault northwest of building TA-9-48, which has 0.5 m (1.5 ft) of down-to-the-east throw on the Unit 3T/4 contact and apparently cuts Qfo (F5, Plate 1). Throw on

the western bounding fault may diminish to the north, or deformation may become more diffuse. About 90 to 120 m (300–400 ft) east of fault F5, the narrow east-west-trending mesa capped by Unit 4u(w) forms a syncline along the axis of the graben (Plate 1). Whether the graben continues to the south of Cañon de Valle is unknown due to extensive cover by anthropogenic works in the vicinity of building TA-16-260 and poor exposure on the north slope of Cañon de Valle near well R-25.

Topographic profiles of contacts between cooling units show the structure of the TA-9 graben (Fig. 8b). Three, closely spaced, high-angle normal faults on the east side account for a total of ~ 6 m (20 ft) of down-to-the-west stratigraphic separation. Synclinal folding adjacent to the eastern bounding fault accounts for about 3 m (10 ft) more of down-to-the-west separation. The western bounding fault (F4) appears as a high-angle normal fault with about 1.5 m (5 ft) of down-to-the-east separation. Directly west of the graben, bedding dips indicate an anticlinal fold contrasting with the gentle easterly dips in the graben and farther east. This folding is apparent in profiles of the topographic surface of the mesa and within the TA-9 trench (see below). A nearly parallel fault (F6, Plate 1) < 150 m (500 ft) to the east of fault F4 has 1.2 m (4 ft) of down-to-the-west apparent dip slip and forms a small graben-within-a-graben structure. Folding associated with graben G2 can be readily appreciated from structure contour maps on the top surface of Unit 3T (Fig. 9a). Dips flatten west and east of the graben. The faults that make up the eastern boundary of the graben coincide with a zone of high conductivity in the canyon bottom identified in electrical resistivity surveys performed by the LANL ER Project (in preparation). There are also three springs in Cañon de Valle associated with the graben (Plate 1), suggesting that these faults influence the hydrology of this part of Cañon de Valle.

A strong inflection in the upper surface of Qoal and the underlying Bandelier Tuff on both sides of Cañon de Valle about 305 m (1,000 ft) east of building TA-16-260 (Gardner et al. 2001) is consistent with the presence of the graben. Gradients in the mesa top abruptly become gentler to the east at the axis of the graben. Low gradients continue at least as far as MDA P and a roadcut on R-site road where a prominent surge within Unit 4 has a very gentle dip to the west. A prominent bench in the structure contour maps on the top surfaces of both Unit 3T and Unit 3 (Figs. 9a and 9b) coincides with the inflections noted by Gardner et al. (2001).

Fractures (possible faults?) in the TA-9 trench. Figure 10 is an east-west profile of surveyed points in the TA-9 gas pipeline trench illustrating topography along the trench and major zones of fracturing. Stratigraphic contacts in post-Bandelier units were traceable in much of the western part of the trench, and no faults were recognized there (Fig. 6). However, recognition of faults and fractures in post-Bandelier clay-rich soils was not always possible because of the locally massive character of the soils, and faults in these units may have been missed in some cases. The upper surface of the Bandelier Tuff in the TA-9 trench had numerous steps at the contact between tuff and overlying alluvium/colluvium (cover photo; Fig. 6). This stepped contact may be partially or entirely depositional and not associated with faulting; plucking of Qbt blocks prior to or during deposition of alluvium/colluvium may create the appearance of fault displacement where there is none.

Two prominent zones of fracturing were mapped in the trench. Zone A (Fig. 10; cover photo) is characterized by numerous steps in the tuff surface, sediment- and clay-filled fractures, and possible domino-style faulting, similar in form to faults described by McCalpin (1998) in tensional structures on the main scarp of the Pajarito fault. Steps on the top surface of the tuff at fractures range from 0.1 to > 1.2 m (0.3 ft to > 4 ft) high. Clay- and sediment-filled fractures are up to 1 m (3 ft) wide. Most fractures in the western portion of zone A strike about N15E; however, strikes vary from N80E to N20W. The eastern end of zone A is dominated by fractures with northerly strikes. The

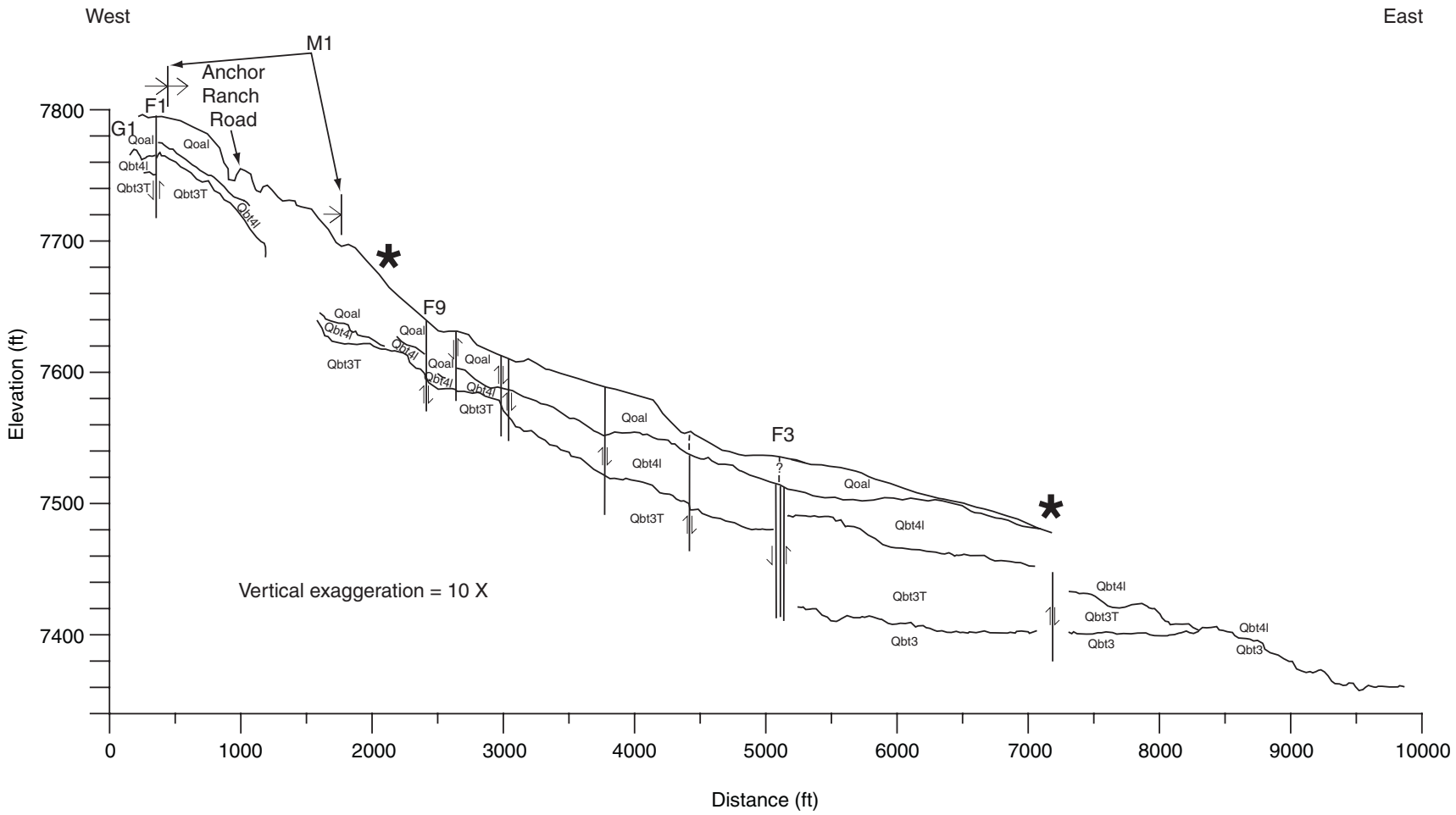

Figure 8a. Pajarito Canyon Profile. This composite profile along the north side of Pajarito Canyon, projected into profile lines on Plate 1, shows the topography, contacts between Qbt units, and the base of Qoal. The profile was created as follows: bedrock contacts were digitized from field maps; elevations along geologic contacts were derived from a DEM; points along contacts were projected from the mesa rim into the profile line; and topography was projected from the crown, or high part, of the mesa (see text for further discussion). Structural features are labeled as in Plate 1. Faults are shown with mostly vertical dips; steep measured dips (> 80°) are made steeper by vertical exaggeration of profiles. Tshirege Member unit designations are as in Plate 1. A large asterisk indicates possible inaccuracy due to projection.

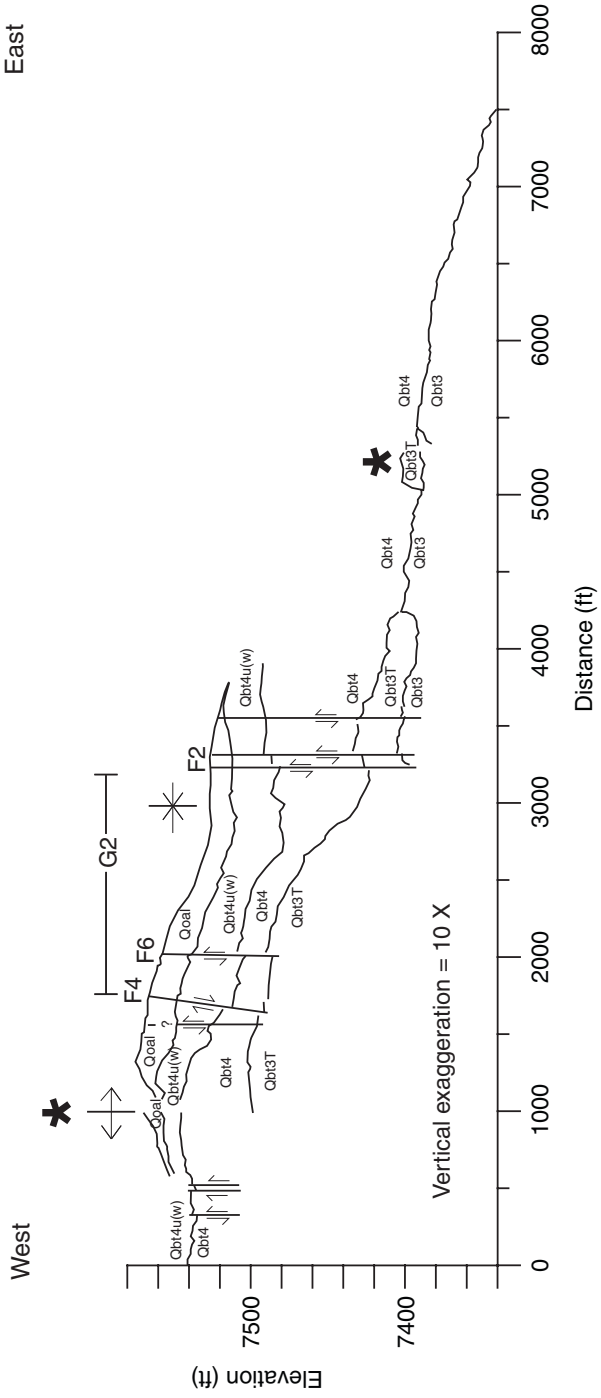

Figure 8b. Cañon de Valle Profile. This composite profile along the north side of Cañon de Valle, projected into profile lines on Plate 1, shows topography, contacts between Qbt units, and the base of Qoal. Graphical notation and methods for creation of the profile are the same as described in the caption for Fig. 8a. A large asterisk indicates possible inaccuracy due to projection.

upper surface of the tuff drops about 3 m (10 ft) down to the east over a 150-m (500-ft) wide zone. We correlate the eastern end of zone A with the western bounding fault (F4, Plate 1) of the TA-9 graben. In Cañon de Valle, fault F4 strikes N30E and has 1.5 m (5 ft) down-to-the-east dip separation on the welding break between Units 4u(npw) and 4u(w).

Zone B (Fig. 10) is also characterized by numerous steps in the tuff surface and possible domino-style faulting. Steps on the top surface of the tuff at fractures are < 60 cm (2 ft) high. The surface of the Bandelier Tuff drops > 3 m (10 ft) down to the west on the western side of this zone, and black, organic-rich soils are present west of the fracture zone. We correlate the west end of zone B with the eastern bounding fault (F2, Plate 1) of the TA-9 graben. In Cañon de Valle, this fault strikes north-south to N5E and has a cumulative dip separation of 3 m (10 ft) down to the west. The number of fractures falls off on the eastern side of zone B. The 460-m (1,500-ft) width of the TA-9 graben and topography on the tuff surface across the bounding fracture zones (Fig. 10) are markedly similar to the same features in the profile of the north side of Cañon de Valle (Fig. 8b).

Examination of post-Bandelier Tuff units in the westernmost 300 m (1,000 ft) of the trench revealed no evidence of faulting (Fig. 6). However, because the trench walls were not continuously cleaned or logged, small faults may have been missed.

continued on page 28

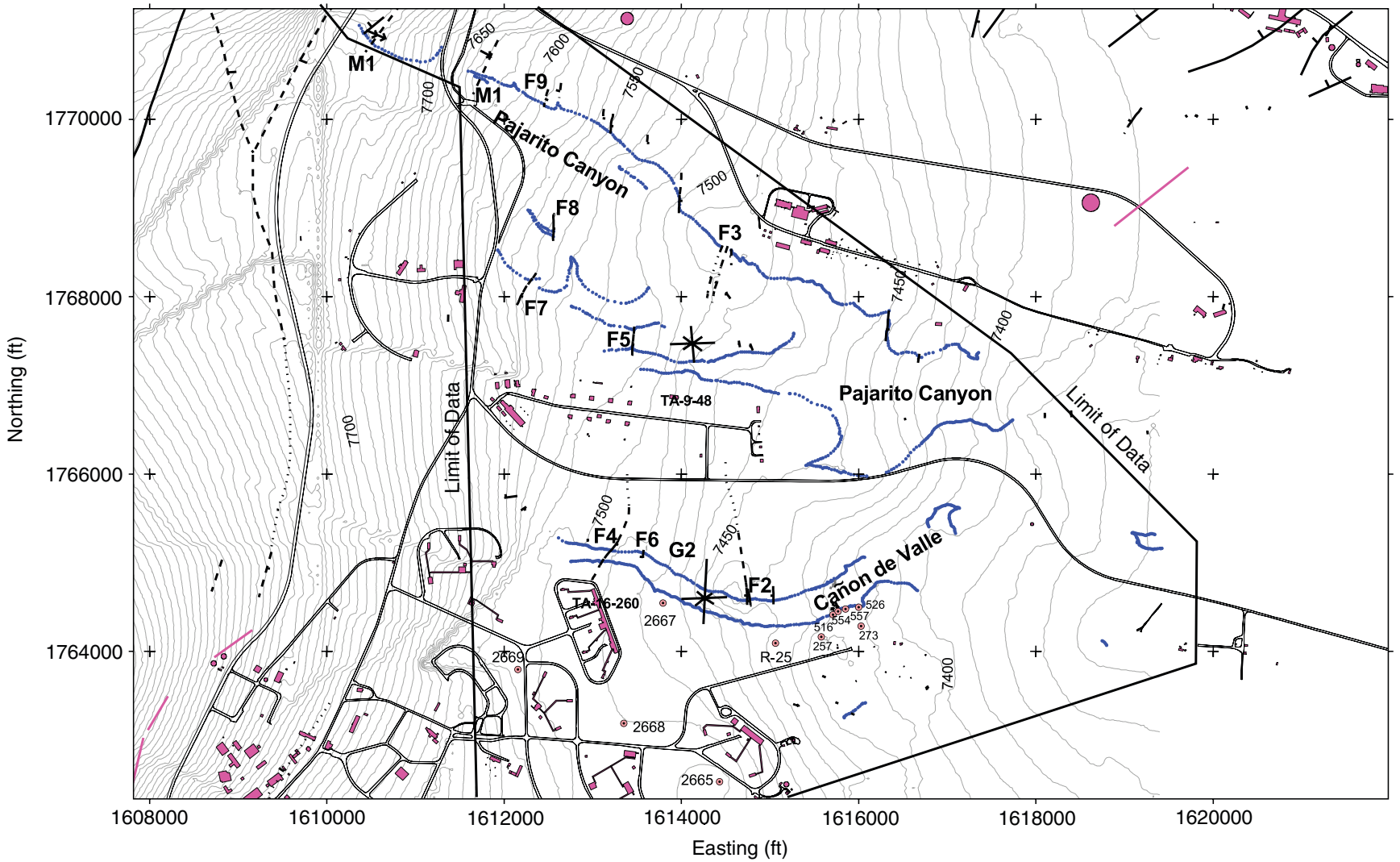

Figure 9a. Contoured Upper Surface of Unit 3T. Blue dots are mapped points on the Unit 3T-Unit 4 contact. Points were derived as for Fig. 8. Contour interval is 10 ft, and the surface was interpolated from a 100-ft grid of data from this study and from Gardner et al. (1999, 2001) using kriging. Mapped points constrain the contouring of the surface model; some spurious topography on the surface may result from limited data. Structural features, boreholes, and buildings are labeled as in Plate 1. Boreholes in the building TA-16-260 area are from LANL ER Project (1998).

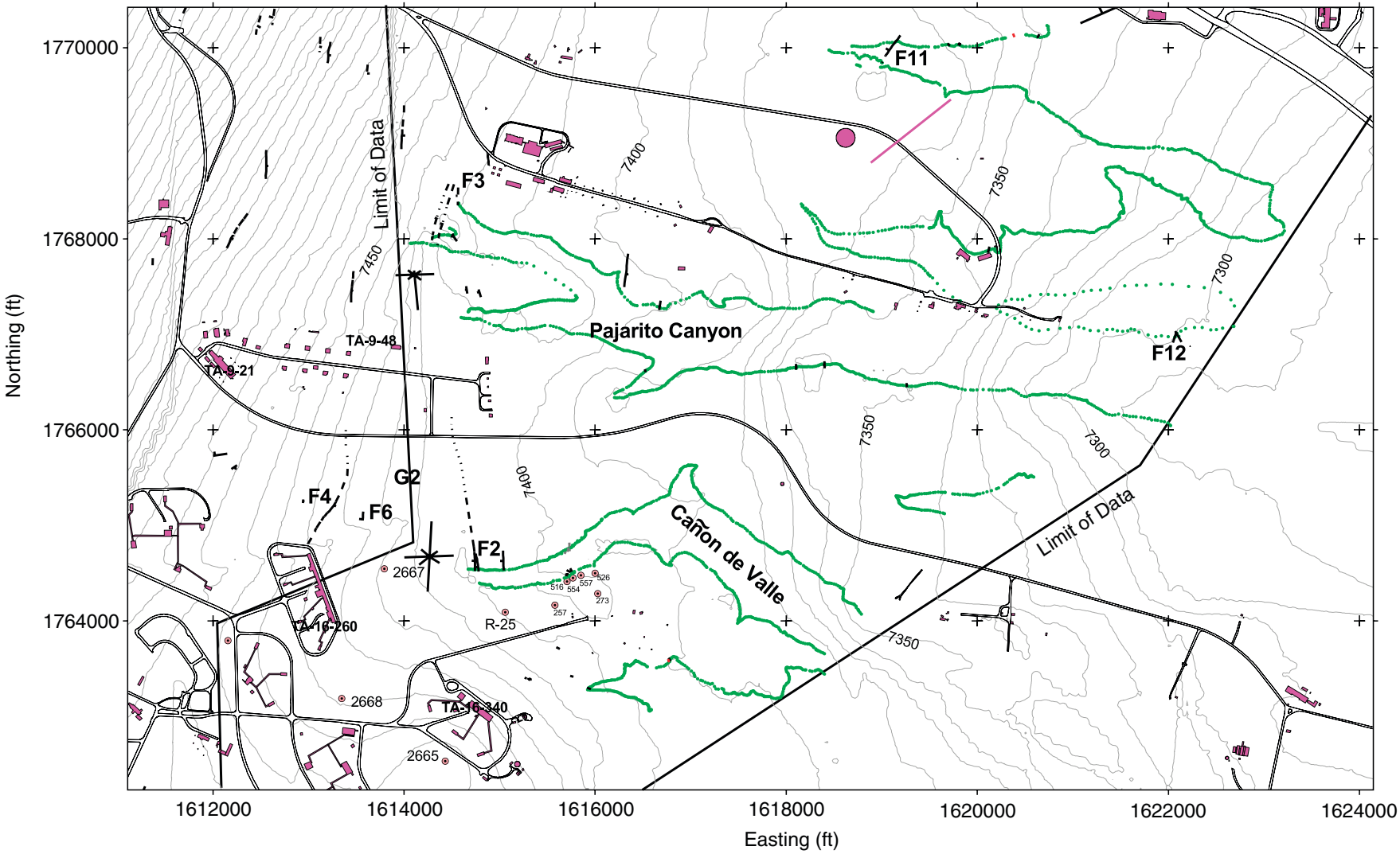

Figure 9b. Contoured Upper Surface of Unit 3. Green dots are mapped points on the Unit 3-Unit 3T contact. The other information is the same as that for Fig. 8a. The surface model was created using the same techniques as Fig. 8a.

continued from page 25

The easternmost surveyed part of the trench lay at the top of a large colluvium-covered scarp that drops 18 m (60 ft) to the east (Fig. 10). The trench in this location exposed the contact between Units 4u(npw) and 4u(w). This scarp is not associated with a fault. Rather it represents the eastern limit of a welded flow lobe of Unit 4u. Outcrops of this part of Unit 4 are sparse to absent east of here.

Small faults north and west of the TA-9 graben. Eight normal faults, all with apparent dip-slip displacements of < 5 m (16 ft), were identified north and west of the TA-9 graben. Their association, if any, with the TA-9 graben is unclear. Several of these faults are somewhat aligned along a north-northeast trend. Two of them, located east and northeast of building TA-8-21, have 3 m (10 ft) and > 1.5 m (5 ft) down-to-the-east separation on contacts in Bandelier Tuff (F7 and F8, Plate 1). Fault F7 is associated with flattening of the mesa top and may offset the post-Bandelier Tuff unit Qfi (deposited prior to 50–60 ka). Assuming this is the case, this feature is the youngest fault offset identified in the study area except for Holocene faulting in trench EOC-2 (Reneau et al. 2002). The other fault (F8), with 1.5 m (5 ft) down-to-the-east separation, is exposed only in Bandelier Tuff, giving a maximum age for the faulting.

Two small faults along this north-northeast trend were mapped in Pajarito Canyon (F9, Plate 1). One of these has 3 to 5 m (10–15 ft) apparent down-to-the-east separation on Qoal, and the other 1.5 to 3.0 m (5–10 ft) of apparent down-to-the-west separation on Qoal. Together, they form a small graben about 60 m (200 ft) wide. These faults are apparent in a profile of stratigraphic contacts along the north side of Pajarito Canyon

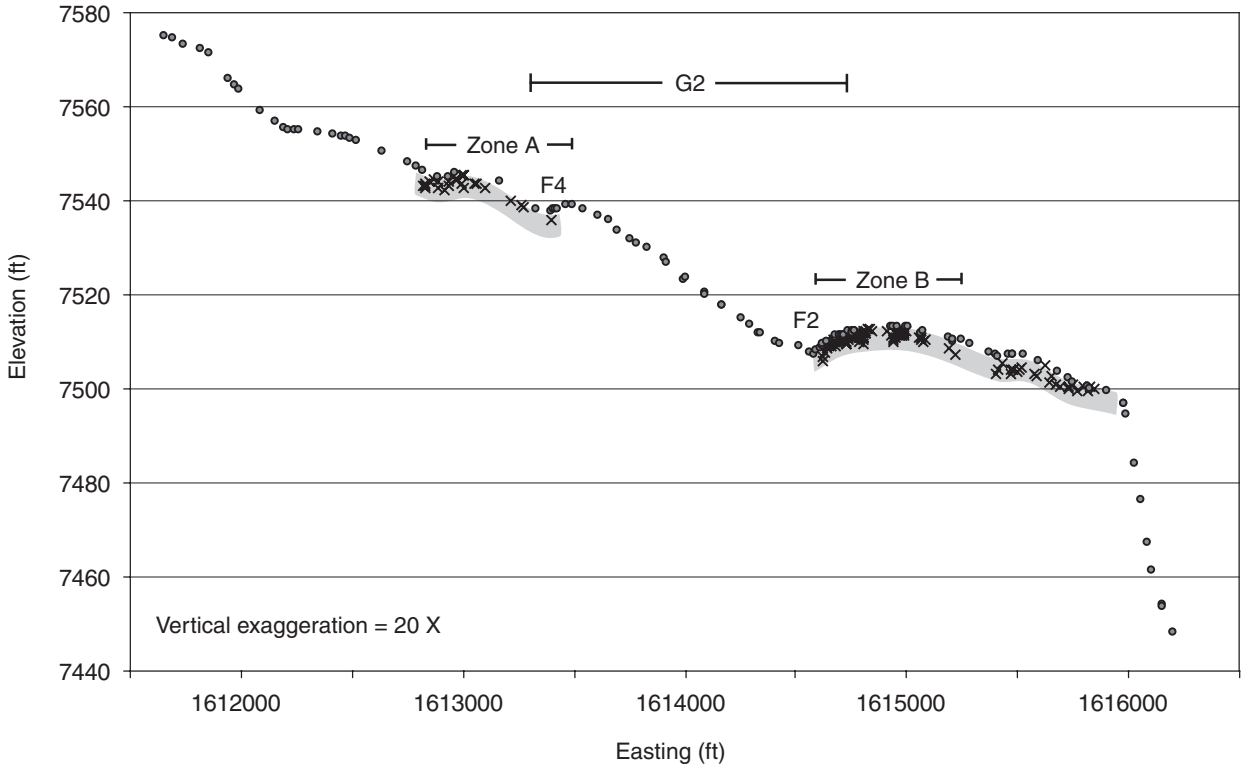

Figure 10. Profile of the TA-9 Trench Showing Surveyed Data. The filled circles are points on the ground surface at the edge of the trench. The X symbols are points at contact between Qbt and post-Qbt strata. Gray bands indicate areas in the trench where Qbt was observed. In all other areas, post-Qbt strata are thicker than the trench depth. Structural features F2, F4, and G2 are as in Plate 1.

(Fig. 8a; Plate 1). The faults are associated with a north-trending tributary canyon that enters Pajarito Canyon at an anomalously high angle, suggestive of structural control. The faults and the tributary canyon trend north-northeast towards the trace of a down-to-the-east fault with > 1.5 m (5 ft) of slip on post-Bandelier Tuff strata beyond the northern limit of the study area, about 460 m (1,500 ft) north of Pajarito Canyon (F10, Plate 1). This fault, where trenched on the south side of Los Alamos Canyon, experienced mid- to late-Pleistocene faulting and possibly Holocene fissuring, but time constraints are equivocal (McCalpin 1998). The continuity among these short faults, none of them with mapped traces longer than about 60 m (200 ft), is difficult to prove. Several springs in the bottom of Pajarito Canyon and its tributaries may be fault-controlled (i.e., springs located between faults F3 and F7 and faults F3 and F9, Plate 1). These springs may be associated with the G2 graben, as suggested above for springs in Cañon de Valle.

Four more small faults, between F9 and F3, offset Bandelier Tuff contacts and the base of Qoal farther east in Pajarito Canyon (Fig. 8a; Plate 1). None of these faults has more than 1.8 m (6 ft) of separation on Bandelier Tuff nor can they be traced more than about 60 m (200 ft) along strike. All of these faults are associated with north-trending tributary canyons that enter Pajarito Canyon at anomalously high angles.

3. Fractures and minor faults at Material Disposal Area P

To help understand a zone of open and filled fractures of large aperture [up to 100 cm (3.3 ft) wide] at MDA P, we measured and analyzed 454 fractures to determine possible tectonic influences on fracturing there. We mapped 9 small-displacement faults at MDA P using total station surveying (Fig. 4; Appendix C, Table C-2), including a fault zone with fissures and a small graben that crops out on both sides of Cañon de Valle. None of these faults appears to have lateral continuity across MDA P. No single large fault transects the site (Plate 1). Therefore, fracture analysis was used to recognize patterns in orientation, density, and aperture of fractures that might indicate their mode of formation.

We measured fractures in three units of the Tshirege Member, the welded Units 3 and 3T and the nonwelded Unit 4l (Fig. 4). Detailed methods are described in Appendix B. Data are compiled in Appendix B, Table B-1. A point density plot (contoured stereonet) of poles to all fracture planes shows a weakly developed clustering of data (Fig. 11a). The fracture set as a whole has a statistically significant north-northwest preferred orientation (mean direction of N15W ± 26°, Fig. 12a). Fracture dips vary from subhorizontal to steep. Despite considerable scatter in strike and dip, these data pass uniformity tests at the 95% confidence level (see Appendix B), indicating that the data are derived from a population of fractures with preferred orientation.

We measured 212 fractures in nonwelded Unit 4l. A point density plot shows a moderately developed girdle with cluster (Fig. 11b). These fractures have a statistically significant north-northwest preferred orientation (mean direction of N14W ± 16°, Fig. 12b). Dips of the Unit 4l fractures are generally steep. The small uncertainty on the mean direction, compared to the fracture set as a whole, indicates less scatter in strike in the nonwelded Unit 4l.

In the densely welded Unit 3T, we measured 129 fractures. A point density plot shows a weakly developed cluster with girdle (Fig. 11c). These fractures have a statistically significant east-northeast preferred orientation (mean direction of N69E ± 32°, Fig. 12c). Dips of the Unit 3T fractures are generally subhorizontal.

In densely welded Unit 3, we measured 113 fractures. A point density plot shows a weakly developed cluster (Fig. 11d). These fractures have a statistically significant north-northwest preferred orientation (mean direction of N25W ± 32°, Fig. 12d).

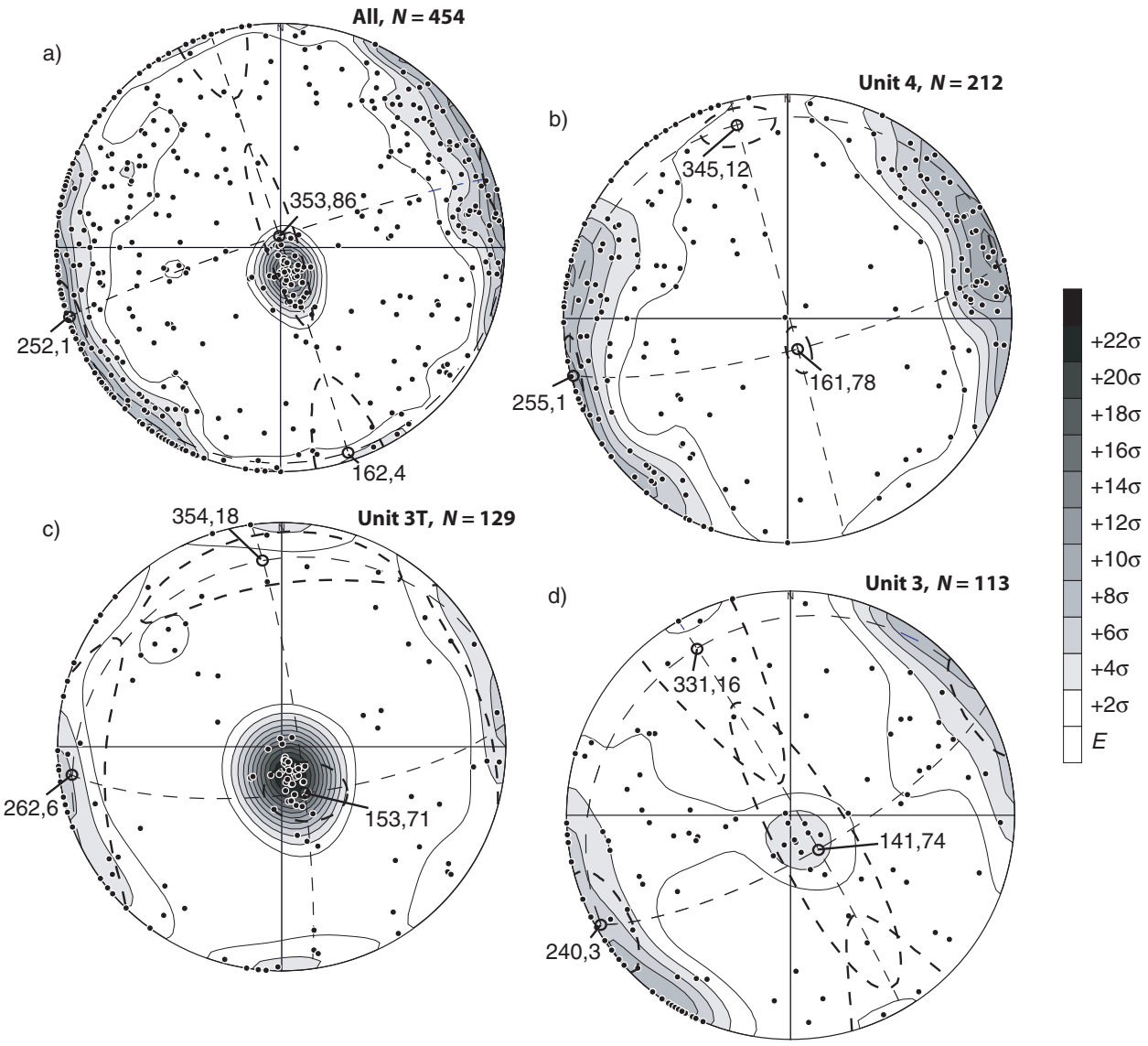

Figure 11. Point Density Plots of Poles to Fracture Planes Measured at MDA P. The plots show a) all data collected, b) data from Unit 4, c) data from Unit 3T, and d) data from Unit 3. Lower hemisphere equal area stereonets are contoured using the Gaussian counting method of Robin and Jowett (1986). Contour intervals are equal to $E + 2\sigma$, $E + 4\sigma$, etc., where E is the number of points expected to be found in the counting circle if points were extracted randomly from a uniform population and σ is the standard deviation. The three orthogonal principal directions are shown with 95% confidence cones for each data set; these show average clustering of each data set (see Appendix B, Table B-2). Only for all data combined and Unit 4 alone do these principal directions have small cones of confidence. Data from Unit 4 show a moderately strong preferred orientation. See Appendix B for further details on the method. Abbreviation: *N*, number of measurements.

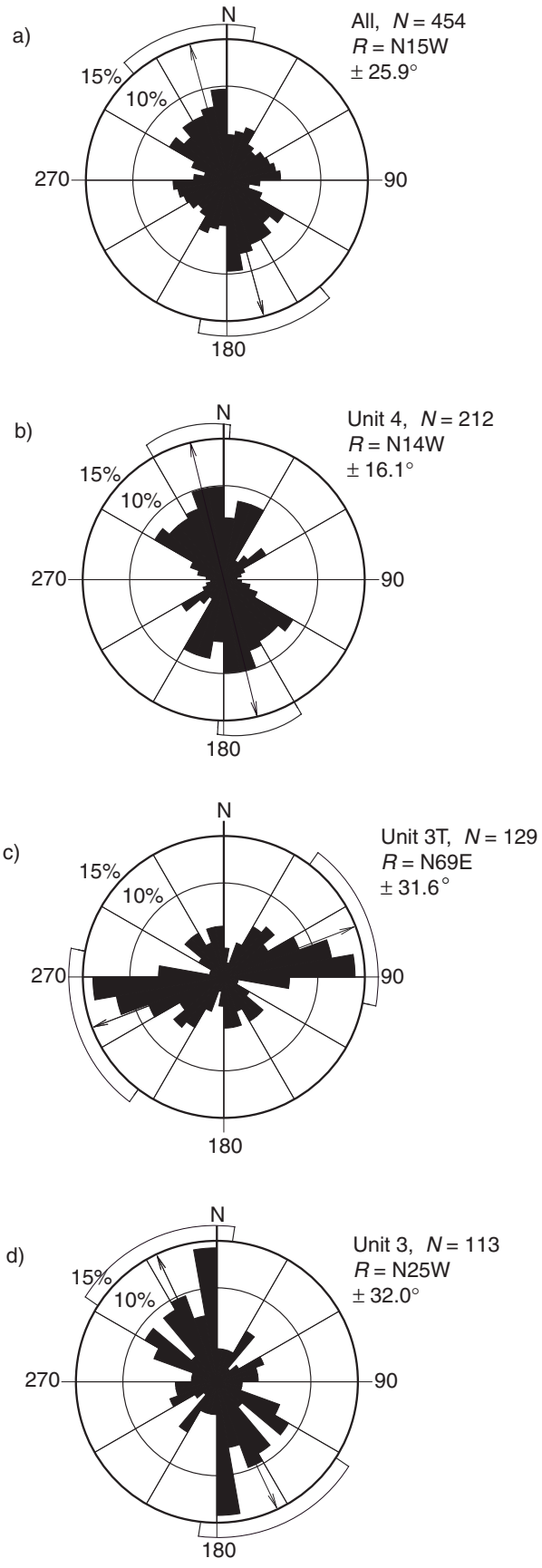

Figure 12. Rose Diagrams of Strikes of Fracture Data from MDA P. The inner circles represent 10% of the data analyzed, and the outer circles 15%. The mean strike, indicated by the arrow, is accompanied by the 95% confidence interval. Abbreviations: *R*, resultant vector, or mean strike; *N*, number of measurements.

Dips of the Unit 3 fractures are a mixture of steep and subhorizontal.

Approximately 37% of the measured fractures are covered at both ends and about 13% at one end, which introduces some uncertainty in interpretations of trace length and style of termination. Nevertheless, 56% of all measured fractures terminate at other fractures. Trace length of the measured fractures in all three units is generally short (Appendix B, Table B-1). Mean trace length of fractures with both ends exposed along our eight traverses is < 3 m (10 ft). Maximum trace length is 25 m (81 ft). The overall map pattern of fractures in all units including Unit 4l is polygonal.

Fracture density (the number of fractures along any one traverse divided by the length of traverse) in nonwelded Unit 4l [~ 20 fractures per 30 m (100 ft)] is significantly lower than in the other units (compare traverses 1 and 2 with traverses 6, 7, and 8; Table 2). Fracture density within Units 3 and 3T [up to about 40 fractures per 30 m (100 ft)] is higher than in Unit 4l. There is a modest increase in fracture density from east to west across MDA P, shown by traverses 3, 4, and 5; traverse 3, the most easterly, has the lowest value, whereas traverse 5, the most westerly, has the highest value. The highest densities were encountered in a zone of abundant fractures in the western third of MDA P. In this zone, exemplified by traverse 8, we measured 40 fractures per 30 m (100 ft).

Apertures (Fig. 13) follow a pattern similar to fracture densities; there are more large aperture fractures in the welded Units 3 and 3T than in the non-

welded Unit 4l (Figs. 13 and 14). Apertures in Unit 4l are generally 1 to 2 mm but locally reach values of about 50 mm. Apertures in Units 3 and 3T are as high as 100 mm. Fracture apertures are bimodal in all units; frequency distribution plots show a large peak at 0 to 5 mm and a smaller one, in all units, at 10 to 15 mm (Fig. 13). The mean aperture for the entire fracture set is 7 ± 10 mm; the large standard deviation is due to a small number of fractures with apertures up to 100 mm (Appendix B, Table B-1).

No consistent, statistically defensible east-to-west spatial variation in aperture is apparent from the fracture set as a whole. Frequency distribution plots of aperture versus easting or northing for all fractures reveal no notable trends due to the discontinuous nature of the sampling along traverses as opposed to uniform coverage of the rock mass. Examination of the outcrop, however, indicates a trend towards higher fracture apertures in western parts of MDA P compared to eastern parts; where traverses 5, 6, and 8 intersect, there is a concentration of fractures of large aperture filled with horizontally stratified sediment. This concentration corresponds to an area of MDA P where there is a mappable, ~ 12-m (40-ft) long, north-northwest-striking fault with a small component of strike slip and a north-trending graben with a small component of dip slip that can be traced about 120 m (400 ft). This spatial association of a fault, a graben, elevated fracture density, and fractures of large aperture appears to mark a north-northwesterly axis of a zone of diffuse deformation.

About 50 of the measured fractures (10% of all measured fractures) at MDA P are filled with brecciated tuff and/or cataclasite (foliated fault material produced by mechanical crushing of host rock and rotation of component grains). Approximately twenty-five of the fractures with cataclasite and/or breccia are in Unit 4l; in some cases cataclasite and breccia are both present. The foliated faults, all but two of which are in Unit 4l, have a preferred orientation of N14W ± 31°.

Table 2. Fracture Density Along MDA P Traverses

Traverse Number	Qbt Unit	Orientation of Traverse	Fracture Density (fractures/30 m)
1	4l	N78E	21
2	4l	N77E	19
3	4l, 3T	N14W	17
4	4l, 3T, 3	N20W	19
5	4l, 3T, 3	N12W	27
6	3T, 3	N76E	31
7	3	N78E	30
8	3	N80E	40

4. Faults and folds in the easternmost part of the study area

Only a few faults of small offset were identified east of the TA-9 graben. One northeast-striking fault in a tributary of Twomile Canyon has 2.4 m (8 ft) down-to-the-west apparent dip slip on the Unit 3/4 contact, which has prominent surge deposits in the contact (F11, Plate 1). We could identify no structures associated with a nearby aerial photo linear noted by Gardner et al. (1999; Plate 1).

Several small faults displace prominent surge deposits in the Unit 3/4 contact 60 cm (2 ft) or less at Twomile Mesa (F12, Plate 1). However, Reneau et al. (1995) surveyed this contact and identified more faults than we were able to map using traditional field mapping techniques.

Within the study area east of MDA P, the dip on the upper surface of Unit 3 increases eastward from < 1° to about 2°. From available data, it is not clear whether this change in dip, apparent on the Unit 3 structure contour map (Fig. 9b) and the Cañon de Valle profile (Fig. 8b), results from deposition on an uneven surface or post-depositional tectonic folding.

V. DISCUSSION

A. Tshirege Member Stratigraphic Units

A number of other workers have also subdivided the Tshirege Member of the Bandelier Tuff in or near our study area into map units or into petrologic units based on detailed petrographic, microprobe, and geochemical studies of samples from measured sections and boreholes (Reneau et al. 1995; Rogers 1995; Broxton et al. 1996, 2002; Warren et al. 1997; LANL ER Project 1998; Gardner et al. 1999, 2001). Most of our Tshirege Member units correlate well with the map units of Rogers (1995) in the study area: her Unit D corresponds to our Unit 3, although there are some differences in actual placement of contacts. Rogers' Unit E combines our Units 3T and 4. Within our study area, Rogers' Unit F corresponds with the upper part of our Unit 4 [clot-rich welded caprock Unit 4u(w)]. However, she carries Unit F well to the north of where our mapping shows it pinches out; we found none of this unit north of Pajarito Canyon.

Some descriptions of Unit 3T and Unit 4 are not entirely consistent with our usage (Warren et al. 1997; LANL ER Project 1998; see discussion in Gardner et al. 2001). We emphasize, however, that our usage of these units is petrographically and chemically consistent over the areas mapped in this study and by Gardner et al. (1999, 2001).

As discussed in Gardner et al. (2001), we define Unit 3T based on its welding characteristics and its phenocryst population. Where Units 3 and 3T are both densely welded, characteristics of the phenocryst and lithic populations combined with major- and trace-element geochemistry provide useful criteria for pinpointing the contact. A study done prior to restoration of MDA P identified a

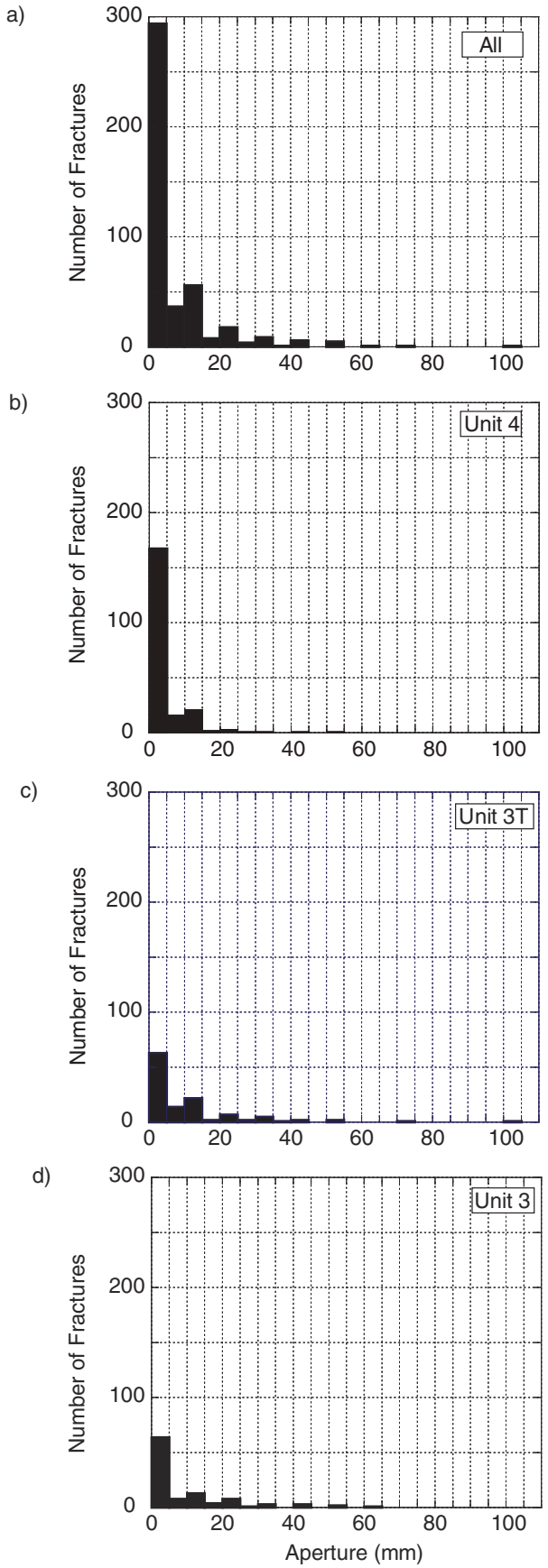

Figure 13. Fracture Aperture Distributions. The histograms show the frequency distributions of apertures taken from measured fractures at MDA P.

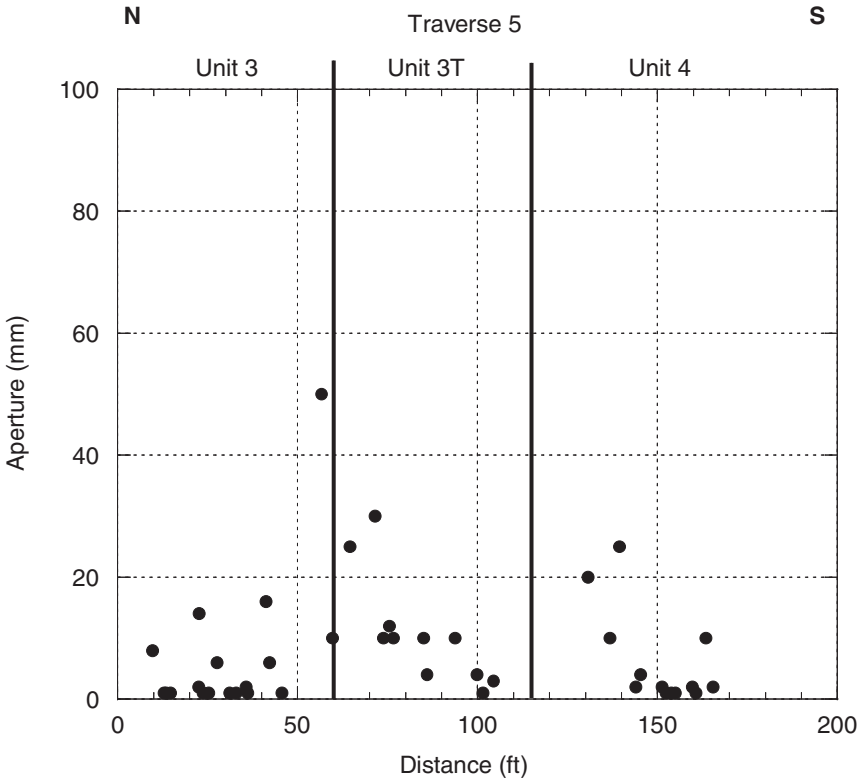

Figure 14. Apertures along Traverse 5. The plot shows the variation in aperture among units of the Bandelier Tuff at MDA P. Data from traverse 5 are shown.

thick section of Unit 3 with no Unit 3T broken out (Broxton et al. 1996). Unit 3T had not been defined, however, at the time that the preliminary MDA P study was done. In well R-25, due west of MDA P, a 21-m (70-ft) thick section of Unit 3T was identified (Broxton et al. 2002). However, based on re-examination of core and cuttings from the R-25 well, we place the contact between Units 3 and 3T shallower in well R-25 [a depth of 36.6 ± 0.6 m (120 ± 2 ft)], making Unit 3 thicker [~ 33.8 m (111 ft)] and Unit 3T thinner [~ 11 m (35 ft)] than previously determined. The revised thickness of Unit 3T is more consistent with mapped thicknesses and thickness trends in Cañon de Valle.

Mapping of the area between TA-3 (Gardner et al. 1999) and TA-16 (Gardner et al. 2001) allows a more definitive interpretation than was possible in either of these previous reports of the stratigraphic relations among the various units near the top of the Tshirege Member. The basal nonwelded ignimbrites of Unit 4l in the study area are the same as Unit 4 of Gardner et al. (1999) in the TA-3 area. The physical and geochemical characteristics of these units, as well as their continuity with Unit 4 of Gardner et al. (1999) in the northern part of the study area (Plate 1), make them unequivocally the same unit. The poorly to densely welded ignimbrites with conspicuous crystal clots [our Units 4u(npw) and 4u(w) and the Unit 4 with conspicuous crystal clots of Gardner et al. (2001)] clearly overlie the phenocryst-poor Unit 4 characteristic of TA-3 (our Unit 4l). The clot-rich Units 4u(npw) and 4u(w) can be traced, in nearly continuous exposure, from Water Canyon to Cañon de Valle, where they overlie Unit 4l.

The uppermost part of the Unit 4 sequence in this study area, our Unit 4u(w), is the same as Unit 5 of Warren et al. (1997) and, at least in part, Unit F of Rogers (1995). Unit 5 was defined informally by Warren et al. (1997) as the caprock above a prominent surge near the top of Unit 4 of Broxton and Reneau (1995). The non- to partially welded, clot-rich Unit 4u(npw) and the densely welded Unit 4u(w) are indistinguishable based on available major- and trace-element geochemistry (Fig. 7). In addition, both units bear conspicuous crystal clots. On some of the mesa tops, a nonwelded, clot-rich unit overlies the caprock (e.g., the mesa where well R-25 was drilled). We interpret this sequence as a cooling unit, with a nonwelded base, densely welded central portion, and a nonwelded top. We therefore map these three zones as one unit, Unit 4u (Plate 1).

After viewing the cores from boreholes at the building TA-16-260 outfall area (LANL ER Project 1998), we revise the stratigraphy somewhat in accordance with our field mapping results. Cores from four boreholes were examined: 2665, 2667, 2668, and 2669 (Plate 1; Table 3). Generally, we moved the upper contact of Unit 3T upwards because we have not been able to reliably distinguish densely welded Unit 4T of Warren et al. (1997) from densely welded Unit 3T (see discussion in Gardner et al. 2001). We place the top of Unit 3T at the top of densely welded tuff in this part of the core, corresponding to the top of Unit 4T of LANL ER Project (1998). Generally, we place the Unit 3/3T contact at the same depth as LANL ER Project (1998) or < 3 m (10 ft) shallower. The thickness of Unit 3T in the boreholes therefore ranges from 11 to 16 m (37 to 54 ft) (37 ft, BH 2665; 54 ft, BH 2667; 52 ft, BH 2668; 46 ft, BH 2669). We were able to distinguish Units 4l and 4u in all boreholes; this division was not made by LANL ER Project (1998). The thickness of Unit 4l varies from around 5 to 22 m (14 to 70 ft) (70 ft, BH 2665; 43 ft, BH 2667; 14 ft, BH 2668; 16 ft, BH 2669). In addition, we recognized Unit 4u(w) in all four boreholes. However, Unit 4u(npw) is present in only two boreholes (2668 and 2669), where it is < 4.3 m (14 ft) thick (0 ft, BH 2665; 0 ft, BH 2667; 4 ft, BH 2668; 14 ft, BH 2669). Unit 4u(w) is up to 14 m (44 ft) thick in the building TA-16-260 boreholes (1 ft, BH 2665; 15 ft, BH 2667; 44 ft, BH 2668; 26 ft, BH 2669). In boreholes 2665 and 2667, Unit 4u(w) directly overlies the nonwelded Unit 4l with no intervening Unit 4u(npw). An additional pyroclastic flow unit and surge are also present in the building TA-16-260 outfall area, as seen in nearby Cañon de Valle. This unit is ~ 5.6 m (18 ft) thick in borehole 2668 and partially to moderately welded.

Despite complexities of the upper Tshirege Member stratigraphy, we have been able to apply an internally consistent tuff stratigraphy over the map area. Most mapped contacts have been walked in their entirety and, together with more local stratigraphic markers, have provided a strong basis for interpretations of geologic structures, their spatial relations, and the style of deformation.

B. Surficial Geologic Units

Units Qoal and Qf both represent post-Bandelier alluvial fan deposits, but a distinction can be made, as we do here, based on lithologic and stratigraphic evidence as to whether the deposits predate or postdate initial Pleistocene incision of drainages on this part of the Pajarito Plateau. Unit Qoal, deposited by streams that emanated from the Sierra de los Valles (west of the study area), constitute remnants of once-extensive alluvial fans that predate development of the present

Table 3. Elevation of Tshirege Member Contacts in Boreholes at Building TA-16-260 Outfall Area, Cañon de Valle* (modified from LANL ER 1998)

	BH 2665	BH 2667	BH 2668	BH 2669
	Elevation (ft)			
Ground surface	7580	7532	7556	7575
Contact (lower/upper unit)				
4u(w)/4u(nw)†	—	—	—	7559
4u(npw)/4u(w)	—	—	7508	7533
4l/4u(w)	7577	7515	—	—
4l/4u(npw)	—	—	7504	7519
3T/4l	7507	7472	7490	7503
3/3T	7470	7418	7438	7457

*"—" signifies not present.
Tshirege Member unit designations are as shown in Fig. 5. The locations of boreholes are on Plate 1.
†The nonwelded top of unit 4u is preserved in one borehole.

main canyons (e.g., Reneau 1995; Reneau et al. 1995; Reneau and McDonald 1996; Gardner et al. 2001). Gravel deposits in shallow tributary canyons that we mapped as Qoal are associated with early stages of canyon development but were originally fed by distributary channels on fans that drained the Sierra de los Valles [Reneau (1995) discusses similar deposits in the Los Alamos Canyon watershed]. We interpret gravel lag deposits mapped as Qoal as remnants of largely eroded older alluvial deposits [Reneau et al. (1995) and Longmire et al. (1996) discuss analogous lag gravels on Pajarito Mesa and on Twomile Mesa, respectively]. These gravels may vary widely in age depending on the local history of canyon development.

Whereas Qoal may be dominated by dacite clasts in a watershed that is completely underlain by Bandelier Tuff, Qf includes clasts that are representative of the modern watersheds. In addition, Qf is topographically related to the modern drainage system and typically inset below the mesa tops. Qf deposits, therefore, postdate Quaternary canyon incision. The occurrence of El Cajete pumice in some fan deposits establishes them as post-El Cajete and therefore relatively young. The steep gradient of these Qfy deposits compared to the modern stream channel is consistent with Qfy recording a period of aggradation associated with an increase in sediment yield from the upper watershed, causing a steepening of the stream channel that was followed by incision. Gentler gradients developed after a subsequent decrease in sediment supply and incision.

C. Structural Geology

1. Origin of fracturing at Material Disposal Area P

Quantitative measures of fracture orientation, fracture density, and aperture from our detailed structural analysis at MDA P differ in some significant respects from previous fracture studies on the Pajarito Plateau (Table 4). Results among fracture studies are not directly comparable in all cases due to variation in data collected and methods of data analysis.

Most fractures in the Bandelier Tuff likely originated by cooling contraction (Wohletz, in preparation), and this origin is probably the case at MDA P as well. The Bandelier Tuff was deposited as a series of hot ash flows that compacted as they cooled, producing tension fractures (Ross and Smith 1961) commonly termed cooling joints. Cooling joints in the Bandelier Tuff are generally vertical, evenly spaced cracks of short lateral extent [< 3 m (10 ft)] and sinuous strike that commonly terminate at other joints, forming irregular polygonal columns with diameters < 3 m (10 ft) (e.g., Rogers et al. 1996). These characteristics also hold at MDA P. The orientation of cooling joints depends on the orientation of principal stresses in the tuff, a combination of regional tectonic stresses and local stresses imposed by underlying topography and the processes of compaction and welding. In addition, pre-existing faults in the substrate may have played a role in formation of cooling joints, imparting stresses in the tuff that were relieved as the tuff cooled and fractured.

Previous studies in the Bandelier Tuff (Table 4) have shown that fracture strikes are widely dispersed but show, in some localities, a crude bimodal distribution that defines a conjugate system of northwesterly and northeasterly oriented fracture sets, resulting in many four-sided columns (e.g., Purtyman et al. 1995; Wohletz 1995, 1996, in preparation). The obtuse angle between these conjugate sets (~ 90–120°) may be bisected by the direction of the regional extensional stress (e.g., Aldrich et al. 1986; Walters 1996). At a few localities, fractures show a strong preferred orientation with little evidence for a conjugate set (Kolbe et al. 1994, 1995; Vaniman and Chipera 1995). The north-northwest preferred orientation for fractures at MDA P (mean for all data: N15W ± 26°) is atypical compared to average strikes at other localities on the Pajarito Plateau but not necessarily distinct within uncertainties (e.g., Kolbe et al. 1994, 1995; Vaniman

Table 4. Comparison of Results from Selected Pajarito Plateau Fracture Studies

Authors	Area	Number of Fractures	Distance (m [ft])	Qbt Unit	Preferred Orientation		Fracture Density (fractures/30 m)		Mean Aperture (mm)
					Strike	Dip	Background	Maximum	
Vaniman and Wohletz (1990)	TA-55 (Pajarito Rd) & E Jemez Rd	1,625	2,225 [7,300]	Units 2, 3	N16E & N4E	76 & 75	20	50	10
Kolbe et al. (1994)*/ Reneau et al. (1995)	TA-67 (Pajarito Mesa)	390*/ 1,417	1,340 [4,400]	Units 3, 4	N4E	85	9.4–13.9*/ 26.4–34.5	13.9*/ 34.5	20.5
Kolbe et al. (1995)*	TA-63 (Mesita del Buey)	194*	685 [2,247]	Unit 3	NNE	90	~ 8–22*	30*	15
Vaniman and Chipera (1995)	TA-67 (Pajarito Mesa)	591†	2,667 [8,750]	Unit 3	N17E ± 15 to isotropic		4†	7.5†	10
Wohletz (1995)	TA-21	1,662	2,229 [7,312]	Unit 2	N43E & N33W (all: N12E)	70–73S	20	70	8–12.5
Purtyman et al.(1995)	Near TA-3	343	165 [540]	Unit 3	N40E, N25W, N65W	70–90	~ 18		10
Wohletz (1996)	TA-2 & TA-41	1,496	1,833 [6,013]	Unit 2	N35W & N47E (all: N8E ± 48)	75–82N	20	50	7
Reneau and Vaniman (1998)	TA-54	438	~ 192 [~ 630]	Unit 2	E-W & N20E	76–77	23–30		3–5
Lewis et al. (this study)	MDA P	454	576 [1,891]	Units 3, 3T, 4	N15W ± 26		20	40	7

*Kolbe et al. (1994, 1995) measured "through-going fractures," or fractures that were logged on both walls of trenches, which biases against fractures strongly oblique to trench walls. The data for Kolbe et al. (1994) are presented above those for Reneau et al. (1995).

†Vaniman and Chipera (1995) measured "mesa-penetrating fractures," or fractures that penetrate both welded and nonwelded parts of Unit 3.

and Chipera 1995). Note that uncertainties on preferred orientations were not determined in most studies.

The polygonal pattern of joints in Unit 4l suggests that even this nonwelded tuff may have been affected by thermal fracturing. The girdle apparent in the point density plot and the short trace lengths of fractures in Unit 4l suggest that some joints propagated from the underlying densely welded Unit 3T into the nonwelded Unit 4l either during cooling of the welded tuff or by tectonic re-activation of cooling joints. The small uncertainty on the north-northwest preferred orientation of the Unit 4l fracture data and association of the fractures with a north-northwest-striking small-offset fault suggest that this direction may represent tectonic rather than thermal fracturing.

Subhorizontal fractures within densely welded Units 3 and 3T appear to be associated with compaction foliation. Unit 3T in many localities consists of a lower part distinguished by platy weathering and an upper part distinguished by a round-edged platform that forms directly beneath Unit 4 (e.g., Gardner et al. 1999). This differential weathering may correspond to slight differences in chemistry of flow units (e.g., Warren et al. 1997; Krier et al. 1998a, 1998b; Stimac et al. 1998; Gardner et al. 2001). On the Pajarito fault escarpment, Unit 3T has a well-developed platy character throughout (e.g., McCalpin 1997; Seismic Hazards Team, unpublished mapping). The platy character may result from downslope creep of the viscous tuff as it cooled and compacted. The overall eastward tapering wedge shape of Unit 3T, with the thickest and platiest sections occurring on the Pajarito escarpment, are consistent with this interpretation.

The greater abundance of fractures in Units 3 and 3T (about 50% more than in Unit 4l) suggests that many of these are cooling joints or weathering features. This outcome is consistent with previous work showing that many fractures in welded tuffs do not penetrate underlying or overlying nonwelded tuffs, imparting greater fracture densities in welded versus nonwelded tuffs (e.g., Reneau et al. 1995; Vaniman and Chipera 1995). The polygonal pattern of fractures in outcrops of Units 3 and 3T, the abundance of fracture terminations by intersection or truncation, and vapor alteration of fracture walls support this interpretation.

The average fracture spacing on the Pajarito Plateau is ~ 1.5 m, resulting in a linear density of ~ 20 fractures/30 m, but fracture densities as high as ~ 70 fractures/30 m have been measured (Wohletz, in preparation). Local maxima are in some cases associated with known faults (Vaniman and Chipera 1995). In other cases, maxima have been used to infer underlying faults (Vaniman and Wohletz 1990; Wohletz 1995, 1996). At TA-67, however, relatively low values of fracture density have been measured near faults, and higher than average values where no faults were identified (Kolbe et al. 1994). Fracture densities at MDA P are similar to other areas (generally ~ 20 fractures/30 m with a local maximum of 40 fractures/30 m). The highest fracture density at MDA P was within a densely welded part of Unit 3.

Mean fracture apertures across the Pajarito Plateau typically range from 7 to 10 mm (Table 4). The highest measured mean apertures are from studies in which only steeply dipping (> 45°) "throughgoing fractures" (fractures identified in both walls of trenches) were measured (Kolbe et al. 1994, 1995). Other investigators have suggested that cooling joints may attain larger apertures if they undergo further opening during tectonism (Walters and Aldrich 1997). Apertures up to 100 mm in Units 3 and 3T at MDA P may indicate post-cooling extension in this area and further opening of pre-existing fractures. However, the data from MDA P and other areas are inconclusive in this regard (e.g., Kolbe et al. 1994; Vaniman and Chipera 1995). Nevertheless, Wohletz (1996) assumed that apertures of fractures at TA-2 and TA-41 developed by vertical displacement along initially closed cooling joints; he calculated a cumulative 3-m down-to-the-west displacement

accommodated by fractures across an inferred Guaje Mountain fault zone. A fractured, welded tuff can conceal several meters of fault displacement over a wide area by accommodating small amounts of strain in a multitude of fractures (Wohletz, in preparation).

We know of no infallible method for distinguishing tectonic fractures from cooling fractures, aside from measurable stratigraphic offset or identification of cataclastic foliation in fracture filling. Cataclasite forms in nonwelded tuffs by grain size reduction, particulate flow, and pore collapse during faulting (Wilson et al. 2001). Fracture filling varies considerably across the Pajarito Plateau. In Unit 2 at TA-21, fracture filling is sparse to absent (Wohletz 1995). Fractures at Pajarito Mesa in Unit 3 are commonly filled with clay, minor gypsum and halite, and tuff breccia (Vaniman and Chipera 1995). Kolbe et al. (1995) recognized slickensides in a few fractures (generally horizontal) in Unit 3 at TA-63 but concluded that they may be due to gravitational slip toward drainages that bound the site. In the TA-67 trenches, Kolbe et al. (1994) found no evidence of gouge, shear fabric, slickensides, or other evidence of faulting along fracture walls in Units 3 and 4. By contrast, we observed numerous examples of slickensides and cataclastic foliation in fractures in nonwelded Unit 4l at MDA P (Appendix B, Table B-1).

Our mapping, however, showed no major faults to the north or south of MDA P, more or less on strike with the preferred orientation of the fractures and small displacement faults. Nevertheless, there is evidence for faulting at MDA P, including five surveyed small-displacement faults (Appendix C, Table C-2) and foliated cataclasite observed in some faults in Unit 4l. We lack stratigraphic markers for estimating displacement on these faults, but displacement is likely to be small because fault traces are on average about 5 m (16 ft) long. Locally high fracture densities at MDA P (40 fractures/30 m) suggest an association with a fault that is not well expressed within Tshirege Member units, as interpreted by Wohletz (1996, in preparation) near the southern end of mapped traces of the Guaje Mountain and Rendija Canyon faults. Along our traverses 1, 2, and 6, we calculate cumulative extension in an east-west direction of 0.4 m, 0.3 m, and 1.1 m, respectively (Appendix B, Table B-1). Thus, a small amount of horizontal extension, over possible deep-seated normal faults, may be accommodated by the fractures at MDA P.

Even so, differential compaction of a tuff may result in small faults, keystone-like grabens, and rotated blocks that resemble folds (Wohletz, in preparation). Some fracture studies on the Pajarito Plateau show a population of north-northwesterly or east-west striking fractures that parallel the modern canyons (e.g., Purtyman et al. 1995; Rogers et al. 1996; Reneau and Vaniman 1998), which may, in some cases, parallel paleocanyons in the substrate. LANL ER Project (1998) identified thickness variations, lateral facies changes, and within-unit elevation differences along Cañon de Valle consistent with differential compaction along the west-to-east course of the canyon. For fracturing observed at MDA P (N15W preferred orientation) to be associated with differential compaction, paleotopography would have had a north-northwesterly trend, strongly oblique to Cañon de Valle and Pajarito Canyon.

The change in dip in Unit 3 identified east of MDA P (Figs. 8b and 9b) coincides roughly with the eastward pinch-out of Units 3T and 4u (Plate 1; Cross-section A-A', Plate 2), suggesting down-to-the-west faulting prior to deposition of Unit 3, which may have influenced the topography on the Unit 3 surface, the distribution of Units 3T and 4, and perhaps the distributed deformation represented by fracturing at MDA P and faulting along the TA-9 graben.

Significantly, the bounding faults of the TA-9 graben (G2) displace Qoal (probably in part 1.13 Ma), indicating tectonic displacements after cooling of the tuff. We conclude that fractures at MDA P result from a combination of thermal contraction and tectonics. Faulting and associat-

ed fracturing at MDA P likely represent distributed deformation associated with the Pajarito fault and may be associated with deep-seated, down-to-the-west normal faulting antithetic to the dominantly down-to-the east displacement on the Pajarito fault. Differential compaction over pre-Bandelier Tuff topography does not appear to play a major role.

2. Structural setting of the study area

We have identified four sets of structures in the area between TA-3 and TA-16 and east of the Pajarito fault zone: a) north-striking faults (F2, F3, F4, F5) defining a graben (G2) in the central part of the study area; b) north-northwest-striking fractures and rare faults (at MDA P) that bound the eastern side of the principal zone of deformation within the study area and may be the surface expression of a subsurface fault or faults; c) rare northeast-striking structures near the northern limit of the area associated with the southern end of the Rendija Canyon fault (F11 and nearby photo linear); and d) several small east-west-striking faults (northwest of building TA-16-260; southwest of MDA P).

The structures in the western half of the study area at Cañon de Valle and Pajarito Canyon accommodate most of the structural deformation that we document east of the main escarpment. We estimate net down-to-the-west throw on Bandelier Tuff to be more than 6 m (20 ft) in the western half of the map area at Cañon de Valle. This estimate must be used with caution, however, due to extensive post-Bandelier deposits in the western quarter of this swath; these deposits may conceal faults or folds of significant displacement. Furthermore, this estimate could be low if the change in dip observed east of MDA P on the top of Unit 3 represents monoclinal folding rather than draping of pre-Unit 3 topography. Farther north, along Pajarito Canyon, the zone of greatest deformation east of the main escarpment also occupies the western half of the study area. East of the Anchor Ranch Road monocline M1, we estimate 3 m (10 ft) of net down-to-the-east throw on Bandelier Tuff and ~ 5 m (16 ft) down-to-the-east throw on the base of Qoal. Monocline M1 and faults west of Anchor Ranch Road account for additional displacement, perhaps as much as 15 m (45 ft) of net down-to-the-east throw on Qbt and the base of Qoal; this amount would be less if the monocline M1 is partly due to the eastward-tapering wedge shape of Unit 3T. However, the higher-than-usual dip of the base of Qoal on the flank of the monocline suggests significant tectonic folding. Down-to-the-east deformation in the northwestern part of the study area is likely associated with evolution of the Pajarito fault zone as a faulted monocline.

Within the Pajarito fault zone, monoclinal folds associated with normal faulting are common (e.g., McCalpin 1997; Gardner et al. 1999, 2001). Analog modeling and field studies show that extensional fault-propagation folds form above steeply dipping normal faults (e.g., Hardy and McClay 1999; Withjack and Callaway 2000; Willsey et al. 2002). Especially where a distinct mechanical contrast exists between basement and cover, discrete normal faulting at depth may be linked to distributed deformation, including folding, at higher levels. Slow displacement rates and thin, strong strata overlying active normal faults favor development of broad monoclines (Withjack and Callaway 2000). Continued displacement can cause propagation of the fault into the cover, resulting in a faulted monocline (M1, for example).

Structures near MDA P, including discontinuous small-displacement faults and fractures, are not clearly associated with any major fault at the surface but may be the surficial expression of deeper-seated normal faulting. Hanging-wall synclines and footwall anticlines adjacent to fault planes, as observed in Cañon de Valle in graben G2, are common in extensional zones and generally indicate breaching of a monocline rather than drag folding (Hardy and McClay 1999).

In general, the structural setting of the study area appears similar in many respects to the setting of

TA-3 to the north (Gardner et al. 1999) and TA-16 to the south (Gardner et al. 2001). At all three locations, a relatively narrow but discontinuous graben lies at the base of and parallel to the main escarpment of the Pajarito fault. Structure to the east of the narrow graben in both TA-3 and TA-16 is dominated by north-northeast and northeast-striking normal faults and monoclines, all of which show significant net down-to-the-west displacements on Bandelier Tuff. At TA-3, the north-northeast and northeast-striking structures are caused by convergence of the Rendija Canyon and Pajarito fault zones, forming the southern end of the 3,650-m (12,000-ft) wide Diamond Drive graben (Gardner et al. 1999) and giving rise to distributed faulting between Los Alamos Canyon and Twomile Canyon. At TA-16, north-northeast-striking open fissure networks are associated with the tensional upper hinge zones of monoclines (Gardner et al. 2001) or with open framework fissure-fill breccias developed at fault surfaces (Wong et al. 1995; McCalpin 1997, 1998; Gardner et al. 1998b, 2001). In the vicinity of TA-16, deformation associated with the Pajarito fault extends at least 1,500 m (5,000 ft) to the east of the Pajarito fault escarpment (Gardner et al. 2001). The dominantly down-to-the-west deformation in that area may be due to accomodation of the eastern, hanging-wall block of the Pajarito fault to either lateral changes in strike or vertical changes in dip of the Pajarito fault. Faulting and fracturing between TA-3 and TA-16 is dominated by north-northeast to north-northwest-striking faults and associated folds with small amounts of down-to-the-east and down-to-the-west displacement. Similar to the TA-16 area, deformation in the present study area extends at least 1,500 m (5,000 ft) to the east of the Pajarito fault escarpment. This deformation appears to be associated with the Pajarito fault and may be caused also by vertical changes in its dip resulting in deep-seated, down-to-the-west normal faulting antithetic to the Pajarito fault.

3. Comparison of structure to previous studies

Rogers (1995) recognized many of the larger structures that we have mapped, but we differ in placement and interpretation of the style of deformation. Rogers (1995) recognized the western bounding fault (F4, Plate 1) of the graben near building TA-16-260 (G2, Plate 1) but inferred the opposite sense of displacement on the fault. She recognized part of the eastern bounding fault where it crosses Pajarito Canyon (F3, Plate 1) with the same sense of displacement we observed. However, Rogers (1995) depicts the connections among these faults quite differently than we do. She further infers a syncline, which we have confirmed with field data, more or less along the axis of the TA-9 graben. She recognized a north-trending, west-dipping monocline crossing Cañon de Valle west of MDA P, but we interpret the horizontal or gentle west dips in the tuffs here to result from down-to-the-west faulting at the east side of graben G2.

Rogers (1995) indicates a north-striking, down-to-the-east fault in the northwestern part of the study area, paralleling Anchor Ranch Road and then cutting directly east of building TA-8-23 (Plate 1). We agree that placing a down-to-the-east normal fault at the surface there is tempting, but the geology does not require it. The Unit 3T/4 contact is folded and climbing steeply westwards there and gives the illusion of down-to-the-east fault offset. Confirmation of folding here comes from the steeper-than-usual dip of the base of Qoal (Fig. 8a).

Rogers (1995) also shows a west-striking fault in the mesa north of Cañon de Valle. We mapped a short segment of a west-striking fault about 610 m (2,000 ft) northwest of building TA-16-260, but we were not able to trace this fault nearly as far west or east as Rogers depicts it. Numerous west-striking faults appear on the Rogers (1995) map in our study area for which we have found no evidence. However, west-southwest of MDA P we identified short segments of west-striking faults that were not mapped by Rogers. West-striking faults are clearly present on the Pajarito Plateau, but they are much less numerous than north-striking faults and play a less important, or less obvious role, in the structural evolution of the area.

Budding and Purtymun (1976) show the "Water Canyon fault" skirting the east side of MDA P. The trace of the fault on their map appears to run from the topographic step at the east end of Campground Mesa (Gardner et al. 2001) and along an aerial photographic linear that Gardner and House (1987) show on their maps. Our mapping revealed no major fault displacements in the Bandelier Tuff contacts between MDA P and the limit of our mapping more than 450 m (1,500 ft) east of MDA P. A major structure on the maps of Rogers (1995) is her "Water Canyon Arch." Gardner et al. (2001) chose not to show this feature in TA-16 because Bandelier Tuff contacts appear to form an arch where an east-southeast-striking fault zone displaces tuff contacts down to the north. Near MDA P, the position of the "Water Canyon Arch" may, in fact, mark a prominent topographic step located at the eastern pinch-out of Unit 4u. The step also corresponds to the pinch-out of Unit 3T. We agree with Gardner et al. (2001) that the topographic step and linear are erosional features formed near the edge of a flow lobe in Unit 4 and not a fault as interpreted by previous workers (Budding and Purtyman 1976). We further propose that lateral stratigraphic changes in the Tshirege Member that give rise to the step and linear may be controlled by deep-seated structure, perhaps down-to-the-west faulting in the underlying Otowi Member. Sufficient time elapsed between deposition of the Otowi Member at 1.61 Ma and the Tshirege Member at 1.22 Ma for deformation to have occurred. The distribution of Units 3T and 4u, especially their eastward pinch-outs, may be fault controlled. We recommend that the terms "Water Canyon fault" and "Water Canyon Arch" be abandoned since they have not been observed either in Water Canyon or in the present study area.

Evidence for a broad north-south-trending graben in the subsurface beneath the study area is sparse but intriguing. Geologic mapping constrains the southerly termination of the Diamond Drive graben, bounded by the Pajarito fault and the Rendija Canyon fault, to lie more or less at TA-3 and the Los Alamos County landfill. However, gravity data (Biehler et al. 1991), fracture data (Wohletz 1996, in preparation), and fault and fracture data (Kolbe et al. 1994; Reneau et al. 1995) suggest possible southwards, subsurface continuations of the down-to-the-west Rendija Canyon and Guaje Mountain faults in the subsurface, although they are not expressed as major faults in Bandelier Tuff (e.g., Gardner et al. 1999). Thickness variations in the Cerro Toledo interval in the general vicinity of the study area are suggestive of faulting after deposition of the Otowi Member. The Cerro Toledo interval is ~ 27.5 m (75 ft) thick in well SHB-3 at TA-16 (Gardner et al. 1993), ~ 36.5 m (120 ft) thick in well R-25 at TA-16 (R-25, LANL ER Project 1998), ~ 42 m (137 ft) thick at TA-55 (Fig. 2; Gardner et al. 1993), and only ~ 15.3 m (50 ft) thick in well R-37-2 [located about 900 m (3,000 ft) southeast of the southeastern corner of the present study area] (LANL ER Project, unpublished data). The greater thickness of the Cerro Toledo interval at well R-25 and TA-55 may indicate down-to-the-west faulting beneath the present study area, which may have influenced the distribution and thickness of Tshirege Member units.

Previous investigators have interpreted a subsurface graben beneath the Pajarito Plateau, but in most cases, its inferred location lies to the east of the study area. Budding (1978) identified a prominent gravity low about 3 km (1.9 mi) east of the city of Los Alamos and interpreted a north-northeast-trending graben in the subsurface that ranges from about 5 km (3.1 mi) wide north of the study area to about 7 km (4.4 mi) wide at Water Canyon. He interpreted the graben as partly syn-depositional and partly post-depositional with the Santa Fe Group, which he modeled as up to 2 km (1.3 mi) thick in the graben. Estimated stratigraphic separation on the bounding normal faults totals more than 2 km in the north, diminishing somewhat to the south. In the vicinity of the study area, the western bounding fault of the graben would be located some 3 km (1.9 mi) east of the Pajarito fault with the eastern bounding fault about 8 km (5 mi) east

of the fault. Electromagnetic sounding surveys also defined a northeast-trending trough beneath the Pajarito Plateau (Williston, McNeil, and Associates 1979). Cordell (1979), as well, interpreted from regional gravity data a northeast-trending graben in about the same position, which he suggested is the southern continuation of the Velarde graben. Modeling of gravity profiles by Williams (1979) identified no graben structure, consistent with seismic reflection lines across the same area. She interpreted the gravity gradient as resulting from a density contrast between the Tschicoma Formation and the Bandelier Tuff and Puye Formation rather than the result of a large fault offset.

Subsequent work by Biehler et al. (1991) demonstrated a pronounced Bouguer gravity anomaly directly east of the Pajarito fault. The deepest part of the anomaly lies due south of the mapped traces of the Rendija Canyon and Guaje Mountain faults and about 5 to 6 km (3–4 mi) east of the Pajarito fault. Thickness variations in Puye Formation beneath the LANL site are consistent with a pre-Bandelier Tuff graben (Vaniman et al., in preparation). The eastern edge of the graben is not well delineated but likely lies well east of the study area. These relations, combined with our results implying structural control of depositional patterns in the Tshirege Member, suggest that further investigation of a possible graben in the subsurface is warranted.

4. Ages of faulting and related deformation

Bounds on the timing of the structural deformation in the study area are not particularly robust. All structures are Quaternary in age in that they postdate the Tshirege Member (1.22 Ma) of the Bandelier Tuff. For many faults (F2, F3, F4, F6, F8, and F9), the only other unit that is clearly faulted or deformed is Qoal, which is probably in part ~ 1.13 million years old. The western bounding fault of the TA-9 graben (F4) apparently cuts Qfo. A small fault (F7) that is part of a series of aligned north-northeast-striking faults apparently cuts Qfi. This fault is aligned with fault F10, which experienced mid- to late-Pleistocene rupture and possible Holocene fissuring (McCalpin 1998). The youngest-known faulting in the study area occurred on fault F1, recently trenched at the site of a new LANL Emergency Operations Center. The most recent paleoseismic event on F1 occurred in Holocene time (Reneau et al. 2002).

The Rendija Canyon fault appears to die out near the northern limit of the study area (Gardner et al. 1999). Paleoseismic trenching of the Rendija Canyon fault about 5 km (3.1 mi) northeast of the study area showed that the most recent earthquake occurred at about 9 or 23 ka (Wong et al. 1995; Kelson et al. 1996). No studies to date have definitively identified a southward continuation of the Rendija Canyon fault south of Twomile Canyon. To the east of the study area, in trenches at Pajarito Mesa, no offset of the buried soil beneath the El Cajete pumice was observed, indicating no faulting for the last 50 to 60 thousand years (Reneau et al. 1995). Therefore, young surface rupture documented on the Rendija Canyon fault terminated north of Pajarito Mesa. Alternatively, displacement was transferred to other faults either east or west of Pajarito Mesa.

To the south of the study area, evidence on the timing of deformation is provided by four structures at TA-16 that are subsidiary to the Pajarito fault (Gardner et al. 2001). A fissured lineament, “fis 1” of Gardner et al. (2001), which projects toward the fault F4 of this study, deforms not only the Tshirege Member of the Bandelier Tuff but possibly also Qoal, which is probably in part about 1.13 million years old. Fault F2 of Gardner et al. (2001) is a down-to-the-west fault that parallels Anchor Ranch Road and projects towards the present study area. This fault appears to truncate deposits of the 50- to 60-thousand-year-old El Cajete pumice (Qec), but field relations are equivocal. Fault F9 of Gardner et al. (2001), which parallels West Jemez Road, appears to truncate an alluvial fan unit, Qfi, but again, field relations are equivocal. Radiocarbon dates from a

borehole at TA-16 led Gardner et al. (2001) to interpret a seismic event on a fissure (their "fis 2") sometime prior to 8.7 to 9.2 cal ka and at least one additional, younger paleoseismic event whose age is not well constrained.

The occurrence of Holocene paleoseismic events on fault F1 (Plate 1), fis 2 of Gardner et al. (2001), and possibly the northward continuation of F10 (Plate 2) suggests that there may well be more structures in the study area that have experienced Holocene events, although we either lack the stratigraphic record or the exposure to demonstrate it. Prevalent fill and disturbed surficial geologic units would require trenching to determine the presence or absence of faults in the western part of the study area, particularly in TA-8, TA-69, and the western half of TA-9.

D. Recommendations

Based on the results of this study, we recommend that the south slope of Pajarito Canyon directly east of building TA-8-21 at fault F7 (Plate 1) be considered as a possible trench site. The identification of faults that may cut post-Bandelier fan units in this area suggests a more or less continuous fault system, at least in the subsurface, that may connect to the north with fault F10, which has undergone 1.5 m (5 ft) down-to-the-east separation on Qbt with possible Holocene rupture (McCalpin 1998). The best potential site for trenching, however, is the site of a gas pipeline installed some years ago.

We also recommend drilling in the area of TA-8 to locate the bases of Units 3T and 3 to resolve the issue of whether steep dips at the Unit 4/3T contact are due to westwards thickening of Unit 3T or to structural deformation. Similarities or differences in trends of the Unit 3/3T contact would bear on this question. In addition, locating the Unit 3/3T contact would give us better control on the dip separation across the Pajarito fault. In this area as well, drilling could determine the thickness of fan units, identifying the depth of the graben at the base of the Pajarito fault. We recommend this action because it is key to understanding the structural setting of the western part of LANL, which would directly aid future seismic hazard evaluations.

The study area clearly lies within the Pajarito fault system, albeit a part of the system that is dominated by subsidiary or distributed ruptures on the major faults. As such, this is an area of generally higher potential for seismic surface rupture, relative to locations farther removed from the Pajarito fault zone. Probabilistic analyses of surface rupture potential at TA-16 by Olig et al. (2001), however, indicate that, even in consideration of 1-in-10,000-year events, seismic surface rupture only becomes a significant hazard on the principal or main trace of the Pajarito fault.

VI. ACKNOWLEDGMENTS

This work was supported by the LANL Seismic Hazards Program under the direction of Larry Goen with funding from the Office of Infrastructure, Facilities, and Construction of the LANL Operations Directorate. We thank Scott Gibbs, Jim Holt, Carolyn Zerkle, Donna Richardson, and Craig Leasure for their support. Yolanda Frazier, from ESA-FM, and Lucille Westerholt, Ken Uher, Harvey Decker, and Cathy Smith from DX Division facilitated access to technical areas. Dave Broxton, Rick Warren, Dave Vaniman, and Ken Wohletz provided discussions and insights on issues regarding the stratigraphy of the Bandelier Tuff. We thank Ken Bostick, MDA P Closure Team Leader, for providing resources, access to the site, access to core, and field personnel. We thank Emily Kluk and Kellie Raven for geochemical analyses, LANL's Geographic Information System Laboratory for invaluable assistance with cartography and database management, Bill Carey for assistance with calculation of point elevations using the 1991 DEM, Anthony Garcia for graphic design, and Ken Wohletz for a helpful review.

VII. REFERENCES

Aldrich, M. J., Jr., Chapin, C. E., and Laughlin, A. W. 1986. Stress history and tectonic development of the Rio Grande rift, New Mexico. *Journal of Geophysical Research 91* (B6): 6199–6211.

Bailey, R. A., Smith, R. L., and Ross, C. S. 1969. Stratigraphic nomenclature of volcanic rocks in the Jemez Mountains, New Mexico. U. S. Geological Survey Bulletin 1274-P, 19 pp.

Baldridge, W. S., Dickerson, P. W., Riecker, R. E., and Zidek, J., editors. 1984. Rio Grande rift: northern New Mexico. *New Mexico Geological Society Guidebook 35*, 379 pp.

Baldridge, W. S., Keller, G. R., Haak, V., Wendlandt, E., Jiracek, G. R., and Olsen, K. H. 1995. The Rio Grande rift. In *Continental Rifts: Evolution, Structure, Tectonics*, Olsen, K. H., editor, pp. 233–275. Amsterdam, Holland: Elsevier.

Bates, R. L., and Jackson, J. A. 1980. *Glossary of Geology*. American Geological Institute, 749 pp.

Biehler, S., Ferguson, J., Baldridge, W. S., Jiracek, G. R., Aldern, J. L., Martinez, M., Fernandez, R., Romo, J., Gilpin, B., Braile, L. W., Hersey, D. R., Luyendyk, B. P., and Aiken, C. L. 1991. A geophysical model of the Española basin, Rio Grande rift, New Mexico. *Geophysics 56* (3): 340–353.

Brown, F., Purtymun, W. D., Stoker, A., and Barr, A. 1988. Site geology and hydrology of Technical Area 16, Area P. Los Alamos National Laboratory report LA-11209-MS, 8 pp.

Broxton, D. E., and Reneau, S. L. 1995. Stratigraphic nomenclature of the Bandelier Tuff for the Environmental Restoration Project at Los Alamos National Laboratory. Los Alamos National Laboratory report LA-13010-MS, 21 pp.

Broxton, D. E., Ryti, R. T., Carlson, D., Warren, R. G., Kluk, E., and Chipera, S. 1996. Natural background geochemistry of the Bandelier Tuff at MDA P, Los Alamos National Laboratory. Los Alamos National Laboratory report LA-UR-96-1151, 42 pp.

Broxton, D., Warren, R., Longmire, P., Gilkeson, R., Johnson, S., Rogers, D., Stone, W., Newman, B., Everett, M., Vaniman, D., McLin, S., Skalski, J., and Larssen, D. 2002. Characterization Well R-25 completion report. Los Alamos National Laboratory report LA-13909-MS, 77 pp. with 8 appendices.

Budding, A. J. 1978. Gravity survey of the Pajarito Plateau, Los Alamos and Santa Fe Counties, New Mexico. Los Alamos Scientific Laboratory report LA-7419-MS, 15 pp.

Budding, A. J., and Purtymun, W. D. 1976. Seismicity of the Los Alamos area based on geologic data. Los Alamos Scientific Laboratory report LA-6278-MS, 9 pp.

Carey, W. J., and Cole, G. 2002. Description of the Cerro Grande fire laser altimetry (LIDAR) data set. Los Alamos National Laboratory report LA-13892-MS, 57 pp.

Chapin, C. E., and Cather, S. M. 1994. Tectonic setting of the axial basins of the northern and central Rio Grande rift. In *Basins of the Rio Grande Rift: Structure, Stratigraphy, and Tectonic Setting*, Keller, G. R., and Cather, S. M., editors. *Geological Society of America Special Paper 291*: 5–25.

Cordell, L. 1979. Gravimetric expression of graben faulting in Santa Fe County and the Española basin, New Mexico. *New Mexico Geological Society Guidebook 30*: 59–64.

Criswell, C. W., Channell, R. A., and others. In preparation. Results of field investigation for bedrock characterization at Material Disposal Area P, Los Alamos National Laboratory, New Mexico. Los Alamos National Laboratory report.

Davis, J. C. 1986. *Statistics and Data Analysis in Geology*. New York, NY: John Wiley and Sons, 646 pp.

Deutsch, C. V., and Journel, A. G. 1998. *GSLIB Geostatistical Software Library and Users Guide*. New York, NY: Oxford University Press, 369 pp.

Dransfield, B. J., and Gardner, J. N. 1985. Subsurface geology of the Pajarito Plateau, Española basin, New Mexico. Los Alamos National Laboratory report LA-10455-MS, 15 pp.

Gardner, J. N., and Goff, F. 1984. Potassium-argon dates from the Jemez volcanic field: Implications for tectonic activity in the north-central Rio Grande rift. *New Mexico Geological Society Guidebook 35*: 75-81.

Gardner, J. N., and House, L. 1987. Seismic hazards investigations at Los Alamos National Laboratory, 1984 to 1985. Los Alamos National Laboratory report LA-11072-MS, 76 pp.

Gardner, J. N., Goff, F., Garcia, S., and Hagan, R. C. 1986. Stratigraphic relations and lithologic variations in the Jemez volcanic field, New Mexico. *Journal of Geophysical Research 91* (B2): 1763–1778.

Gardner, J. N., Baldridge, W. S., Gribble, R., Manley, K., Tanaka, K., Geissman, J. W., Gonzalez, M., and Baron, G. 1990. Results from Seismic Hazards Trench #1 (SHT-1), Los Alamos Seismic Hazards Investigations. Los Alamos National Laboratory unpublished report EES1-SH90-19, 57 pp.

Gardner, J. N., Kolbe, T., and Chang, S. 1993. Geology, drilling, and some hydrologic aspects of seismic hazards program core holes, Los Alamos National Laboratory, New Mexico. Los Alamos National Laboratory Report LA-12460-MS, 19 pp.

Gardner, J. N., Lavine, A., Vaniman, D., and WoldeGabriel, G. 1998a. High-precision geologic mapping to evaluate the potential for seismic surface rupture at TA-55, Los Alamos National Laboratory. Los Alamos National Laboratory report LA-13456-MS, 13 pp.

Gardner, J. N., Lavine, A., WoldeGabriel, G., Krier, D. J., Vaniman, D., and McCalpin, J. 1998b. Evolution of the western boundary of the Rio Grande rift, northern New Mexico. *EOS, Transactions of the American Geophysical Union 79* (45): F614.

Gardner, J. N., Lavine, A., WoldeGabriel, G., Krier, D., Vaniman, D., Caporuscio, F., Lewis, C., Reneau, P., Kluk, E., and Snow, M. J. 1999. Structural geology of the northwestern portion of Los Alamos National Laboratory, Rio Grande rift, New Mexico: Implications for seismic surface rupture potential from TA-3 to TA-55. Los Alamos National Laboratory report LA-13589-MS, 112 pp.

Gardner, J. N., Reneau, S. L., Lewis, C. J., Lavine, A., Krier, D., WoldeGabriel, G., and Guthrie, G. 2001. Geology of the Pajarito fault zone in the vicinity of S-Site (TA-16), Los Alamos National Laboratory, Rio Grande rift, New Mexico. Los Alamos National Laboratory report LA-13831-MS, 86 pp.

Golombek, M. P., McGill, G. E., and Brown, L. 1983. Tectonic and geologic evolution of the Española basin, Rio Grande rift: Structure, rate of extension, and relation to the state of stress in the western U. S. *Tectonophysics 94*: 483–507.

Griggs, R. L. 1964. Geology and ground water resources of the Los Alamos area, New Mexico. U. S. Geological Survey Water-Supply Paper 1753, 107 pp.

Hardy, S., and McClay, K. 1999. Kinematic modelling of extensional fault-propagation folding. *Journal of Structural Geology 21* (7): 695–702.

Hext, G. R. 1963. The estimation of second-order

tensors, with related tests and designs. *Biometrika 50*: 353–373.

Izett, G. A., and Obradovich, J. D. 1994. $^{40}Ar/^{39}Ar$ age constraints for the Jaramillo Normal Subchron and the Matuyama-Brunhes geomagnetic boundary. *Journal of Geophysical Research 99* (B2): 2925–2934.

Keller, G. R., editor. 1986. Special section on the Rio Grande rift. *Journal of Geophysical Research 91* (B6): 6142–6345.

Kelley, V. C. 1979. Tectonics, middle Rio Grande rift, New Mexico. In *Rio Grande Rift: Tectonics and Magmatism*, Riecker, R. E., editor, pp. 57–70. Washington, D.C.: American Geophysical Union.

Kelson, K. I., and Olig, S. S. 1995. Estimated rates of Quaternary crustal extension in the Rio Grande rift, northern New Mexico. *New Mexico Geological Society Guidebook 46*: 9–12.

Kelson, K. I., Hemphill-Haley, M. A., Olig, S. S., Simpson, G. D., Gardner, J. N., Reneau, S. L., Kolbe, T. R., Forman, S. L., and Wong, I. G. 1996. Late-Pleistocene and possibly Holocene displacement along the Rendija Canyon fault, Los Alamos County, New Mexico. *New Mexico Geological Society Guidebook 47*: 153–160.

Kolbe, T., Sawyer, J., Gorton, A., Olig, S., Simpson, D., Fenton, C., Reneau, S., Carney, J., Bott, J., and Wong, I. 1994. Evaluation of the potential for surface faulting at the proposed Mixed Waste Disposal Facility, TA-67. Unpublished consulting report prepared for Los Alamos National Laboratory by Woodward-Clyde Federal Services, Oakland, CA, 3 volumes.

Kolbe, T., Sawyer, J., Springer, J., Olig, S., Reneau, S., Hemphill-Haley, M., and Wong, I. 1995. Evaluation of the potential for surface faulting at TA-63. Unpublished consulting report prepared for Los Alamos National Laboratory by Woodward-Clyde Federal Services, Oakland, CA.

Krier, D., Caporuscio, F., Lavine, A., and Gardner, J. N. 1998a. Stratigraphy and geologic structure at the SCC and NISC building sites, Technical Area 3, Los Alamos National Laboratory. Los Alamos National Laboratory report LA-13507-MS, 23 pp.

Krier, D., Caporuscio, F., Gardner, J. N., and Lavine, A. 1998b. Stratigraphy and geologic structure at the Chemical and Metallurgy (CMR) building, Technical Area 3, Los Alamos National Laboratory. Los Alamos National Laboratory report LA-13522-MS, 32 pp.

LANL ER Project (Los Alamos National Laboratory Environmental Restoration Project). 1998. RFI Report for Potential Release Site 16-021 (c). Los Alamos National Laboratory report LA-UR-98-4101, 3 volumes.

Lavine, A., Gardner, J. N., Vaniman, D., and WoldeGabriel, G. 1997. Southward splaying and termination of the Rendija Canyon fault, Pajarito Plateau, New Mexico. *Geological Society of America Abstracts with Programs 29* (6): A-259.

Lavine, A., Gardner, J. N., Reneau, S. L., WoldeGabriel, G., Vaniman, D. T., and Carney, J. 1998. High-precision geologic mapping to evaluate the potential for seismic surface rupture at Los Alamos National Laboratory, New Mexico. *EOS, Transactions of the American Geophysical Union 79* (45): F614.

Longmire, P. A., Reneau, S. L., Watt, P. M., McFadden, L. D., Gardner, J. N., Duffy, C. J., and Ryti, R. T. 1996. Natural background geochemistry, geomorphology, and pedogenesis of selected soil profiles and Bandelier Tuff, Los Alamos, New Mexico. Los Alamos National Laboratory report LA-12913-MS, 176 pp.

Machette, M. N., Personius, S. F., Kelson, K. I., Haller, K. M., and Dart, R. L. 1998. Map and data for Quaternary faults and folds in New Mexico.

U. S. Geological Survey, open-file report 98-521, 443 pp., 1 plate, scale 1:750,000.

Manley, K. 1979. Stratigraphy and structure of the Española basin, Rio Grande rift, New Mexico. In *Rio Grande Rift: Tectonics and Magmatism*, Riecker, R. E., editor, pp. 71–86. Washington, D.C.: American Geophysical Union.

Mardia, K. V. 1972. *Statistics of Directional Data*. London: Academic Press, 357 pp.

McCalpin, J. P. 1997. Geomorphology and structure of the Pajarito fault zone west of Los Alamos National Laboratory, New Mexico. Unpublished consulting report prepared for Los Alamos National Laboratory by GEO-HAZ Consulting, Inc., Estes Park, CO, 22 pp.

McCalpin, J. P. 1998. Late Quaternary faulting on the Pajarito fault, west of Los Alamos National Laboratory, north-central New Mexico: Results from the seven-trench transect excavated in summer of 1997. Unpublished consulting report prepared for Los Alamos National Laboratory by GEO-HAZ Consulting, Inc., Estes Park, CO, 112 pp., 4 appendices.

McCalpin, J. P. 1999. Late Quaternary Faulting on the Pajarito Fault, west of Los Alamos National Laboratory, north-central New Mexico: Results from seven trenches excavated in summer of 1998. Unpublished consulting report prepared for Los Alamos National Laboratory by GEO-HAZ Consulting, Inc., Estes Park, CO, 104 pp.

McDonald, E. V., Reneau, S. L., and Gardner, J. N. 1996. Soil-forming processes on the Pajarito Plateau: Investigation of a soil chronosequence in Rendija Canyon. *New Mexico Geological Society Guidebook 47*: 367–374.

Olig, S. S., Kelson, K. I., Gardner, J. N., Reneau, S. L., and Hemphill-Haley, M. 1996. The earthquake potential of the Pajarito fault system, New Mexico. *New Mexico Geological Society Guidebook 47*: 143–151.

Olig, S., Youngs, R., and Wong, I. 2001. Probabilistic seismic hazard analysis for surface fault displacement at TA-16, Los Alamos National Laboratory. Unpublished report prepared for Los Alamos National Laboratory by URS Computing Corporation, Oakland, CA.

Phillips, W. M., McDonald, E. V., Reneau, S. L., and Poths, J. 1998. Dating soils and alluvium with cosmogenic ^{21}Ne depth profiles: Case studies from the Pajarito Plateau, New Mexico. *Earth and Planetary Science Letters 160*: 209–223.

Purtyman, W. D., Koenig, E., Morgan, T., and Sagan, E. 1995. Joint orientation and characteristics as observed in a trench excavated near TA-3 and a basement excavated at TA-55. Los Alamos National Laboratory report LA-13036-MS, 42 pp.

Reneau, S. L. 1995. Geomorphic studies at DP Mesa and vicinity. In "Earth science investigations for environmental restoration—Los Alamos National Laboratory Technical Area 21," Broxton, D. E., and Eller, P. G., editors, Los Alamos National Laboratory report LA-12934-MS, pp. 65–92.

Reneau, S. L. 2000. Stream incision and terrace development in Frijoles Canyon, Bandelier National Monument, New Mexico, and the influence of lithology and climate. *Geomorphology 32*: 171–193.

Reneau, S. L., and McDonald, E. V. 1996. Landscape history and processes on the Pajarito Plateau, northern New Mexico. "Rocky Mountain Cell, Friends of the Pleistocene Field Trip Guidebook," unpublished Los Alamos National Laboratory report LA-UR-96-3035, 195 pp.

Reneau, S. L., and Vaniman, D. T. 1998. Fracture characteristics in a disposal pit on Mesita del Buey, Los Alamos National Laboratory. Los Alamos

National Laboratory report LA-13539-MS, 21 pp.

Reneau, S. L., Kolbe, T., Simpson, D., Carney, J. S., Gardner, J. N., Olig, S. S., and Vaniman, D. T. 1995. Surficial materials and structure at Pajarito Mesa. In "Geological site characterization for the proposed Mixed Waste Disposal Facility, Los Alamos National Laboratory," Reneau, S. L., and Raymond, R., editors, Los Alamos National Laboratory report LA-13089-MS, pp. 31–69.

Reneau, S. L., McDonald, E. V., Gardner, J. N., Kolbe, T. R., Carney, J. S., Watt, P. M., and Longmire, P. A. 1996a. Erosion and deposition on the Pajarito Plateau, New Mexico, and implications for geomorphic responses to late Quaternary climatic changes. *New Mexico Geological Society Guidebook 47*: 391–397.

Reneau, S. L., Gardner, J. N., and Forman, S. L. 1996b. New evidence for the age of the youngest eruptions in the Valles caldera, New Mexico. *Geology 24*: 7–10.

Reneau, S. L., Gardner, J. N., Lavine, A., McDonald, E. V., Lewis, C., Katzman, D., WoldeGabriel, G., Krier, D., Bergfeld, D., and Heikoop, J. 2002. Paleoseismic investigation of Trench EOC-2, Pajarito fault zone, Los Alamos National Laboratory, New Mexico. Los Alamos National Laboratory report LA-13939-MS, 65 pp.

Riecker, R. E., editor. 1979. *Rio Grande Rift: Tectonics and Magmatism*. Washington, D.C.: American Geophysical Union, 438 pp.

Robin, P.-Y. F., and Jowett, E. C. 1986. Computerized density contouring and statistical evaluation of orientation data using counting circles and continuous weighting functions. *Tectonophysics 121*: 207–223.

Rogers, M. A. 1995. *Geologic Map of Los Alamos National Laboratory Reservation*. Santa Fe, NM: State of New Mexico Environment Department, scale 1:400.

Rogers, M. A., Budding, K. E., and Christie, C. V. L. 1996. Distinguishing tectonic joints from cooling joints in the Bandelier Tuff (Pleistocene), Pajarito Plateau, Los Alamos County, New Mexico. *New Mexico Geological Society Guidebook 47*: 293–301.

Ross, C. S., and Smith, R. L. 1961. Ash-flow tuffs: Their origin, geologic relations, and identification. U.S. Geological Survey Professional Paper 366, 81 pp.

Sanford, A. R., Jaksha, L. H., and Cash, D. J. 1991. Seismicity in the Rio Grande rift. In *Neotectonics of North America, Decade Map Volume 1*, Slemmons, D. B., Engdahl, E. R., Zoback, M. D., and Blackwell, D. D., editors, pp. 229–244. Boulder, CO: Geological Society of America.

Smith, R. L., Bailey, R. A., and Ross, C. S. 1970. Geologic map of the Jemez Mountains, New Mexico. U.S. Geological Survey miscellaneous investigations map I-571, scale 1:125,000.

Spell, T. L., and Harrison, T. M. 1993. $^{40}Ar/^{39}Ar$ geochronology of post-Valles caldera rhyolites, Jemez volcanic field, New Mexico. *Journal of Geophysical Research 98*: 8031–8051.

Starkey, J. 1977. The contouring of orientation data represented in spherical projection. *Canadian Journal of Earth Sciences 14*: 268–277.

Steck, L. K., Thurber, C. H., Fehler, M. C., Lutter, W. J., Roberts, P. M., Baldridge, W. S., Stafford, D. G., and Sessions, R. 1998. Crust and upper mantle P-wave velocity structure beneath Valles caldera, New Mexico: Results from the Jemez teleseismic tomography experiment. *Journal of Geophysical Research 103* (B10): 24,301–24,320.

Stimac, J. A., Broxton, D. E., Kluk, E. C., and Chipera, S. J. 1998. Preliminary stratigraphy of tuffs from borehole 49-2-700-1 at Technical Area

49. Los Alamos National Laboratory unpublished report, 21 pp.

Toyoda, S., Goff, F., Ikeda, S., and Ikeya, M. 1995. ESR dating of quartz phenocrysts in the El Cajete and Battleship Rock Members of the Valles Rhyolite, Valles caldera, New Mexico. J*ournal of Volcanology and Geothermal Research 67*: 29–40.

Vaniman, D., and Chipera, S. 1995. Mesa-penetrating fractures, fracture mineralogy, and fault traces at Pajarito Mesa. In "Geological Site Characterization for the Proposed Mixed Waste Disposal Facility," Reneau, S. L., and Raymond, R., Jr., editors, Los Alamos National Laboratory report LA-13089-MS, pp. 71–85.

Vaniman, D., and Wohletz, K. 1990. Results of geological mapping/fracture studies: TA-55 area. Los Alamos National Laboratory Seismic Hazards Program memo EES1-SH90-17, 25 pp., 3 plates, 23 figures.

Vaniman, D., Cole, G., and Broxton, D. In preparation. From drill-hole data to 3-D geologic models. In "Groundwater Annual Status Report—2001," Nylander, C., editor. Los Alamos National Laboratory report.

Walters, M. C. 1996. Fracture analysis of the Bandelier Tuff, Pajarito Plateau, north-central Rio Grande rift, New Mexico. M.S. thesis, Texas Christian University, Fort Worth, TX, 91 pp.

Walters, M. C., and Aldrich, M. J., Jr. 1997. Distinguishing cooling and tectonic joints in the Bandelier Tuff, Pajarito Plateau, north-central Rio Grande rift, New Mexico. *Geological Society of America Abstracts with Programs 29* (6): A-417.

Warren, R. G., McDonald, E. V., and Ryti, R. T. 1997. Baseline geochemistry of soil and bedrock Tshirege Member of the Bandelier Tuff. Los Alamos National Laboratory report LA-13330-MS, 69 pp.

Williams, L. M. 1979. Gravity study of the Los Alamos area, New Mexico. Los Alamos Scientific Laboratory report LA-8154-MS, 18 pp.

Williston, McNeil, and Associates. 1979. A time domain survey of the Los Alamos region, New Mexico. Los Alamos Scientific Laboratory report LA-7657-MS, 32 pp.

Willsey, S. P., Umhoefer, P. J., and Hilley, G. E. 2002. Early evolution of an extensional monocline by a propagating normal fault: 3D analysis from combined field study and numerical modeling. *Journal of Structural Geology 24* (4): 651–669.

Wilson, J. E., Goodwin, L. B., and Lewis, C. J. 2001. Petrophysical controls on fault-zone deformation in ash-flow tuffs—Deformation bands versus fractures and implications for fluid-fault interaction. *EOS, Transactions of the American Geophysical Union 82*: F1191.

Withjack, M. O., and Callaway, S. 2000. Active normal faulting beneath a salt layer: An experimental study of deformation patterns in the cover sequence. *American Association of Petroleum Geologists Bulletin 84* (5): 627–651.

Wohletz, K. H. 1995. Measurement and analysis of rock fractures in the Tshirege Member of the Bandelier Tuff along Los Alamos Canyon adjacent to Technical Area-21. In "Earth Science Investigations for Environmental Restoration—Los Alamos National Laboratory Technical Area 21," Broxton, D. E., and Eller, P. G., editors, pp. 19–32. Los Alamos National Laboratory report LA-12934-MS.

Wohletz, K. H. 1996. Fracture characterization of the Bandelier Tuff in OU-1098 (TA-2 and TA-41). Los Alamos National Laboratory report LA-13194-MS, 19 pp.

Wohletz, K. H. In preparation. Fractures in welded tuff. In *The Tuff Handbook*, Heiken, G., and Broxton, D. E., editors. *Geological Society of America Special Paper*. Los Alamos National

Laboratory report LA-UR-99-6556.

Wolff, J. A., and Gardner, J. N. 1995. Is the Valles caldera entering a new cycle of activity? *Geology 23*: 411–414.

Wong, I., Kelson, K., Olig, S., Kolbe, T., Hemphill-Haley, M., Bott, J., Green, R., Kanakari, H., Sawyer, J., Silva, W., Stark, C., Haraden, C., Fenton, C., Unruh, J., Gardner, J., Reneau, S., and House, L. 1995. Seismic hazards evaluation of the Los Alamos National Laboratory. Unpublished consulting report prepared for Los Alamos National Laboratory by Woodward-Clyde Federal Services, Oakland, CA, 3 volumes.

Woodcock, N. H. 1977. Specification of fabric shapes using an eigenvalue method. *Geological Society of American Bulletin 88*: 1231–1236.

APPENDIX A. WHOLE ROCK GEOCHEMISTRY

Table A-1. Locations of Bandelier Tuff Samples

Sample Number*	Stratigraphic Unit	Coordinates† Northing (ft)	Easting (ft)	Elevation (ft)
CDV-1	Qbt3	1764589	1615570	7336
CDV-2	Qbt3	1764702	1615684	7355
CDV-3	Qbt3	1764706	1615665	7377
CDV-4	Qbt3T	1764705	1615643	7381
CDV-5	Qbt3T	1764728	1615618	7397
CDV-6	Qbt4l	1764747	1615603	7402
CDV-7	Qbt4l	1764770	1615574	7417
CDV-8	Qbt4u	1764838	1615505	7465
CDV-9	Qbt4u	1764853	1615497	7477
CDV-10	Qbt4u	1764849	1615468	7494
MDAP-257-0.2	Qbt4?	1764163	1615576	7464
MDAP-257-9.8	Qbt4l	1764163	1615576	7454
MDAP-257-25.8	Qbt4l	1764163	1615576	7438
MDAP-257-40.2	Qbt4l	1764163	1615576	7424
MDAP-257-54.9	Qbt4l	1764163	1615576	7409
MDAP-257-55.3	Qbt3T	1764163	1615576	7409
MDAP-257-66.4	Qbt3T	1764163	1615576	7398
MDAP-257-70.1	Qbt3T	1764163	1615576	7394
MDAP-257-134.4	Qbt3	1764163	1615576	7330
MDAP-257-139.5	Qbt3	1764163	1615576	7325
MDAP-257-144.0	Qbt3	1764163	1615576	7320
MDAP-273-42.0	Qbt4	1764283	1616023	7411
MDAP-273-42.4	Qbt3T	1764283	1616023	7410
MDAP-273-49.8	Qbt3T	1764283	1616023	7403
MDAP-273-49.9	Qbt3T	1764283	1616023	7403
MDAP-273-82.1	Qbt3T	1764283	1616023	7371
MDAP-273-84.2	Qbt3T	1764283	1616023	7369
MDAP-273-96.7	Qbt3	1764283	1616023	7356
MDAP-273-117.0	Qbt3	1764283	1616023	7336

*Abbreviations as follows: CDV, Cañon de Valle; MDAP, Material Disposal Area P.

†Northing and easting coordinates for CDV were digitized from topographic maps. The elevation for CDV-10 was drawn from the DEM, and the remaining sample elevations were calculated from the measured section. The coordinates for MDA P boreholes were surveyed by the LANL ER Project, and sample elevations were measured from cores. Northing and easting coordinates are in the State Plane Coordinate System, New Mexico Central Zone, 1983 North American Datum.

Table A-2. Major and Trace Element Geochemistry of Bandelier Tuff (notes on page 55)

Sample	Major Elements (wt %)†												Trace Elements (ppm)						
Number*	SiO_2	TiO_2	Al_2O_3	Fe_2O_3T	MnO	MgO	CaO	Na_2O	K_2O	P_2O_5	LOI	Total	Zn	Rb	Sr	Y	Zr	Nb	Ba
CDV-1	75.99	0.128	12.17	1.57	0.052	BD	0.27	4.10	4.52	0.022	0.44	98.82	53.6	101.5	35.6	34.7	243.1	45.7	135.2
CDV-2	75.15	0.150	12.70	1.73	0.061	0.07	0.28	3.92	4.60	BD	0.73	98.66	52.1	97.5	45.7	31.3	254.8	47.1	231.3
CDV-3	74.56	0.151	12.94	1.72	0.056	0.07	0.26	3.99	4.66	0.027	0.64	98.43	72.3	104.7	40.3	45.1	273.6	53.2	255.5
CDV-4	74.62	0.147	12.78	1.95	0.049	BD	0.23	4.15	4.63	0.032	0.59	98.59	56.2	104.5	38.2	48.0	295.9	47.8	168.4
CDV-5	75.45	0.159	12.64	1.87	0.063	0.07	0.28	4.29	4.65	0.019	0.38	99.50	56.4	102.5	39.2	33.9	308.7	49.9	187.7
CDV-6	74.49	0.196	13.19	2.13	0.061	0.11	0.32	4.07	4.64	0.022	0.75	99.22	53.7	96.3	35.7	40.6	326.0	41.1	181.8
CDV-7	70.73	0.286	13.56	2.46	0.073	0.31	0.76	4.85	4.90	0.057	1.08	97.99	75.2	81.7	108.8	33.1	350.8	43.8	378.9
CDV-8	73.64	0.244	12.97	2.42	0.074	0.30	0.73	4.05	4.47	0.045	0.80	98.96	63.5	80.4	89.8	55.6	325.4	40.7	379.5
CDV-9	72.96	0.242	12.96	2.32	0.087	0.27	0.69	3.79	4.76	0.117	1.82	98.19	64.2	83.3	74.6	54.7	344.4	46.2	311.4
CDV-10	72.78	0.235	14.08	1.71	0.016	BD	0.33	4.75	4.84	0.053	0.48	98.80	25.3	78.5	90.6	22.0	361.7	34.2	467.3
MDAP-257-0.2	70.62	0.252	13.59	3.36	0.021	0.34	0.78	4.04	4.48	0.056	1.22	97.55	42.0	77.3	99.2	49.6	29.01	50.8	416.9
MDAP-257-9.8	72.04	0.288	13.58	2.46	0.077	0.26	0.81	4.64	4.56	0.053	0.45	98.77	71.7	80.6	96.2	27.3	353.0	33.0	466.7
MDAP-257-25.8	71.05	0.345	13.67	2.73	0.088	0.35	0.94	4.67	4.50	0.069	0.39	98.41	73.4	79.3	120.8	30.0	404.6	28.6	489.6
MDAP-257-40.2	70.05	0.370	14.26	2.86	0.091	0.37	1.17	4.87	4.41	0.086	0.41	98.54	63.8	73.7	144.8	41.1	384.8	35.3	600.8
MDAP-257-54.9	71.77	0.354	13.69	2.75	0.093	0.33	1.03	4.64	4.26	0.073	0.52	99.01	84.6	81.8	127.7	32.7	395.8	45.3	566.1
MDAP-257-55.3	75.38	0.150	12.41	1.70	0.060	0.06	0.33	4.34	4.61	0.013	0.15	99.05	58.5	102.7	37.8	34.4	277.3	43.1	236.7
MDAP-257-66.4	75.11	0.153	12.50	1.78	0.063	0.08	0.32	4.35	4.60	0.014	0.11	98.96	61.7	103.6	37.4	45.2	285.1	52.1	168.7
MDAP-257-70.1	75.81	0.147	12.19	1.70	0.056	0.08	0.33	4.18	4.42	0.014	0.19	98.92	54.8	84.4	39.8	50.3	267.3	49.0	188.4
MDAP-257-134.4	76.62	0.130	11.79	1.51	0.053	BD	0.24	4.10	4.33	0.000	0.20	98.76	55.2	92.6	36.5	41.3	240.5	45.8	183.6
MDAP-257-139.5	76.59	0.131	11.79	1.50	0.051	BD	0.24	4.09	4.39	0.000	0.14	98.78	62.7	96.9	33.9	37.4	232.6	47.7	96.5
MDAP-257-144.0	76.80	0.118	11.85	1.44	0.050	BD	0.23	4.04	4.34	0.011	0.19	98.89	55.2	92.8	32.6	35.7	234.6	35.3	183.9
MDAP-273-42.0	70.92	0.357	14.20	2.81	0.095	0.35	1.08	4.87	4.39	0.080	0.40	99.15	77.3	83.2	140.0	44.7	392.9	29.7	571.5
MDAP-273-42.4	74.89	0.157	12.69	1.80	0.055	0.09	0.36	4.31	4.59	0.015	0.25	98.96	51.1	96.6	31.4	48.7	278.4	43.2	173.6
MDAP-273-49.8	74.87	0.156	12.69	1.81	0.065	0.10	0.35	4.37	4.66	0.017	0.24	99.09	70.1	104.7	42.5	37.8	274.2	50.4	144.5
MDAP-273-49.9	74.58	0.163	12.98	1.88	0.055	0.14	0.38	3.99	4.40	0.018	0.70	98.59	64.6	95.0	49.7	39.9	240.6	40.1	182.7
MDAP-273-82.1	75.66	0.152	12.51	1.74	0.057	0.09	0.34	4.10	4.43	0.016	0.40	99.10	68.2	94.3	46.1	37.5	256.1	54.9	217.0

Table A-2 Continued. Major and Trace Element Geochemistry of Bandelier Tuff

Sample Number*	Major Elements (wt %)†												Trace Elements (ppm)						
	SiO_2	TiO_2	Al_2O_3	Fe_2O_3T	MnO	MgO	CaO	Na_2O	K_2O	P_2O_5	LOI	Total	Zn	Rb	Sr	Y	Zr	Nb	Ba
MDAP-273-84.2	76.33	0.137	12.16	1.66	0.055	0.08	0.26	4.00	4.36	0.014	0.38	99.05	59.2	94.0	39.0	40.3	236.0	41.3	144.6
MDAP-273-96.7	75.86	0.135	12.09	1.59	0.058	BD	0.22	4.20	4.42	0.015	0.17	98.58	95.7	101.0	37.1	41.6	248.0	45.8	135.1
MDAP-273-117.0	76.40	0.121	12.04	1.50	0.054	BD	0.23	4.11	4.37	0.010	0.14	98.84	51.4	94.5	28.8	28.3	233.4	45.8	154.8

*Abbreviations as follows: CDV, Cañon de Valle; MDAP, Material Disposal Area P.

†Analytical uncertainties are available on request from the authors. V, Cr, and Ni concentrations are below detection limits and therefore not reported. Abbreviations: LOI, loss on ignition; BD, below detection limits.

APPENDIX B. STRUCTURAL ANALYSIS

We performed a detailed fracture analysis of the restored MDA P site [~ 0.3 km^2 (0.1 mi^2)], taking advantage of nearly complete (88%) exposure. We located and measured 454 fractures and faults along eight traverses covering 576 linear meters (1,891 linear ft) of exposure (Fig. 4; Table B-1). The longest individual traverse was 134 m (440 ft). Data collected for each fracture are as follows: distance along traverse, strike, dip, trace length, aperture, and characteristics of the fracture terminations and the material filling the fracture. End points of traverses were located at grid points with an 18-m (60-ft) spacing surveyed by the LANL ER Project. Five traverses were oriented roughly east-west. Three were oriented approximately north-south. Distance along each traverse was measured with a tape stretched between surveyed grid points. Fracture strike and dip were measured to an accuracy of ± 2° with a Brunton compass. Aperture of fractures was measured perpendicular to fracture faces. In addition, fractures were mapped at a scale of 1:360 on a topographic base with 2-ft contours derived from the LANL ER Project 1991 DEM. The fracture map was then digitized, georeferenced, and imported into ArcGIS (© ESRI). Intersections of fractures and traverse lines were calculated in ArcGIS.

With the fracture data, we performed a geometric analysis, identifying preferred orientations in the directional data and spatial variation in aperture. Using the computer program Spheristat (© Pangaea Scientific), we determined preferred orientations using a Gaussian counting routine (Robin and Jowett 1986) that allows determination of the principal directions of the strain ellipse with 2σ uncertainties (Fig. 11). Point density is estimated by counting the number of data points (poles to fracture planes) within a certain angular distance of the particular direction at which the point density is being estimated. We used a Gaussian counting function in which counting is weighted according to angular distance from the counting station. Specifically, we used the Fisher function, $w = e^{k(\cos\theta - 1)}$, where θ is the angular distance and k is the kurtosis. The value of k determines the rate at which the weighting function decreases with angular distance. We chose a k value that produces a result equivalent to the Starkey method, which adjusts the size of the counting circle according to sample size, resulting in statistically significant density estimates (Starkey 1977).

In addition to making graphical plots of contoured density distributions, which demonstrate visually the clustering of directions, we also calculated principal directions (eigenvectors), which show the average clustering of the whole sample, and the 95% cones of confidence for each of the principal directions (Fig. 11; Table B-2, page 76). The difference between the point density distribution and the principal directions is similar to the difference between the mode (most frequent) and the mean (overall average). The smallest eigenvector points in the direction of the normal to the best-fitting plane through the set of poles to fracture planes. The largest eigenvector is in the direction of the statistically greatest clustering. Quantitative comparison can be made of eigenvectors and uncertainties for different data sets, whereas only graphical comparison can be made of contoured point densities.

As a further measure of preferred orientation, we plotted Rose diagrams of fracture strikes in 10° classes and calculated mean strikes with 95% confidence intervals (Fig. 12). Rose diagrams can be compared directly to the results of fracture analyses in other parts of the Laboratory (e.g., Wohletz 1995; Vaniman and Chipera 1995).

We also applied a number of statistical tests that analyze whether a sample might have been taken from a uniform (random) population of directions. Due to the abundance of cooling joints in our measured fracture data, there is a tendency for girdle distributions. Therefore, we used the Mardia test and the Woodcock/Maylor test (Mardia 1972;

Woodcock 1977), avoiding uniformity tests that are not reliable for girdle data.

We calculated mean fracture density at MDA P for each traverse but did not perform running averages of fracture density as done by Wohletz (1995). The short length of the traverses and small areas of colluvial cover (despite 88% exposure) resulted in spurious values of low density at the ends of each traverse as well as within and adjacent to areas of cover.

Finally, we investigated changes in aperture across MDA P by frequency distribution analysis. We first explored trends in aperture size by counting the number of fractures of a certain aperture (Fig. 13). We then plotted aperture versus distance along traverse to investigate variation amongst units of the Bandelier Tuff and spatial variations from east to west (Fig. 14).

Table B-1. MDA P Fracture Data (notes on page 74)

Traverse 1, N78E Trend, 440' Total Length — **Start Grid Point 421*: 1764430, 1616108** — **End Grid Point 407+20': not surveyed**

Fracture Number[†]	Distance along traverse (ft)	Coordinates[‡] Northing (ft)	Coordinates[‡] Easting (ft)	Bedrock unit	Strike[#]	Dip	Aperture (mm)	Fracture filling[¥]	Trace length[§] (ft) S	Trace length[§] (ft) N	Total length (ft)	Termination[&] Type: S	Termination[&] Type: N
1-1	3.0	1764430	1616108	4l	7	73	1	C	1.3	8.6	9.9	Te	Sp
1-2	4.5	1764429	1616106	4l	343	43	1	C/R	1.1	4.1	5.2	Tr	Tr
1-3	9.5	1764428	1616101	4l	352	69	1	C/R	1.2	5.3	6.5	Tr	C
1-4	13.1	1764427	1616097	4l	313	80	10	C/R	10.7	38.0	48.7	Sp	C
1-5	16.4	1764427	1616095	4l	202	48	> 10	C/R/OX	4.7	4.1	8.8	Tr	Tr
1-6	22.1	1764425	1616089	4l	204	63	10	C/R	8.8	5.2	14.0	Tr	Tr
1-7	36.3	1764421	1616074	4l	323	60	3	C/R	7.8	2.7	10.5	C	Tr
1-8	40.6	1764420	1616071	4l	216	79	5	C/R	8.3	26.6	34.9	Sp	Tr
1-9	44.7	1764419	1616068	4l	348	80	1	C/R	2.4	0.55	3.0	Tr	Tr
47' to 50' Covered													
1-10	51.2	1764418	1616062	4l	100	63	2	C/R/OX	2	4.4	6.4	C	C
1-11	53.1	1764417	1616059	4l	202	74	2	C/R	3.2	1.0	4.2	Tr	Tr
1-12	56.6	1764416	1616056	4l	22	78	2	C/R	4.6	9.4	14.0	C	Tr
1-13	64.9	1764414	1616048	4l	150	58	3	C/R	4.7	2.6	7.3	C	Tr
1-14	68.9	1764413	1616044	4l	28	76	2	C	1.0	6.0	7.0	Tr	C
1-15	69.9	1764413	1616043	4l	303	75	5	C	5.4	4.9	10.3	C	Tr
1-16	72.5	1764412	1616040	4l	349	90	2	C	1.8	2.4	4.2	Tr	Tr
1-17	73.5	1764411	1616038	4l	338	90	2–4	C	1.8	2.4	4.2	Tr	Tr
1-18	77.5	1764411	1616036	4l	345	56	2	C	2.7	3.1	5.8	Tr	Tr
22.3' to 34.5' Covered													
1-19	85.7	1764409	1616028	4l	23	50	2–3	C	0.6	5.7	6.3	C	Tr
1-20	91.8	1764407	1616023	4l	16	43	5	C/R	0.2	4.2	4.4	Tr	Tr
1-21	91.9	1764407	1616022	4l	131	84	4	C/R	0.0	4.6	4.6	C	Tr
34.6' to 36.8' Covered													
1-22	98.6	1764405	1616015	4l	140	53	1	C	3.2	3.3	6.5	Tr	C
1-23	103.5	1764404	1616010	4l	332	85	10	F/C/B	5.8	3.8	9.6	C	Tr
1-24	104.1	1764404	1616010	4l	174	83	5	C/R	0.0	3.6	3.6	C	Tr
44.4' to 51.7' Covered													
1-25	111.7	1764402	1616003	4l	300	80	2	C	0.0	1.5	1.5	Tr	Te
1-26	113.9	1764401	1616001	4l	173	69	3	C/R	4.4	5.1	9.5	C	Tr
53.9' to 56.5' Covered and likely brecciated													
1-27	116.5	1764401	1615998	4l	334	88	10	F/B	7.0	4.5	11.5	C	Tr
1-28	128.4	1764398	1615987	4l	51	90	1	C	6.2	7.3	13.5	Tr	C
1-29	130.8	1764397	1615985	4l	322	90	1	C	1.3	10.7	12.0	Tr	Tr
1-30	130.9	1764397	1615984	4l	210	86	1	C	3.5	3.0	6.5	Tr	C

Table B-1 Continued. MDA P Fracture Data (notes on page 74)

Traverse 1 Continued

Fracture Number[†]	Distance along traverse (ft)	Coordinates[‡] Northing (ft)	Coordinates[‡] Easting (ft)	Bed-rock unit	Strike[#]	Dip	Aper-ture (mm)	Frac-ture filling[¥]	Trace length[§] (ft) S	Trace length[§] (ft) N	Total length (ft)	Termi-nation[&] Type: S	Termi-nation[&] Type: N
1-31	135.7	1764396	1615979	4l	149	77	10	F/C/R	0.6	4.4	5.0	Tr	Tr
1-32	138.0	1764395	1615978	4l	80	90	3	C	2.7	0.5	3.2	Tr	Tr
1-33	138.8	1764395	1615977	4l	173	88	5	C	3.8	4.1	7.9	Tr	Tr
1-34	170.1	1764387	1615945	4l	59	76	1	C	0.0	4.8	4.8	Tr	Tr
1-35	170.4	1764386	1615945	4l	163	83	1	B/C/F	4.8	24.3	29.1	Tr	Sp
1-36	172.0	1764386	1615944	4l	162	86	2	B/C	3.8	15.2	19.0	C	Tr
1-37	178.6	1764385	1615939	4l	6	70	5	C/B/F	4.9	0.9	5.8	Tr	Tr
5' to 12.6' Covered													
1-38	193.3	1764381	1615925	4l	199	63	3	C/R	3.3	3.4	6.7	C	Tr
14.2' to 18.0' Covered													
1-39	205.8	1764378	1615912	4l	8	90	5	C	2.0	1.1	3.1	Tr	Tr
1-40	207.3	1764379	1615919	4l	NA	82	10	C	2.8	5.4	8.2	Sp	Tr
34.3' to 41.3' Covered													
1-41	224.9	1764373	1615894	4l	132	88	3	C	0.8	2.4	3.2	Tr	Tr
1-42	226.5	1764372	1615892	4l	187	87	2	C/F	26.0	3.8	29.8	C	Tr
1-43	228.0	1764372	1615891	4l	97	78	15	C	1.5	4.2	5.7	Tr	Tr
1-44	234.8	1764370	1615884	4l	4	90	4	F/C	7.8	0.9	8.7	Te	Tr
1-45	237.3	1764370	1615882	4l	359	90	1	C	14.2	2.55	16.8	Tr	Tr
1-46	243.3	1615876	1764368	4l	2	72	2	C	5.5	2.6	8.1	Tr	Sp
1-47	254.2	1615866	1764365	4l	133	63	1	C/R	1.9	3.0	4.9	Tr	Tr
1-48	258.3	1615863	1764364	4l	10	80	1	C/R	3.6	2.5	6.1	Tr	C
1-49	258.5	1615861	1764364	4l	175	64	2	C/R	1.8	2.0	3.8	Tr	C
1-50	264.3	1615857	1764363	4l	19	60	1	C/R	1.3	3.8	5.1	T	Tr
1-51	266.2	1615854	1764362	4l	170	79	1	C/R	1.8	4.2	6.0	Tr	Tr
1-52	266.8	1615853	1764362	4l	128	70	1	OX/R	0.7	3.3	4.0	Tr	Tr
1-53	269.4	1615851	1764361	4l	339	90	50	B/C	0.7	2.3	3.0	Sp	Tr
1-54	270.6	1615850	1764361	4l	175	71	1	C	0.4	2.5	2.9	Tr	Tr
1-55	271.1	1615849	1764361	4l	10	76	1	C	0.8	1.3	2.1	Tr	Tr
1-56	281.2	1615840	1764358	4l	158	76	1	C	1.9	1.8	3.7	Tr	Tr
1-57	282.6	1615838	1764358	4l	138	65	10	C/F	22.4	0.2	22.6	Tr	Tr
1-58	283.0	1615838	1764358	4l	29	75	22	F/C/B	6.5	9.2	15.7	Tr	Tr
1-59	288.0	1615833	1764356	4l	115	80	2	C	3.4	3.2	6.6	Tr	Tr
1-60	291.6	1615829	1764355	4l	125	70	4	C	7.2	3.1	10.3	Sp	C
1-61	293.8	1615826	1764355	4l	160	82	1	C	3.8	1.9	5.7	Tr	Tr
1-62	302.3	1615818	1764353	4l	332	78	2	C/R	1.2	0.9	2.1	Tr	Tr

Table B-1 Continued. MDA P Fracture Data (notes on page 74)

Traverse 1 Continued

Fracture Number[†]	Distance along traverse (ft)	Coordinates[‡] Northing (ft)	Coordinates[‡] Easting (ft)	Bedrock unit	Strike[#]	Dip	Aperture (mm)	Fracture filling[¥]	Trace length[§] (ft) S	Trace length[§] (ft) N	Total length (ft)	Termination[&] Type: S	Termination[&] Type: N
3.1' to 9.4' Covered													
1-63	312.6	1764350	1615807	4l	240	69	2	C	10.9	1.6	12.5	Tr	C
1-64	314.1	1764350	1615808	4l	170	67	1	C/B	0.9	9.9	10.8	Tr	Tr
1-65	324.6	1764347	1615798	4l	174	71	1	C/R	11.9	6.7	18.6	Sp	Tr
1-66	325.3	1764347	1615797	4l	345	90	1	C	14.0	6.4	20.4	Sp	Tr
1-67	334.4	1764344	1615788	4	125	85	1	C	16.7	3.4	20.1	Tr	Tr
1-68	339.6	1764343	1615783	4l	20	90	12	C/B	49.0	11.7	60.7	Sp	Sp
1-69	340.5	1764343	1615782	4l	145	8	2	C	0.7	14.0	14.7	Tr	Tr
1-70	352.8	1764340	1615770	4	135	77	1	C	10.4	15.3	25.7	Tr	Sp
1-71	355.6	1764339	1615767	4l	121	72	6	C	7.0	5.9	12.9	Tr	C
1-72	361.7	1764337	1615762	4l	150	89	1	C	4.1	4.5	8.6	Tr	Tr
1-73	363.9	1764337	1615760	4l	187	83	4	C	7.4	1.6	9.0	Tr	Te
1-74	368.2	1764336	1615755	4l	143	74	1	C/R	4.5	1.3	5.8	C	Te
1-75	373.5	1764334	1615751	4l	165	72	1	C	13.0	4.7	17.7	C	Sp
1-76	382.9	1764332	1615741	4l	341	74	1	C	5.5	1.0	6.5	Sp	Tr
1-77	384.2	1764332	1615740	4l	15	90	22	C/R/F	32.7	16.1	48.8	Tr	Tr
1-78	387.0	1764331	1615737	4l	297	90	1	C/R	2.5	7.0	9.5	Tr	Tr
1-79	397.0	1764328	1615728	4l	20	78	4	C/R	0.6	6.0	6.6	Tr	Tr
1-80	397.8	1764328	1615727	4l	5	83	6	C	0.3	3.5	3.8	Tr	Tr
1-81	398.2	1764328	1615727	4l	292	90	8	C/F	14.0	2.0	16.0	Tr	Tr
1-82	402.1	1764327	1615723	4l	54	90	8	C/R	0.2	12.0	12.2	Tr	C
1-83	402.4	1764327	1615721	4l	155	80	2	C/R	3.2	11.6	14.8	Tr	C
1-84	406.8	1764326	1615718	4l	132	67	1	R	3.0	3.3	6.3	Tr	Tr
1-85	413.0	1764324	1615712	4l	190	71	1	C	1.5	8.7	10.2	Tr	C
1-86	414.5	1764324	1615711	4l	309	84	4	C	4.7	3.5	8.2	Tr	Tr
1-87	418.7	1764323	1615706	4l	348	70	2	C	5.9	0.7	6.6	Tr	Tr
1-88	422.9	1764322	1615703	4l	25	72	4	C/F	3.1	2.9	6.0	Sp	Tr
1-89	433.0	1764319	1615693	4l	322	90	16	C/R	3.7	11.7	15.4	Tr	Tr
1-90	437.3	1764318	1615688	4l	310	84	1	C	15.5	2.7	18.2	Tr	C

Aperture (mm): mean: 4; max: 50; min: 1; sum: 383

Trace length (ft): mean: 11.0; max: 60.7; min: 1.5

Cumulative extension: 0.4 m

Fracture density: 21 fractures/100 ft

Table B-1 Continued. MDA P Fracture Data (notes on page 74)

Traverse 2, N77E Trend, 421' Total Length							Start Grid Point 478*: 1764371, 1615658 End Grid Point 492: not surveyed						
Fracture Number[†]	Distance along traverse (ft)	Coordinates[‡] Northing (ft)	Coordinates[‡] Easting (ft)	Bed-rock unit	Strike[#]	Dip	Aper-ture (mm)	Frac-ture filling[¥]	Trace length[§] (ft) S	Trace length[§] (ft) N	Total length (ft)	Termi-nation[&] Type: S	Termi-nation[&] Type: N
2-1	4.5	1764373	1615665	4l	341	90	1	C	1.1	2.2	3.3	Tr	C
5.0' to 8.3' Covered													
2-2	8.7	1764374	1615669	4l	320	81	1	C	9.7	4.0	13.7	Sp	C
2-3	18.2	1764377	1615678	4l	340	80	2	C/R	0.5	2.6	3.1	Tr	C
2-4	18.6	1764377	1615679	4l	0	61	1	C/R	0.7	2.0	2.7	Tr	Tr
2-5	19.7	1764377	1615680	4l	40	70	1	C	0.9	4.2	5.1	Tr	C
2-6	20.9	1764378	1615682	4l	122	66	1	C	2.0	4.0	6.0	Tr	C
2-7	30.0	1764380	1615690	4l	314	80	2	C/B	3.7	4.0	7.7	C	C
2-8	32.6	1764381	1615693	4l	137	72	32	C/R	5.1	5.0	10.1	C	C
2-9	39.2	1764382	1615698	4l	322	90	2	C	5.8	11.3	17.1	C	C
2-10	48.6	1764385	1615707	4l	150	76	1	C	1.5	2.8	4.3	Tr	Tr
2-11	54.5	1764386	1615714	4l	166	85	40	C/R	4.3	21.0	25.3	Sp	C
2-12	75.1	1764391	1615733	4l	164	66	3	C	10.1	9.2	19.3	Sp	C
2-13	77.1	1764392	1615736	4l	115	90	2	C	9.8	1.1	10.9	C	Tr
2-14	86.3	1764395	1615744	4l	150	85	1	C	2.0	10.2	12.2	C	Tr
0' to 6' Covered													
2-15	97.6	1764397	1615755	4l	19	72	2	C/R	1.4	1.6	3.0	C	Tr
2-16	98.9	1764398	1615757	4l	151	70	8	C/F	0.7	3.2	3.9	C	C
2-17	103.3	1764399	1615760	4l	165	90	1	C	13.0	2.0	15.0	Te	Sp
2-18	108.6	1764400	1615766	4l	109	73	10	C/R	8.0	9.4	17.4	C	Tr
2-19	113.5	1764401	1615770	4l	30	90	1	C	3.0	9.7	12.7	Tr	Tr
2-20	122.5	1764404	1615779	4l	161	71	1	C/R	7.5	6.0	13.5	Tr	Tr
2-21	125.4	1764405	1615782	4l	308	80	2	C	5.2	7.5	12.7	Tr	Tr
2-22	126.3	1764405	1615782	4l	140	76	1	C/R	0.5	2.0	2.5	Tr	Tr
2-23	129.4	1764405	1615784	4l	128	74	1	C	3.1	4.7	7.8	Tr	C
2-24	132.1	1764406	1615787	4l	140	84	2	C	6.5	0.6	7.1	Tr	C
2-25	137.4	1764407	1615792	4l	150	81	2	C/R	1.5	3.6	5.1	Tr	Tr
2-26	138.0	1764408	1615793	4l	147	74	1	C	1.7	2.9	4.6	Tr	Tr
2-27	141.0	1764409	1615797	4l	60	90	12	C/R	8.1	12.9	21.0	Sp	Sp
2-28	151.7	1764412	1615807	4l	314	88	1	C	1.7	3.7	5.4	Tr	Tr
2-29	154.2	1764412	1615809	4l	150	80	10	C/R	1.9	11.0	12.9	Tr	Tr
2-30	158.8	1764413	1615813	4l	15	90	1	C	5.6	1.1	6.7	Tr	Tr
2-31	160.9	1764414	1615816	4l	170	73	1	C	15.0	5.6	20.6	Tr	Tr
2-32	163.8	1764414	1615818	4l	169	77	3	C	2.4	2.9	5.3	C	Tr
2-33	165.7	1764415	1615820	4l	15	90	1	C	1.2	5.1	6.3	Tr	Tr

Table B-1 Continued. MDA P Fracture Data (notes on page 74)

Traverse 2 Continued

Fracture Number[†]	Distance along traverse (ft)	Coordinates[‡] Northing (ft)	Coordinates[‡] Easting (ft)	Bedrock unit	Strike[#]	Dip	Aperture (mm)	Fracture filling[¥]	Trace length[§] (ft) S	Trace length[§] (ft) N	Total length (ft)	Termination[&] Type: S	Termination[&] Type: N
2-34	168.8	1764416	1615823	4l	178	83	1	C	3.3	2.9	6.2	C	Sp
2-35	172.2	1764417	1615828	4l	276	85	8	C/F?	4.8	3.5	8.3	Tr	Tr
2-36	176.7	1764418	1615831	4l	339	90	10	C	0.3	5.3	5.6	Tr	Tr
2-37	176.9	1764418	1615832	4l	155	82	10	C	5.6	6.0	11.6	Tr	C
2-38	181.1	1764419	1615835	4l	170	74	1	C	2.3	1.1	3.4	Tr	Tr
2-39	183.7	1764420	1615839	4l	270	90	1	C	0.8	3.7	4.5	Tr	C
2-40	184.2	1764420	1615839	4l	133	76	1	C	1.8	7.0	8.8	Tr	Tr
2-41	187.6	1764421	1615841	4l	25	90	2	C	2.4	6.3	8.7	Tr	C
98.3' to 117.4' Covered													
2-42	209.7	1764426	1615863	4l	171	61	NA	NA	5.2	1.2	6.4	C	C
2-43	214.8	1764428	1615868	4l	0	74	1	C	11.3	5.7	17.0	Tr	Tr
2-44	218.5	1764429	1615871	4l	176	76	1	C	0.9	4.3	5.2	Sp	Tr
2-45	221.3	1764430	1615874	4l	305	63	1	C	0.8	7.5	8.3	Tr	C
2-46	221.5	1764430	1615875	4l	25	44	1	C	0.8	1.7	2.5	Tr	C
2-47	222.8	1764430	1615876	4l	175	40	1	C	0.9	2.6	3.5	Tr	C
2-48	226.2	1764431	1615879	4l	336	90	4	C	8.0	11.3	19.3	C	Te
2-49	227.2	1764431	1615879	4l	234	81	10	C	1.4	15.0	16.4	Tr	Tr
2-50	229.6	1764432	1615882	4l	20	69	2	C	3.6	2.0	5.6	Tr	Tr
2-51	239.7	1764434	1615891	4l	172	86	1	C	2.9	2.2	5.1	Tr	Te
2-52	240.2	1764434	1615892	4l	169	75	8	C/R	9.8	4.6	14.4	C	Sp
2-53	248.3	1764437	1615902	4l	286	77	2	C	2.0	7.5	9.5	Tr	Tr
2-54	250.4	1764437	1615902	4l	5	77	1	C	1.2	2.5	3.7	Tr	Tr
2-55	254.0	1764438	1615907	4l	290	90	10	C	2.2	15.4	17.6	Tr	Tr
2-56	257.3	1764439	1615908	4l	230	71	10	C	7.0	6.7	13.7	Tr	Te
2-57	281.8	1764445	1615932	4l	11	90	1	C	13.0	1.6	14.6	C	Tr
2-58	284.6	1764446	1615935	4l	178	71	1	C	3.0	0.5	3.5	Te	Tr
2-59	285.8	1764447	1615937	4l	290	70	1	C	6.3	3.7	10.0	Sp	Tr
2-60	295.3	1764449	1615945	4l	349	43	1	C	4.2	2.4	6.6	Tr	C
2-61	309.2	1764451	1615955	4l	57	50	2	Ca	3.3	3.0	6.3	Te	Tr
2-62	313.0	1764453	1615963	4l	303	30	2	C/R	0.7	2.6	3.3	Tr	Tr
2-63	315.1	1764454	1615965	4l	325	50	2	C/R	6.0	4.8	10.8	Tr	Tr
2-64	312.0	1764453	1615960	4l	19	90	1	Ca/R	9.2	7.4	16.6	Tr	Tr
2-65	317.8	1764455	1615967	4l	323	50	2	C/R	4.6	6.6	11.2	Tr	Tr
2-66	323.3	1764456	1615971	4l	3	90	2	F/B	4.7	3.9	8.6	Tr	C
2-67	325.4	1764456	1615974	4l	3	90	1	C	9.3	8.0	17.3	Tr	Tr
2-68	333.6	1764459	1615983	4l	303	90	2	C/R	0.6	6.5	7.1	Tr	Tr

Table B-1 Continued. MDA P Fracture Data (notes on page 74)

Traverse 2 Continued

Fracture Number[†]	Distance along traverse (ft)	Coordinates[‡] Northing (ft)	Coordinates[‡] Easting (ft)	Bed-rock unit	Strike[#]	Dip	Aper-ture (mm)	Frac-ture filling[¥]	Trace length[§] (ft) S	Trace length[§] (ft) N	Total length (ft)	Termi-nation[&] Type: S	Termi-nation[&] Type: N
2-69	338.3	1764459	1615984	4l	50	58	1	C/R	2.4	0.6	3.0	Tr	Te
2-70	348.2	1764463	1615997	4l	310	63	4	F/B	10.6	4.0	14.6	C	Te
2-71	356.1	1764464	1616003	4l	350	54	4	C/R	3.6	1.6	5.2	C	C
59' to 60' Covered													
0' to 2' Covered													
2-72	366.0	1764467	1616014	4l	326	90	2	F	15.0	2.0	17.0	Tr	Tr
2-73	370.9	1764468	1616018	4l	23	62	1	R	3.0	2.4	5.4	Tr	Tr
2-74	371.8	1764469	1616019	4l	18	90	1	R	3.1	1.8	4.9	Tr	Tr
2-75	374.2	1764469	1616022	4l	300	80	2	C	3.0	20.0	23.0	Tr	Sp
2-76	377.3	1764470	1616024	4l	18	90	2	C	0.4	13.3	13.7	Tr	
20' to 34' Covered													
40' to 41' Covered													
45' to 56' Covered													
2-77	418.2	1764481	1616064	4l	27	66	2	C/R	2.5	1.3	3.8	C	Tr
2-78	420.6	1764481	1616066	4l	347	84	5	F/B	20.0	0.6	20.6	Tr	C

Aperture (mm): mean: 4; max: 40; min: 1; sum: 280

Trace length (ft): mean: 9.7; max: 25.3; min: 2.5

Cumulative extension: 0.3 m

Fracture density: 19 fractures/100 ft

Table B-1 Continued. MDA P Fracture Data (notes on page 74)

Traverse 3, N14W Trend, 207' Total Length — **Start Grid Point 418*: 1764407, 1616021** — **End Grid Point 562: 1764523, 1615990**

Fracture Number†	Distance along traverse (ft)	Coordinates‡ Northing (ft)	Coordinates‡ Easting (ft)	Bedrock unit	Strike#	Dip	Aperture (mm)	Fracture filling¥	Trace length§ (ft) S	Trace length§ (ft) N	Total length (ft)	Termination& Type: S	Termination& Type: N
3-1	4.1	1764411	1616022	4l	309	90	4	C/R/F	3.0	9.7	12.7	Te	Sp
3-2	9.5	1764417	1616021	4l	44	90	2	C/R	7.0	3.6	10.6	C	Tr
3-3	12.0	1764419	1616020	4l	305	65	1	C/R	2.4	2.3	4.7	Tr	Tr
3-4	14.7	1764421	1616020	4l	67	90	1	C	14.3	7.1	21.4	Tr	Tr
3-5	22.9	1764430	1616017	4l	284	64	1	C/R	5.3	6.5	11.8	Sp	Sp
3-6	27.2	1764433	1616016	4l	148	36	2	R	2.4	1.4	3.8	C	Tr
3-7	30.1	1764436	1616016	4l	116	60	2	C	3.7	3.0	6.7	Tr	C
3-8	30.4	1764438	1616015	4l	11	59	1	C/R	4.8	0.6	5.4	Tr	Tr
3-9	34.2	1764441	1616014	4l	15	48	1	R	1.4	4.0	5.4	Tr	Tr
3-10	35.5	1764441	1616014	4l	101	80	1	C	9.3	5.2	14.5	C	Sp
3-11	39.7	1764447	1616013	4l	22	53	3	C/R	2.5	4.3	6.8	Tr	Tr
3-12	43.9	1764450	1616012	4l	65	90	1	C	8.1	1.9	10.0	Sp	Sp
3-13	48.0	1764455	1616011	4l	355	82	1	C	2.0	3.5	5.5	Te	Sp
3-14	58.0	1764463	1616008	4l	355	79	1	C	7.6	0.6	8.2	Te	Sp
3-15	67.1	1764472	1616006	4l	75	32	2	R/B	5.9	7.6	13.5	Tr	Tr
3-16	69.1	1764474	1616006	4l	103	60	3	R	9.1	6.2	12.3	Tr	Tr
3-17	75.7	1764481	1616004	4l	225	72	1	R	3.4	6.6	10.0	C	Sp
3-18	76.6	1764482	1616003	4l	266	70	1	R	1.2	4.1	5.3	Tr	C
3-19	83.6	1764488	1616002	4l	296	90	1	C	5.2	1.7	6.9	C	C
3-20	92.5	1764497	1615999	4l	243	79	3	C/R	4.5	9.7	14.2	Te	Tr
3-21	104.4	1764508	1615996	4l	190	64	10	C/R/B	12.1	2.2	14.3	C	C
3-22	114.3	1764518	1615994	3T	260	72	1	C	1.5	0.7	2.2	Tr	C
86.4' to 91.2' Covered													
0' to 5.8' Trench													
5.8' to 13.0' Covered													
3-23	133.3	1764536	1615989	3T	261	81	10	C	8.0	9.0	17.0	C	C
3-24	138.6	1764541	1615988	3T	276	90	3	C	1.9	8.7	10.6	Tr	C
3-25	140.8	1764547	1615986	3T	72	90	1	O	2.4	0.9	3.3	Tr	Tr
3-26	141.7	1764544	1615987	3T	260	33	1	C	2.5	0.7	3.2	Tr	C
3-27	143.2	1764544	1615987	3T	279	90	8	C/R	16.2	7.6	23.8	Tr	Tr
3-28	148.6	1764552	1615985	3T	86	84	4	C/R	1.3	8.1	9.4	C	C
3-29	162.1	1764565	1615981	3T	41	41	1	C	0.9	2.0	2.9	C	C
3-30	166.0	1764567	1615980	3T	274	90	2	C	2.0	2.9	4.9	C	C
3-31	167.7	1764569	1615980	3T	48	35	5	C/R	6.3	1.7	8.0	C	Tr
3-32	176.2	1764578	1615978	3T	200	64	6	C	4.0	9.5	13.5	Te	C

Table B-1 Continued. MDA P Fracture Data (notes on page 74)

Traverse 3 Continued

Fracture Number[†]	Distance along traverse (ft)	Coordinates[‡] Northing (ft)	Coordinates[‡] Easting (ft)	Bedrock unit	Strike[#]	Dip	Aperture (mm)	Fracture filling[¥]	Trace length[§] (ft) S	Trace length[§] (ft) N	Total length (ft)	Termination[&] Type: S	Termination[&] Type: N
3-33	182.3	1764551	1615985	3T	264	8	2	C	7.9	5.3	13.2	Tr	Tr
3-34	186.2	1764542	1615987	3T	243	12	10	C	2.4	9.1	11.5	Tr	Tr
3-35	189.3	1764540	1615988	3T	256	14	NA	O	1.6	8.9	10.5	Tr	Tr
3-36	197.1	1764532	1615990	3T	263	13	2	C	4.0	0.5	4.5	Tr	C

Aperture (mm): mean: 3; max: 10; min: 1

Trace length (ft): mean: 9.5; max: 23.8; min: 2.2

Fracture density: 17 fractures/100 ft

Table B-1 Continued. MDA P Fracture Data (notes on page 74)

Traverse 4, N20W Trend, 165' Total Length — **Start Grid Point 667+15.2'*: not surveyed**; **End Grid Point 595: 1764528, 1615895**

Fracture Number[†]	Distance along traverse (ft)	Coordinates[‡] Northing (ft)	Coordinates[‡] Easting (ft)	Bedrock unit	Strike[#]	Dip	Aperture (mm)	Fracture filling[¥]	Trace length[§] (ft) S	Trace length[§] (ft) N	Total length (ft)	Termination[&] Type: S	Termination[&] Type: N
4-1	6.0	1764595	1615880	3	82	57	1	C	2.2	5.2	7.4	Tr	C
4-2	9.6	1764592	1615881	3	99	37	1	C/R	2.5	7.1	9.6	C	C
4-3	16.3	1764586	1615883	3	130	72	1	C	5.0	7.3	12.3	Tr	Te
4-4	21.0	1764580	1615884	3	75	90	1	R	4.1	1.7	5.8	Tr	Sp
4-5	21.7	1764579	1615884	3	70	63	1	C	3.2	0.5	3.7	Tr	Tr
4-6	24.5	1764577	1615885	3	234	87	10	C/R	9.4	11.5	20.9	Tr	C
4-7	29.0	1764570	1615887	3	168	70	20	C/R	6.2	5.1	11.3	Tr	Tr
4-8	42.1	1764561	1615889	3T	138	75	10	C/R	31.5	9.3	40.8	C	Tr
4-9	46.8	1764557	1615890	3T	250	39	4	C	0.3	5.1	5.4	C	C
4-10	51.3	1764553	1615891	3T	271	88	10	C/B	1.1	13.4	14.5	Tr	Tr
4-11	55.3	1764548	1615893	3T	72	90	25	C/R	8.0	21.0	29.0	Tr	Tr
4-12	67.5	1764537	1615896	3T	255	18	1	C	6.3	10.4	16.7	C	Tr
4-13	68.3	1764530	1615898	3T	85	63	1	C	1.9	4.8	6.7	Tr	Te
4-14	74.7	1764535	1615896	3T	62	65	1	C	1.6	0.7	2.3	Sp	C
4-15	75.7	1764522	1615900	3T	82	90	8	C/R/B	4.9	3.3	8.2	Tr	C
4-16	81.3	1764526	1615899	3T	42	90	100	C/R/B	4.6	0.4	5.0	Tr	C
4-17	78.5	1764526	1615899	3T	271	9	6	C	2.0	1.5	3.5	Tr	C
4-18	75.2	1764528	1615898	3T	275	10	1	C	2.2	3.9	6.1	Tr	C
4-19	77.2	1764526	1615899	3T	314	90	2	C	8.2	1.4	9.6	C	Tr
4-20	76.8	1764527	1615899	3T	252	4	20	C	2.7	1.1	3.8	Tr	Tr
4-21	77.8	1764524	1615899	3T	215	80	50	C/R/B	8.4	12.4	20.8	C	C
4-22	79.7	1764522	1615900	3T	252	9	10	C/R/B	1.1	3.4	4.5	Tr	Tr
4-23	81.6	1764520	1615900	3T	50	82	35	C	1.8	1.1	2.9	Tr	Tr
4-24	82.6	1764521	1615900	3T	124	64	14	C	3.4	4.1	7.5	Tr	Tr
10.1' to 20.3' Covered													
4-25	98.9	1764505	1615905	4I	49	74	1	C	3.2	1.3	4.5	Tr	C
4-26	105.1	1764500	1615906	4I	309	46	2	R	2.0	2.3	4.3	C	C
4-27	124.8	1764481	1615911	4I	310	62	2	C	0.8	1.0	1.8	C	Sp
4-28	126.9	1764476	1615913	4I	70	90	1	C	0.3	3.0	3.3	Tr	C
4-29	149.2	1764457	1615918	4I	129	80	4	C	4.1	1.7	5.8	Tr	C
4-30	153.2	1764454	1615919	4I	51	67	2	C	8.0	5.2	13.2	C	Tr
4-31	163.1	1764445	1615921	4I	57	90	1	C	7.2	4.7	11.9	Sp	Tr

Aperture (mm): mean: 11; max: 100; min: 1

Trace length (ft): mean: 9.8; max: 40.8; min: 1.8

Fracture density: 19 fractures/100 ft

Table B-1 Continued. MDA P Fracture Data (notes on page 74)

Traverse 5, N12W Trend, 165' Total Length									Start Grid Point 662*: 1764547, 1615735 End Grid Point 482: 1764403, 1615773				
Fracture Number†	Distance along traverse (ft)	Coordinates‡ Northing (ft)	Coordinates‡ Easting (ft)	Bed-rock unit	Strike#	Dip	Aper-ture (mm)	Frac-ture filling¥	Trace length§ (ft) S	Trace length§ (ft) N	Total length (ft)	Termi-nation& Type: S	Termi-nation& Type: N
5-1	9.7	1764541	1615739	3	320	90	8	C/R	1.2	1.3	2.5	C	C
5-2	12.9	1764537	1615740	3	104	56	1	C	0.4	11.7	12.1	Tr	C
5-3	13.5	1764535	1615741	3	347	35	1	C/OX	0.6	9.2	9.8	C	Tr
5-4	14.7	1764534	1615741	3	240	43	1	OX/R	0.6	1.2	1.8	Te	Tr
5-5	22.5	1764528	1615743	3	94	84	2	C	7.8	8.3	16.1	Tr	C
5-6	22.7	1764526	1615743	3	218	79	14	C/R/F	6.0	2.7	8.7	C	Tr
5-7	23.7	1764526	1615743	3	139	55	1	C	3.5	0.2	3.7	Tr	Tr
5-8	25.3	1764524	1615743	3	119	64	1	C/R	2.3	2.4	4.7	Te	Tr
5-9	27.6	1764522	1615744	3	296	90	6	C/R/B	12.0	7.4	19.4	Tr	Tr
5-10	31.2	1764518	1615745	3	29	67	1	C	3.1	6.6	9.7	Tr	Tr
5-11	33.0	1764518	1615745	3	268	59	1	C	3.4	1.6	5.0	Tr	Tr
5-12	35.8	1764515	1615746	3	293	16	2	R	0.5	1.7	2.2	Tr	Te
5-13	36.1	1764512	1615747	3	51	76	1	R	2.0	3.3	5.3	Tr	Tr
5-14	41.3	1764510	1615747	3	295	90	16	C/B/OX	2.1	1.4	3.5	Tr	Tr
5-15	42.3	1764507	1615748	3	245	88	6	C/R/OX	9.0	16.0	25.0	Tr	C
5-16	45.7	1764504	1615749	3	22	2	1	C	4.9	7.0	11.9	Tr	Tr
5-17	56.7	1764495	1615751	3	303	90	50	C/R/B	11.0	18.0	29.0	Tr	C
5-18	59.7	1764491	1615752	3	265	82	10	C/R	10.6	15.0	25.6	Tr	C
5-19	64.6	1764485	1615754	3T	227	11	25	C/R	5.2	7.1	12.3	Tr	C
5-20	67.8	1764481	1615755	3T	220	11	0	O	2.4	2.6	5.0	Tr	Tr
5-21	71.5	1764479	1615756	3T	238	88	30	C	1.5	11.0	12.5	Tr	Tr
5-22	73.9	1764477	1615756	3T	245	11	10	C	0.3	3.7	4.0	Tr	Tr
5-23	75.6	1764476	1615756	3T	98	70	12	C/R	2.8	1.0	3.8	C	C
5-24	76.7	1764472	1615758	3T	1	79	10	C/R/B	21.0	7.0	28.0	C	C
5-25	82.8	1764469	1615758	3T	262	8	0	O	0.9	1.8	2.7	Tr	Te
5-26	85.0	1764466	1615759	3T	260	83	10	C	2.0	5.5	7.5	Tr	C
5-27	89.0	1764462	1615760	3T	254	7	4	C/R	4.0	5.0	9.0	Tr	C
5-28	93.8	1764458	1615761	4I	311	80	10	C	6.0	3.1	9.1	C	C
5-29	99.8	1764452	1615763	4I	45	69	4	C	1.0	2.1	3.1	C	C
5-30	101.5	1764449	1615764	4I	25	1	1	C	0.9	1.6	2.5	C	C
5-31	104.5	1764446	1615765	4I	29	81	3	C	3.6	2.9	6.5	C	C
5.0' to 24.4' Covered													
5-32	130.7	1764436	1615767	4I	52	30	20	R	2.4	2.1	4.5	C	C
26.0' to 31.0' Covered													
5-33	136.8	1764430	1615769	4I	39	45	10	R	2.1	8.5	10.6	C	Tr

Table B-1 Continued. MDA P Fracture Data (notes on page 74)

Traverse 5 Continued

Fracture Number[†]	Distance along traverse (ft)	Coordinates[‡] Northing (ft)	Coordinates[‡] Easting (ft)	Bedrock unit	Strike[#]	Dip	Aperture (mm)	Fracture filling[¥]	Trace length[§] (ft) S	Trace length[§] (ft) N	Total length (ft)	Termination[&] Type: S	Termination[&] Type: N
5-34	139.5	1764428	1615770	4l	55	35	25	C/R	5.7	2.2	7.9	C	Tr
5-35	144.0	1764424	1615771	4l	87	72	2	C/R	3.7	5.3	9.0	Tr	Tr
5-36	145.3	1764423	1615771	4l	96	86	4	C/R	21.9	6.3	28.2	Tr	Tr
5-37	151.3	1764417	1615773	4l	9	90	2	C	2.8	1.2	4.0	Sp	Tr
5-38	152.4	1764416	1615773	4l	72	52	1	C	1.3	3.5	4.8	Tr	Sp
5-39	153.9	1764414	1615773	4l	38	90	1	C/OX	1.5	2.5	4.0	Tr	Tr
5-40	155.0	1764413	1615773	4l	18	90	1	C/OX	9.4	2.3	11.7	Tr	Tr
5-41	159.7	1764410	1615774	4l	138	83	2	C	14.1	15.4	29.5	Sp	C
5-42	160.7	1764408	1615775	4l	40	68	1	C	0.8	11.6	12.4	Tr	Tr
5-43	163.5	1764405	1615776	4l	41	51	10	C	1.4	3.1	4.5	Tr	Tr
5-44	165.4	1764403	1615776	4l	72	90	2	C	2.1	7.7	9.8	Tr	Tr

Aperture (mm): mean: 8; max: 50; min: 1

Trace length (ft): mean: 10.1; max: 29.5; min: 1.8

Fracture density: 27 fractures/100 ft

Table B-1 Continued. MDA P Fracture Data (notes on page 74)

Traverse 6, N76E Trend, 360' Total Length — **Start Grid Point 599*: not surveyed** — **End Grid Point 587: 1764466, 1615663**

Fracture Number[†]	Distance along traverse (ft)	Coordinates[‡] Northing (ft)	Coordinates[‡] Easting (ft)	Bed-rock unit	Strike[#]	Dip	Aper-ture (mm)	Frac-ture filling[¥]	Trace length[§] (ft) S	Trace length[§] (ft) N	Total length (ft)	Termi-nation[&] Type: S	Termi-nation[&] Type: N
6-1	7.1	1764558	1616007	3T	159	32	1	R	1.4	0.8	2.2	Tr	C
8.0' to 23.5' Covered													
6-2	26.0	1764554	1615989	3T	301	73	70	C	2.5	0.9	3.4	C	C
6-3	26.5	1764553	1615988	3T	260	5	2	C	3.9	0.6	4.5	Tr	C
6-4	30.1	1764552	1615984	3T	291	11	4	C/R	2.5	0.3	2.8	C	Tr
6-5	30.7	1764552	1615984	3T	21	25	54	C	1.2	0.4	1.6	C	Tr
6-6	31.5	1764552	1615983	3T	24	62	20	C/R	1.8	0.8	2.6	C	C
6-7	33.7	1764552	1615982	3T	141	62	1	C	1.4	0.5	1.9	C	Tr
6-8	34.2	1764551	1615980	3T	52	59	4	C	1.0	1.3	2.3	C	C
6-9	35.1	1764551	1615981	3T	138	5	4	C	0.8	1.2	2.0	C	Tr
6-10	36.5	1764551	1615979	3T	34	90	6	C	0.4	1.0	1.4	C	C
6-11	38.8	1764550	1615977	3T	350	5	6	C	1.2	1.5	2.7	C	Tr
41.0' to 50.6' Covered													
6-12	50.8	1764547	1615964	3T	321	90	4	C	4.6	1.8	6.4	C	C
6-13	51.8	1764547	1615965	3T	245	12	1	C	1.1	1.3	2.4	Tr	Tr
6-14	52.8	1764546	1615962	3T	327	81	2	C	4.8	3.1	7.9	C	C
6-15	54.7	1764546	1615960	3T	339	90	4	C	1.0	1.4	2.4	Tr	C
6-16	55.4	1764546	1615959	3T	254	14	2	C	1.7	0.6	2.3	C	Tr
6-17	58.2	1764545	1615957	3T	315	16	4	C/OM	1.5	0.7	2.2	Tr	Tr
6-18	58.7	1764545	1615957	3T	217	82	20	C/R	10.5	3.0	13.5	Tr	C
6-19	59.9	1764545	1615957	3T	150	65	10	C/OM	1.9	1.5	3.4	C	C
6-20	61.4	1764544	1615954	3T	305	81	30	C/R	1.1	4.1	5.2	Tr	C
6-21	65.0	1764543	1615950	3T	100	1	4	C/R	0.8	2.7	3.5	C	Tr
6-22	68.6	1764542	1615947	3T	326	77	20	C/R	13.3	2.7	16.0	C	Tr
6-23	69.4	1764542	1615947	3T	39	62	4	C	2.4	0.8	3.2	C	Tr
6-24	73.6	1764542	1615944	3T	240	12	0	O	6.9	3.8	10.7	Tr	Tr
6-25	77.7	1764540	1615939	3T	345	90	20	R/C	10.4	49.0	59.4	C	C
6-26	80.6	1764540	1615939	3T	245	6	0	O	8.3	4.7	13.0	C	Tr
6-27	83.4	1764539	1615934	3T	351	90	2	C	27.0	27.4	54.4	C	C
6-28	87.0	1764536	1615924	3T	257	5	1	C	4.0	5.7	9.7	Tr	Tr
6-29	90.5	1764537	1615927	3T	171	87	4	C	30.7	1.6	32.3	Sp	Tr
6-30	92.9	1764536	1615924	3T	260	6	1	C	1.4	2.0	3.4	C	Tr
6-31	95.3	1764536	1615921	3T	330	62	1	C	1.4	2.0	3.4	C	C
6-32	97.2	1764535	1615919	3T	343	90	1	C	1.1	1.3	2.4	C	C
6-33	99.3	1764535	1615919	3T	240	10	0	O	0.8	4.0	4.8	C	Tr

Table B-1 Continued. MDA P Fracture Data (notes on page 74)

Traverse 6 Continued

Fracture Number[†]	Distance along traverse (ft)	Coordinates[‡] Northing (ft)	Coordinates[‡] Easting (ft)	Bedrock unit	Strike[#]	Dip	Aperture (mm)	Fracture filling[¥]	Trace length[§] (ft) S	Trace length[§] (ft) N	Total length (ft)	Termination[&] Type: S	Termination[&] Type: N
6-34	101.6	1764534	1615916	3T	160	39	2	C	1.3	3.5	4.8	C	C
6-35	103.3	1764534	1615915	3T	359	90	1	C	28.0	52.7	80.7	C	Tr
6-36	106.0	1764532	1615910	3T	260	20	2	C	2.8	3.0	5.8	Tr	Tr
6-37	108.7	1764532	1615908	3T	319	90	2	C/R	16.7	1.7	18.4	Tr	Tr
6-38	109.7	1764532	1615909	3T	263	20	2	C	6.1	1.8	7.9	Tr	Tr
6-39	110.6	1764532	1615907	3T	184	87	8	C/R	10.8	2.0	12.8	C	C
6-40	111.5	1764532	1615906	3T	253	9	10	C	1.7	3.4	5.1	Tr	Tr
6-41	112.4	1764531	1615905	3T	324	90	10	C/R	2.3	1.0	3.3	Tr	Tr
6-42	113.0	1764531	1615904	3T	260	12	6	C	0.8	0.9	1.7	C	Tr
6-43	113.6	1764531	1615903	3T	217	84	2	C	2.5	1.2	3.7	C	Tr
6-44	115.9	1764531	1615903	3T	13	90	30	R/C	17.0	1.7	18.7	C	C
6-45	118.0	1764529	1615897	3T	255	5	10	C	2.0	1.2	3.2	Tr	Tr
6-46	124.7	1764529	1615897	3T	285	88	1	C	0.4	0.6	1.0	Tr	Tr
6-47	125.5	1764528	1615893	3T	80	3	4	C	0.3	0.7	1.0	C	Tr
6-48	126.2	1764528	1615891	3T	225	61	10	C	1.4	0.9	2.3	C	Tr
6-49	129.7	1764527	1615890	3T	229	9	2	C/R	0.7	2.6	3.3	C	Tr
6-50	136.1	1764528	1615893	3T	239	15	1	C	0.5	1.8	2.3	C	Tr
6-51	137.2	1764525	1615881	3T	323	84	2	C	0.2	1.6	1.8	Tr	Tr
6-52	137.8	1764525	1615880	3T	260	20	2	C	0.6	1.6	2.2	Tr	Tr
6-53	138.3	1764525	1615880	3T	184	81	34	C/R/B	0.5	1.6	2.1	C	Tr
6-54	138.7	1764525	1615884	3T	236	78	1	C	1.9	0.3	2.2	Tr	Tr
6-55	140.0	1764524	1615878	3T	247	6	2	C	0.3	1.1	1.4	Tr	Tr
6-56	140.6	1764524	1615878	3T	343	76	1	R/C	0.6	1.2	1.8	C	C
6-57	141.3	1764524	1615880	3T	245	27	6	C	0.6	1.1	1.7	C	Tr
6-58	141.6	1764524	1615877	3T	216	65	4	R/C	1.1	1.6	2.7	C	Tr
6-59	151.4	1764522	1615870	3T	22	90	22	C	1.1	0.1	1.2	C	Tr
6-60	152.4	1764521	1615869	3T	33	64	1	C	0.9	0.3	1.2	Tr	Tr
6-61	155.0	1764520	1615865	3T	355	90	10	C	0.7	1.5	2.2	C	C
6-62	155.8	1764520	1615862	3T	255	36	5	R/C	0.7	2.0	2.7	C	Tr
6-63	162.5	1764519	1615858	3T	119	78	1	C	1.4	1.0	2.4	C	Tr
6-64	163.3	1764519	1615858	3T	347	90	10	C	1.2	1.2	2.4	Tr	Tr
6-65	165.6	1764518	1615856	3T	277	23	6	C/R	1.9	2.4	4.3	C	Tr
6-66	167.9	1764518	1615854	3T	201	52	1	C	0.7	2.0	2.7	C	C
6-67	170.8	1764516	1615848	3T	310	70	2	C	1.6	1.4	3.0	C	C
6-68	173.6	1764515	1615846	3T	256	22	10	C	2.5	2.1	4.6	Tr	Tr
6-69	176.3	1764515	1615844	3T	345	90	15	C/R	2.4	0.5	2.9	C	C

Table B-1 Continued. MDA P Fracture Data (notes on page 74)

Traverse 6 Continued

Fracture Number[†]	Distance along traverse (ft)	Coordinates[‡] Northing (ft)	Coordinates[‡] Easting (ft)	Bedrock unit	Strike[#]	Dip	Aperture (mm)	Fracture filling[¥]	Trace length[§] (ft) S	Trace length[§] (ft) N	Total length (ft)	Termination[&] Type: S	Termination[&] Type: N
6-70	178.2	1764515	1615843	3T	265	16	2	R/C	1.7	5.7	7.4	Tr	Tr
6-71	185.7	1764512	1615835	3T	152	87	20	C/R	14.9	16.5	31.4	C	C
6-72	186.3	1764512	1615834	3T	169	36	30	R/C	1.8	6.0	7.8	C	C
6-73	190.6	1764511	1615830	3T	42	54	15	C	2.5	4.0	6.5	Tr	Tr
6-74	195.2	1764510	1615826	3T	251	23	2	C/R	1.1	1.2	2.3	C	Tr
6-75	196.2	1764510	1615825	3T	354	90	10	C	0.4	1.1	1.5	C	Tr
17.5' to 36.0' Covered													
6-76	216.4	1764509	1615823	3T	276	90	2	C	0.3	1.9	2.2	C	C
6-77	223.4	1764505	1615805	3T	148	78	2	C	0.8	5.7	6.5	C	C
6-78	223.6	1764504	1615804	3T	46	62	40	C	0.7	2.1	2.8	C	Tr
46.4' to 55.5' Covered													
6-79	237.3	1764499	1615786	3T	238	15	0	O	1.3	1.0	2.3	Tr	Tr
6-80	238.5	1764499	1615784	3T	186	75	6	C	1.9	0.3	2.2	C	C
6-81	241.9	1764498	1615781	3T	306	90	40	C/B/R	24.1	18.0	42.1	C	C
6-82	244.3	1764498	1615780	3T	245	20	2	R/C	2.8	2.3	5.1	C	Tr
6-83	246.8	1764497	1615775	3T	36	90	10	C	16.8	4.3	21.1	Tr	Tr
6-84	252.6	1764495	1615771	3T	240	19	2	C	3.7	5.7	9.4	C	Tr
6-85	258.3	1764494	1615765	3T	358	85	12	C/R/OM	10.7	16.8	27.5	C	C
6-86	260.7	1764493	1615762	3T	233	10	10	C/R	4.0	1.5	5.5	C	Tr
6-87	262.9	1764492	1615760	3T	17	90	8	R/C/OM	10.7	1.0	11.7	C	Tr
6-88	266.0	1764492	1615757	3T	314	15	2	C	3.8	4.0	7.8	Tr	Tr
6-89	269.0	1764491	1615754	3	355	73	40	C/R	11.5	14.6	26.1	C	C
6-90	271.4	1764490	1615752	3	225	9	4	C/R	3.0	2.6	5.6	Tr	Tr
6-91	273.8	1764490	1615750	3	350	38	10	B/R/C	1.1	1.0	2.1	C	C
6-92	274.9	1764489	1615749	3	356	20	15	C	2.2	3.0	5.2	C	C
6-93	275.8	1764489	1615747	3	210	6	2	C	2.0	1.9	3.9	C	Tr
6-94	276.6	1764489	1615746	3	208	43	1	R/OM	1.8	9.8	11.6	C	Tr
39.0' to 51.4' Covered													
6-95	298.0	1764483	1615726	3	323	90	12	O/C	3.1	4.0	7.1	C	C
6-96	300.0	1764483	1615725	3	308	90	1	O	0.7	1.5	2.2	C	Tr
6-97	301.5	1764482	1615722	3	197	77	2	C	0.9	1.3	2.2	C	C
6-98	303.6	1764482	1615722	3	333	90	1	C	1.1	2.0	3.1	C	C
6-99	306.8	1764481	1615719	3	60	42	2	O	1.8	3.3	5.1	C	Tr
6-100	310.8	1764481	1615716	3	330	82	44	O	0.8	2.2	3.0	C	Tr
6-101	311.9	1764480	1615715	3	301	90	30	O	0.7	1.7	2.4	C	Tr
6-102	312.4	1764480	1615714	3	302	90	34	O	1.0	1.3	2.3	C	Tr

Table B-1 Continued. MDA P Fracture Data (notes on page 74)

Traverse 6 Continued

Fracture Number[†]	Distance along traverse (ft)	Coordinates[‡] Northing (ft)	Coordinates[‡] Easting (ft)	Bedrock unit	Strike[#]	Dip	Aperture (mm)	Fracture filling[¥]	Trace length[§] (ft) S	Trace length[§] (ft) N	Total length (ft)	Termination[&] Type: S	Termination[&] Type: N
6-103	313.4	1764480	1615713	3	210	50	20	O	2.7	4.0	6.7	C	C
6-104	319.8	1764478	1615707	3	20	84	1	C/R	1.7	1.4	3.1	C	C
6-105	324.2	1764477	1615702	3	31	60	4	O	3.7	2.5	6.2	C	C
6-106	326.8	1764477	1615700	3	298	90	50	O	2.0	4.0	6.0	Tr	C
6-107	330.5	1764475	1615696	3	259	10	0	O	1.5	1.3	2.8	C	Tr
6-108	334.4	1764474	1615692	3	338	62	2	C/R	0.9	7.3	8.2	C	C
6-109	337.0	1764474	1615690	3	254	14	0	O	1.9	4.0	5.9	C	Tr
6-110	345.9	1764472	1615682	3	308	90	20	C/R	3.1	2.4	5.5	Tr	Tr
6-111	348.6	1764471	1615679	3	168	78	40	O	2.3	0.9	3.2	C	Tr
6-112	351.9	1764470	1615676	3	16	85	2	O	1.2	0.5	1.7	C	Tr

Aperture (mm): mean: 10; max: 70; min: 1; sum: 1097

Trace length (ft): mean: 7.6; max: 80.7; min: 1.0

Cumulative extension: 1.1 m

Fracture density: 31 fractures/100 ft

Table B-1 Continued. MDA P Fracture Data (notes on page 74)

Traverse 7, N78E Trend, 137' Total Length — **Start Grid Point 670*: 1764610, 1615966** — **End Grid Point 666+17': not surveyed**

Fracture Number[†]	Distance along traverse (ft)	Coordinates[‡] Northing (ft)	Coordinates[‡] Easting (ft)	Bed-rock unit	Strike[#]	Dip	Aper-ture (mm)	Frac-ture filling[¥]	Trace length[§] (ft) S	Trace length[§] (ft) N	Total length (ft)	Termi-nation[&] Type: S	Termi-nation[&] Type: N
7-1	25.8	1764603	1615944	3	282	11	0	O	1.5	3.8	5.3	C	Tr
7-2	31.4	1764602	1615939	3	288	3	0	O	1.0	3.1	4.1	Tr	Tr
7-3	32.6	1764602	1615938	3	219	72	1	C/R	2.7	1.9	4.6	Tr	Tr
7-4	34.1	1764601	1615937	3	355	90	10	C/R/B	6.4	7.0	13.4	Sp	Tr
7-5	34.9	1764601	1615936	3	213	13	0	O	0.6	1.2	1.8	Tr	Tr
7-6	35.7	1764601	1615935	3	355	90	1	C	3.3	3.5	6.8	Te	Tr
7-7	37.8	1764600	1615933	3	182	83	6	C/R	5.8	4.0	9.8	Sp	Sp
7-8	39.6	1764600	1615931	3	155	62	2	C	9.8	9.5	19.3	C	C
7-9	41.0	1764599	1615928	3	60	90	2	C/R	5.6	1.3	6.9	Tr	Tr
7-10	47.5	1764598	1615925	3	305	77	10	C/R/B	0.4	3.5	3.9	Sp	C
7-11	51.4	1764597	1615921	3	350	24	1	C	2.8	3.0	5.8	Te	C
7-12	53.4	1764596	1615917	3	141	48	12	C/R	4.0	9.1	13.1	C	C
7-13	57.4	1764595	1615914	3	155	31	1	C	2.8	0.7	3.5	C	Tr
7-14	57.7	1764595	1615914	3	170	44	6	C	3.4	5.0	8.4	C	Sp
7-15	60.0	1764595	1615912	3	222	35	0	O	0.7	0.8	1.5	Tr	Tr
7-16	61.2	1764594	1615910	3	161	51	20	C/R	5.8	8.6	14.4	C	Tr
7-17	63.0	1764594	1615908	3	260	72	15	C/R	1.8	2.9	4.7	Tr	Tr
7-18	65.9	1764593	1615906	3	174	41	2	C	2.9	3.8	6.7	Te	Tr
7-19	67.1	1764593	1615904	3	315	86	15	C/R	3.2	17.1	20.3	C	Tr
7-20	71.4	1764592	1615900	3	326	90	6	C/R/B	1.7	11.0	12.7	Sp	C
7-21	72.1	1764591	1615899	3	250	21	10	C	1.9	5.0	6.9	Tr	Tr
7-22	77.0	1764590	1615895	3	330	73	20	C/R/B	4.7	4.4	9.1	Tr	Tr
7-23	80.3	1764589	1615892	3	239	56	2	C/R	0.8	1.1	1.9	Tr	Tr
7-24	81.0	1764590	1615893	3	240	25	4	C/R	1.9	1.6	3.5	Tr	Tr
7-25	82.9	1764589	1615889	3	318	90	6	C/R/B	16.2	1.2	17.4	C	Tr
7-26	84.6	1764588	1615889	3	16	90	4	C/R	12.8	9.3	22.1	Tr	Sp
7-27	87.9	1764587	1615884	3	330	90	1	C	0.5	5.9	6.4	Sp	Tr
7-28	95.3	1764585	1615877	3	330	90	28	C/R	0.9	13.1	14.0	Sp	C
7-29	96.4	1764585	1615875	3	148	67	1	C	6.2	6.7	12.9	Tr	C
7-30	112.4	1764581	1615861	3	300	73	30	C/R/B	1.5	9.1	10.6	C	C
7-31	113.3	1764581	1615860	3	355	90	60	C/R/B	2.1	1.3	3.4	C	Tr
7-32	115.4	1764580	1615858	3	353	90	10	C/R	1.1	1.6	2.7	C	Te
7-33	116.0	1764580	1615857	3	261	9	2	C/R	1.4	1.3	2.7	C	Tr
7-34	120.6	1764579	1615854	3	178	21	1	C/R	5.8	0.7	6.5	Tr	Tr
7-35	121.0	1764579	1615852	3	155	69	1	C/R	1.9	5.2	7.1	Te	C

Table B-1 Continued. MDA P Fracture Data (notes below)

Traverse 7 Continued

Fracture Number[†]	Distance along traverse (ft)	Coordinates[‡] Northing (ft)	Coordinates[‡] Easting (ft)	Bedrock unit	Strike[#]	Dip	Aperture (mm)	Fracture filling[¥]	Trace length[§] (ft) S	Trace length[§] (ft) N	Total length (ft)	Termination[&] Type: S	Termination[&] Type: N
7-36	122.5	1764578	1615851	3	141	58	2	C/R	0.9	0.7	1.6	Te	Tr
7-37	126.0	1764577	1615847	3	297	71	20	C/R/B	2.4	11.2	13.6	Tr	C
7-38	127.2	1764577	1615846	3	305	90	2	C	2.4	0.3	2.7	Tr	Tr
7-39	128.5	1764577	1615846	3	65	85	2	C	5.2	0.9	6.1	Tr	Sp
7-40	134.5	1764575	1615840	3	323	90	4	C	12.3	3.5	15.8	C	C
7-41	135.7	1764575	1615838	3	301	90	4	C	3.9	2.3	6.2	Tr	C

Aperture (mm): mean: 9; max: 60; min: 1

Trace length (ft): mean: 8.3; max: 22.1; min: 1.5

Fracture density: 30 fractures/100 ft

*Grid points surveyed by LANL ER Project; coordinates are northing and easting in State Plane Coordinate System, New Mexico Central Zone, 1983 North American Datum.
[†]The fracture number is the traverse number followed by the fracture number counting from the beginning of traverse.
[‡]The northing and easting coordinates are of the intersection between the fracture and the traverse.
[#]Fracture orientations are presented according to the right hand rule. Abrreviation: NA, not available.
[¥]Fracture filling abbreviations: B, breccia; C, clay; Ca, cataclasite; F, foliated; O, open; OM, organic matter; OX, oxidized; R, roots; NA, not available.
[§]Trace lengths are measured to the south (S) and to the north (N) of the line of traverse.
[&]Termination abbreviations: C, covered; SP, splays; Te, terminates by dying out; Tr, truncates.

Table B-1 Continued. MDA P Fracture Data (notes on page 74)

Traverse 8, N80E Trend, 57' Total Length — **Start Grid Point 627*: not surveyed** — **End Grid Point 626+27': 1764518, 1615742+27'**

Fracture Number[†]	Distance along traverse (ft)	Coordinates[‡] Northing (ft)	Coordinates[‡] Easting (ft)	Bedrock unit	Strike[#]	Dip	Aperture (mm)	Fracture filling[¥]	Trace length[§] (ft) S	Trace length[§] (ft) N	Total length (ft)	Termination[&] Type: S	Termination[&] Type: N
8-1	3.6	1764526	1615771	3	2	56	2	C	2.2	3.1	5.3	Tr	Tr
8-2	6.3	1764525	1615768	3	3	37	4	C/R/OM	1.1	4.9	6.0	Tr	Tr
8-3	8.0	1764525	1615766	3	300	90	2	C/R	9.4	9.5	18.9	Tr	Sp
8-4	10.8	1764524	1615764	3	161	55	2	C	8.3	3.1	11.4	Tr	Tr
8-5	13.7	1764523	1615761	3	345	36	12	C/R	3.4	3.5	6.9	Tr	Tr
8-6	14.1	1764523	1615761	3	357	53	1	C	3.8	1.9	5.7	Tr	Te
8-7	15.7	1764523	1615759	3	324	76	10	C	3.2	3.4	6.6	Tr	Tr
8-8	16.7	1764523	1615758	3	349	71	1	C	1.2	6.2	7.4	Tr	Tr
8-9	17.8	1764522	1615757	3	353	90	20	C/R/B	8.0	39.7	47.7	Sp	C
8-10	18.5	1764522	1615756	3	141	76	1	C	3.0	13.0	16.0	Tr	Sp
8-11	21.9	1764521	1615753	3	358	90	1	C	1.1	5.1	6.2	Tr	Tr
8-12	23.6	1764521	1615752	3	348	90	2	C	0.5	8.7	9.2	Tr	Sp
8-13	24.4	1764521	1615751	3	299	90	4	C	3.2	16.5	19.7	Sp	Tr
8-14	27.4	1764520	1615748	3	9	63	1	C	3.2	1.9	5.1	Tr	Tr
8-15	28.5	1764520	1615747	3	352	71	1	C	4.5	2.9	7.4	Tr	Tr
8-16	31.7	1764519	1615743	3	275	72	1	C	1.5	1.6	3.1	Te	Tr
8-17	33.7	1764518	1615742	3	30	62	4	C	4.6	6.2	10.8	Tr	Tr
8-18	38.2	1764517	1615738	3	335	62	1	C	2.6	10.9	13.5	Tr	C
8-19	41.4	1764517	1615735	3	293	90	12	C/R/B	14.5	9.3	23.8	Tr	C
8-20	44.4	1764516	1615732	3	15	59	4	C	8.1	1.1	9.2	C	Tr
8-21	47.0	1764515	1615729	3	326	51	2	C/R	6.4	5.7	12.1	C	C
8-22	53.5	1764513	1615723	3	350	44	8	C/OM	2.2	2.4	4.6	Tr	C
8-23	56.9	1764512	1615719	3	338	90	22	C/B/F	8.0	6.1	14.1	C	C

Aperture (mm): mean: 5; max: 22; min: 1

Trace length (ft): mean: 11.8; max: 47.7; min: 3.1

Fracture density: 40 fractures/100 ft

Cumulative for all traverses:

Aperture (mm): mean: 7; max: 100; min: 1

Trace length (ft): mean: 9.4; max: 80.7; min: 1

Fracture density: 24 fractures/100 ft

Table B-2. Eigenvectors and Uncertainties for MDA P Fracture Data

Data Set	Eigenvector*			Eigen-value	Maximum Angle	Minimum Angle	Average Angle	Orientation	Standard Deviation
		Trend	Plunge						
All data	1	353	86	111.2	35.22	5.87	20.54	–0.42	0.2874
N = 454	2	162	4	125.1	35.22	9.17	22.19	–0.26	0.3511
	3	252	1	217.8	9.25	5.78	7.52	–4.79	0.3251
Unit 4	1	161	78	24.2	8.72	4.36	6.54	–1.10	0.2755
N = 212	2	345	12	62.8	10.60	8.60	9.60	6.75	0.3020
	3	255	1	125.0	10.51	4.37	7.44	0.01	0.1667
Unit 3T	1	354	18	31.6	40.69	11.52	26.11	0.02	0.3001
N = 129	2	262	6	39.5	40.74	14.35	27.54	–1.67	0.3539
	3	153	71	57.9	15.06	10.86	12.96	12.39	0.4273
Unit 3	1	331	16	27.7	62.06	14.74	38.40	0.47	0.2721
N = 113	2	141	74	30.4	62.06	13.70	37.88	0.55	0.3487
	3	240	3	54.9	14.87	13.80	14.33	–6.07	0.3291

*For each data set (with *N* data points), trends and plunges of eigenvectors are listed in that section from the smallest to largest eigenvalue (1, 2, 3). For a full explanation of eigenvector analysis, see, for example, Davis (1986) and Hext (1963).

APPENDIX C. TOTAL STATION SURVEY DATA

Table C-1. TA-9 Trench Total Station Survey Data (notes on page 94)

Mapped Contact*	Coordinates†			Comments‡
	Northing (ft)	Easting (ft)	Elevation (ft)	
BTR	1766795.15	1611654.02	7571.04	
BTR	1766773.81	1611691.38	7570.71	
BTR	1766722.11	1611737.76	7569.21	
BTR	1766643.46	1611817.41	7568.39	
BTR	1766605.59	1611853.14	7567.87	
BTR	1766516.14	1611939.65	7562.44	
BTR	1766490.17	1611967.64	7560.04	
BTR	1766470.51	1611990.49	7559.92	
BTR	1766381.11	1612090.21	7555.45	
BTR	1766284.09	1612198.29	7552.34	
BTR	1766271.19	1612211.51	7551.43	
BTR	1766229.80	1612262.10	7551.63	
BTR	1766184.69	1612348.54	7551.16	
BTR	1766149.45	1612418.28	7550.24	
BTR	1766129.87	1612456.33	7549.20	
BTR	1766122.07	1612470.06	7549.08	
BTR	1766109.54	1612494.43	7549.25	
BTR	1766098.11	1612517.31	7548.44	
BTR	1766034.92	1612640.95	7546.73	
BTR	1765978.38	1612750.07	7544.16	
BTR	1765958.96	1612786.97	7543.36	
BTR	1765942.91	1612817.33	7542.88	
BTR	1765938.59	1612826.32	7542.02	
BTR	1765915.78	1612870.38	7541.21	
BTR	1765909.05	1612884.52	7540.95	
BTR	1765816.26	1613068.02	7541.73	
BTR	1765777.42	1613211.81	7538.68	
BTR	1765769.76	1613265.71	7536.33	
BTR	1765768.87	1613270.55	7536.42	
BTR	1765747.31	1613399.42	7534.15	
BTR	1765736.53	1613468.86	7535.11	
BTR	1765732.88	1613491.74	7535.36	
BTR	1765724.10	1613545.76	7534.18	
BTR	1765714.64	1613605.49	7533.00	
BTR	1765699.88	1613692.29	7529.54	
BTR	1765680.60	1613782.60	7527.51	

Table C-1 Continued. TA-9 Trench Total Station Survey Data (notes on page 94)

Mapped Contact*	Coordinates†			Comments‡
	Northing (ft)	Easting (ft)	Elevation (ft)	
BTR	1765660.07	1613906.07	7522.97	
BTR	1765649.18	1613999.39	7519.55	
BTR	1765634.95	1614090.61	7516.62	
BTR	1765617.80	1614172.38	7514.06	
BTR	1765598.83	1614296.40	7509.99	
BTR	1765596.81	1614336.61	7508.28	
BTR	1765582.02	1614407.24	7506.25	
BTR	1765565.36	1614517.38	7505.58	
BTR	1765553.57	1614616.79	7505.55	
BTR	1765519.78	1614804.71	7508.84	
BTR	1765489.11	1614986.79	7510.06	
BTR	1765488.36	1614998.05	7510.20	
BTR	1765469.73	1615248.26	7506.40	
BTR	1765483.36	1615285.36	7506.25	
BTR	1765516.58	1615373.10	7503.88	
BTR	1765534.45	1615406.28	7503.30	
BTR	1765538.05	1615415.07	7503.03	
BTR	1765618.71	1615619.79	7501.21	
BTR	1765648.25	1615701.23	7499.21	
F	1765938.59	1612826.32	7545.82	S55W 80NE; fracture zone 0.3 m (1 ft) wide
F	1765928.42	1612846.02	7545.56	N42E 66SE
F	1765915.78	1612870.38	7545.21	N15E 85–90NW
F	1765908.03	1612888.39	7544.92	N15E > 60NW; fissure fill 0.8 m (2.5 ft) wide with clay-rich matrix and Qbt blocks
F	1765899.76	1612903.11	7544.70	S55W 90
F	1765897.34	1612908.10	7544.60	N65E 90
F	1765893.27	1612915.60	7544.45	N15W 90
F	1765882.09	1612938.91	7544.94	S15W 90
F	1765860.84	1612977.50	7546.03	N12E 68NW
F	1765853.84	1612991.71	7545.88	N60E > 60SE; fissure fill 0.9 m (3 ft) wide
F	1765850.90	1612997.91	7546.05	N20W; fissure fill
F	1765846.14	1613007.49	7545.89	N55E > 45SE; fissure fill
F	1765816.26	1613066.02	7545.73	
F	1765814.05	1613070.50	7545.70	
F	1765808.27	1613081.65	7545.36	N50E 90
F	1765806.40	1613086.17	7545.27	N30W > 45NE
F	1765787.69	1613126.20	7544.92	N80E 85–90NW

Table C-1 Continued. TA-9 Trench Total Station Survey Data (notes on page 94)

Mapped Contact*	Coordinates†			Comments‡
	Northing (ft)	Easting (ft)	Elevation (ft)	
F	1765790.53	1613132.63	7544.46	N7W 90; graben/fissure fill 0.5 m (1.5 ft) wide; no tuff in bottom
F	1765786.18	1613135.55	7544.74	N35W 86SW
F	1765785.10	1613164.50	7543.77	
F	1765778.27	1613207.66	7542.39	N70W 74SW
F	1765777.42	1613211.81	7542.28	N14W 90; fissure fill 0.6 m (2 ft) wide
F	1765775.74	1613224.92	7541.95	N20E 66SW; fissure fill < 0.3 m (1 ft) wide
F	1765774.64	1613229.97	7541.86	N5W 90; fissure 1.5 m (5 ft) wide at T-C and 0.3 m (1 ft) in tuff
F	1765772.53	1613242.39	7541.27	N5W 90; fissure 1.5 m (5 ft) wide at T-C and 0.3 m (1 ft) in tuff
F	1765768.16	1613244.88	7541.68	N20W 80SW; fissure fill
F	1765771.89	1613248.85	7541.00	N70E 85SE; fissure fill
F	1765767.44	1613251.81	7541.05	N13E 86NW
F	1765766.69	1613257.35	7540.96	N70W 90
F	1765770.12	1613259.31	7540.62	N55W 52SW
F	1765766.17	1613260.95	7540.85	N17E 87SE
F	1765769.76	1613265.71	7540.33	N28W 28–75SW
F	1765768.87	1613270.55	7540.12	N37E 44–87NW; alluvium 0.5 m (1.5 ft) thick over tuff
F	1765766.56	1613285.20	7539.16	N3E 72SE
F	1765766.28	1613287.88	7539.39	N27E 84NW
F	1765763.06	1613308.58	7538.32	N3W 90
F	1765759.97	1613324.03	7537.67	N20W 85–90SW
F	1765759.61	1613328.66	7537.97	N15W 70NE; W side of channel incised into top of tuff; channel fill up to 0.9 m (3 ft) thick
F	1765758.58	1613333.97	7537.99	N20W 90; E side of channel
F	1765755.76	1613350.55	7538.10	center of 0.9-m (3-ft) wide rubble zone; clay-filled shear planes N15W 80SW and N50E 70NW
F	1765751.57	1613375.74	7538.00	N60E 68NW
F	1765750.95	1613378.15	7538.00	N37E 87NW; fissure fill
F	1765749.18	1613388.20	7538.01	N3W 55NE
F	1765749.18	1613390.20	7538.01	
F	1765551.68	1614633.96	7509.78	
F	1765550.17	1614637.16	7510.15	N15E 85SE; clay-filled fracture
F	1765548.75	1614647.65	7510.48	clay-filled fracture; 18.3-cm (7.2-in) wide fissure with large block in clay
F	1765547.94	1614653.27	7510.62	N4W 84NE; clay-filled fracture

Table C-1 Continued. TA-9 Trench Total Station Survey Data (notes on page 94)

Mapped Contact*	Coordinates†			Comments‡
	Northing (ft)	Easting (ft)	Elevation (ft)	
F	1765546.42	1614659.44	7510.70	
F	1765543.02	1614674.01	7510.76	
F	1765540.27	1614690.03	7510.98	
F	1765538.12	1614701.89	7511.18	N5W 36NE; rubble zone 0.6 m (2 ft) thick at top to 5 cm (2 in) at base
F	1765536.09	1614715.77	7511.21	N7E 82–85NW; center of 1.3-m (4.3-ft) wide fissure
F	1765530.08	1614748.34	7511.88	N5W 83NE; 6-cm (2.4-in) wide clay-filled fracture
F	1765525.98	1614756.21	7512.00	N2W 78SW; brecciated but no apparent offset; 3-cm (1.2-in) thick clay
F	1765528.49	1614759.01	7511.94	N7W 57NE; fissure
F	1765524.39	1614766.60	7512.18	N60W 89SW; 3-cm (1.2-in) thick clay
F	1765523.79	1614770.79	7512.15	N13E 37SE; 5-cm (2-in) thick clay
F	1765522.20	1614778.99	7512.20	
F	1765521.05	1614786.50	7512.28	N5W 85SW; 27-cm (11-in) wide brecciated zone
F	1765520.79	1614786.87	7512.25	N30W 33SW
F	1765522.93	1614791.87	7512.26	N10E 86SE
F	1765522.66	1614794.37	7512.31	
F	1765521.40	1614802.37	7512.61	
F	1765520.45	1614806.01	7511.85	N25E 30SE
F	1765519.53	1614814.61	7512.96	N35E 83NW; 0.3-m (1-ft) wide fissure
F	1765517.02	1614827.88	7513.12	N5E 68SE
F	1765516.91	1614830.19	7513.06	2.5-cm (1-in) wide hackly fracture with no apparent offset
F	1765515.51	1614838.50	7513.31	
F	1765509.44	1614854.52	7513.52	
F	1765503.31	1614908.51	7513.47	N36W 54NE
F	1765501.59	1614918.86	7513.14	N28W 90
F	1765500.50	1614926.52	7513.00	N25W 82SW; clay-filled fracture
F	1765496.20	1614954.00	7513.05	
F	1765494.86	1614959.80	7511.54	N33W 73NE
F	1765492.11	1614978.01	7513.32	
F	1765490.23	1614991.08	7513.26	N30W 85–90SW; fissure filled with 5 cm (2 in) clay
F	1765485.89	1615017.20	7513.00	N7E 90; fissure 0.5 m (1.6 ft) wide at T-C to 5 cm (2 in) wide in tuff at base; filled with silt
F	1765484.26	1615025.27	7512.77	N10E 85–90SE; T-C undulates 0.5 m (1.5 ft) for 5 m (16.4 ft) E of here

Table C-1 Continued. TA-9 Trench Total Station Survey Data (notes on page 94)

Mapped Contact*	Coordinates†			Comments‡
	Northing (ft)	Easting (ft)	Elevation (ft)	
F	1765480.66	1615046.99	7512.25	N20E 22NW; 2.5-cm (1-in) wide clay-filled fracture; next to 2–3 other fractures
F	1765480.10	1615050.43	7512.14	N32E 90; 10-cm (4-in) wide clay filled
F	1765478.90	1615058.15	7512.14	N8E 34NW clay-filled fracture and N8W 67NE 15-cm (6-in) wide clay-filled fracture
F	1765476.59	1615070.11	7509.79	N25W 17SW
F	1765476.40	1615071.60	7509.96	N65W 87NE
F	1765544.29	1615431.54	7507.25	N70W 48NE; 15 cm (6 in) wide at T-C; W edge of cobbly Holocene colluvium
F	1765581.72	1615526.33	7505.29	N50E 55SE
F	1765590.08	1615546.81	7507.14	colluvium 0.7–1.0 m (2.4–3.4 ft) thick
F	1765607.07	1615597.35	7501.93	N2W 90; fissure 12 cm (4.8 in) wide
F	1765612.82	1615605.23	7505.70	N75W vertical to steep NE; fissure 2.5–6.4 cm (1–2.5 in) wide
F	1765618.71	1615619.79	7505.11	N2E 90; fissure 0.3 m (1 ft) wide filled with sandy orange silt; tuff bleached to 2.5 cm (1 in) depth
F	1765679.36	1615782.82	7500.59	N33W 62NE
F	1765686.71	1615795.57	7500.55	N36E 90
F	1765699.06	1615826.73	7500.18	N18W 52NE; U-shaped fracture; 3 m (10 ft) wide
F	1765709.84	1615852.65	7499.69	N10E 85SE; fracture filled with silty clay
F	1765713.96	1615864.82	7499.68	N20W 80NE; fracture 5 cm (2 in) wide
F	1765723.47	1615890.36	7499.61	
F	1765730.14	1615906.60	7499.24	N48E 68SE; fissure filled with sandy silt
F	1765729.79	1615911.22	7496.93	N20W 90; fissure at T-C 15 cm (6 in) wide filled with clayey sand
F	1765740.02	1615935.55	7497.92	N6E 65SE; fissure < 14 cm (5.4 in) wide; lower 0.5 m (1.5 ft) clay filled; upper part, sand and tuff
F	1765745.04	1615945.12	7493.99	0.3-m (1-ft) wide fissure with angular tuff blocks in clay; 3 main vertical fractures in zone
F	1765751.57	1615970.17	7496.91	N23E 88–90SE; fracture 10.2 cm (4 in) wide filled with Holocene colluvium
G	1765508.86	1614893.01	7513.42	
S	1765767.29	1616007.92	7490.03	sample from 0.6 m (2 ft) above surge within Unit 4
S	1765768.86	1616012.29	7487.05	sample from below surge
S	1765807.84	1616121.73	7457.31	sample of tuff
S4	1765772.83	1616015.44	7488.23	attitude on surge within Unit 4: N20W 3SW

Table C-1 Continued. TA-9 Trench Total Station Survey Data (notes on page 94)

Mapped Contact*	Coordinates† Northing (ft)	Easting (ft)	Elevation (ft)	Comments‡
STRAT	1766643.46	1611817.41	7570.39	top of pumice-rich gravel
STRAT	1766516.14	1611939.65	7563.74	top of pumice with prominent Bt lamellae; base of pumice at base of trench
STRAT	1766470.51	1611990.49	7561.22	base of reworked pumice with prominent Bt lamellae
STRAT	1766381.11	1612090.21	7558.95	base of reworked pumice with prominent Bt lamellae, 0.6 m (1.8 ft) thick
STRAT	1766322.50	1612155.77	7553.94	base of channel
STRAT	1766271.19	1612211.51	7553.93	top of white ashy unit
STRAT	1766129.87	1612451.33	7551.70	top of 3-m (10-ft) wide pocket of coarse cobbles, maximum 0.3-m (1-ft) diameter of Tschicoma dacite and even more Qbt
STRAT	1766122.07	1612470.06	7551.38	top of pocket of coarse cobbles, maximum 0.3-m (1-ft) diameter Tschicoma dacite and even more Qbt
STRAT	1766109.54	1612494.43	7550.85	top of cobble gravel
STRAT	1766098.11	1612517.31	7549.04	top of cobble gravel
STRAT	1766034.92	1612640.95	7547.53	top of ashy fine clay-rich unit
STRAT	1766034.92	1612640.95	7548.23	top of fine clay-rich unit; base organic A horizon developed on loess
STRAT	1765978.38	1612750.07	7544.66	top of silty ashy orange unit; base pebbly unit
STRAT	1765978.38	1612750.07	7546.06	top of pebbly unit; base organic rich unit
STRAT	1765958.96	1612786.97	7544.56	top of orange silty unit; base ashy unit
STRAT	1765958.96	1612786.97	7545.86	top of ashy unit; base dirt
STRAT	1765942.91	1612817.33	7544.18	top of orange silty unit; base white ashy unit
STRAT	1765942.91	1612817.33	7544.88	top of white ashy unit; base dirt
STRAT	1765899.76	1612903.11	7544.70	western edge of black organic-rich sediments
STRAT	1765897.34	1612908.10	7543.10	bottom of organic-rich sediments
STRAT	1765743.14	1613428.00	7534.38	tuff dives below base of trench here; to E > 1.2-m (4-ft) thick alluvium
STRAT	1765736.53	1613468.86	7538.11	top of dk orange to brownish orange massive f sparse pebbles
STRAT	1765736.53	1613468.86	7538.71	top f whitish unit; base Holocene organic-rich duff
STRAT	1765732.88	1613491.74	7536.16	top of f sandy orange; base orange massive unit
STRAT	1765732.88	1613491.74	7537.36	base of white ashy unit
STRAT	1765732.88	1613491.74	7537.56	base of organic-rich dk brn massive unit
STRAT	1765732.88	1613491.74	7538.66	base of white f loess

Table C-1 Continued. TA-9 Trench Total Station Survey Data (notes on page 94)

Mapped Contact*	Coordinates†			Comments‡
	Northing (ft)	Easting (ft)	Elevation (ft)	
STRAT	1765732.88	1613491.74	7538.86	base of Holocene duff
STRAT	1765724.10	1613545.76	7534.78	top of lt orange v f sand with sparse pebbles; base of white ashy unit
STRAT	1765724.10	1613545.76	7535.28	top of white ashy unit; base of dk orange massive unit
STRAT	1765724.10	1613545.76	7537.08	top of dk orange massive unit; base of lt gray to white f-grained unit
STRAT	1765724.10	1613545.76	7537.28	top of lt gray to white f-grained unit; base of massive, f clay-rich orange unit
STRAT	1765714.64	1613605.49	7533.30	top of white ashy unit; base of lt orange v f unit that becomes massive up-section
STRAT	1765714.64	1613605.49	7534.60	base of dk to lt orange massive unit
STRAT	1765714.64	1613605.49	7536.00	base of lt gray to v lt orange loess
STRAT	1765699.88	1613692.29	7530.14	top of f to pebbly lt orange sand; base dk orange massive unit
STRAT	1765699.88	1613692.29	7531.94	base of lt orange f massive unit
STRAT	1765699.88	1613692.29	7532.84	base of lt gray to lt orange Holocene Bt horizon
STRAT	1765680.60	1613782.60	7528.11	top of v dk brn orange clay-rich unit; base of v lt orange pebbly gravel (sample white ashy unit)
STRAT	1765680.60	1613782.60	7529.11	base of dk orange massive clayey unit
STRAT	1765680.60	1613782.60	7530.51	base of lt gray to lt orange Holocene Bt horizon
STRAT	1765660.07	1613906.07	7524.17	top of v coarse lam'd sand with f pebbles (abundant small pumice); base of gravel lens
STRAT	1765660.07	1613906.07	7524.47	top of gravel lens with sparse pebbles up to 0.3 m (1 ft) long; color change from lt to dk orange
STRAT	1765660.07	1613906.07	7525.87	base of lt orange to grey unit
STRAT	1765660.07	1613906.07	7526.87	base of lt grey to lt orange Holocene Bt horizon
STRAT	1765649.18	1613999.39	7520.25	top of v coarse lam'd sand with f pebbles (abundant small pumice); base of choc brn clayey unit
STRAT	1765649.18	1613999.39	7520.45	base of lt orange sandy, powdery v f sand unit
STRAT	1765649.18	1613999.39	7521.25	base of med orange brn f sand with some gravel
STRAT	1765649.18	1613999.39	7522.45	base of lt gray to lt orange Holocene Bt horizon
STRAT	1765634.95	1614090.61	7517.32	top of v f lt orange sand (mottled lt to dk orange); base of lt to dk orange mottled silt
STRAT	1765634.95	1614090.61	7518.42	base of lt brn orange massive silt with 2% small gravel
STRAT	1765634.95	1614090.61	7519.32	base of lt gray to lt orange Holocene Bt horizon with 3–4-mm laminae

Table C-1 Continued. TA-9 Trench Total Station Survey Data (notes on page 94)

Mapped Contact*	Coordinates†			Comments‡
	Northing (ft)	Easting (ft)	Elevation (ft)	
STRAT	1765617.80	1614172.38	7514.96	top of v f lt orange massive hard sand; base of lt orange to choc brn mottled gravel
STRAT	1765617.80	1614172.38	7516.16	base of choc brn massive silt with 1–3% gravel
STRAT	1765617.80	1614172.38	7516.96	base of massive lt orange brn eolian silt
STRAT	1765617.80	1614172.38	7517.46	base of lt gray to lt orange Holocene Bt horizon with 3–4-mm laminae
STRAT	1765598.83	1614296.40	7510.59	top of v f choc brn wet sand; base of v f lt orange sand
STRAT	1765598.83	1614296.40	7511.09	base of massive v f med orange sand
STRAT	1765598.83	1614296.40	7511.99	base of lt orange to med orange platy porous and striped (from root mats) unit
STRAT	1765598.83	1614296.40	7512.19	base of choc brn massive silty clay
STRAT	1765598.83	1614296.40	7512.59	base of lt orange-brn massive eolian silt
STRAT	1765598.83	1614296.40	7513.19	base of lt orange-brn massive platy eolian silt
STRAT	1765596.81	1614336.61	7509.98	top of dk orange to choc brn massive unit with good peds; base of v lt gray to lt gray porous unit
STRAT	1765596.81	1614336.61	7510.38	base of unit grading from v lt orange at base to v dk orange at top
STRAT	1765596.81	1614336.61	7510.88	base of unit grading into black organic bog deposit
STRAT	1765596.81	1614336.61	7511.88	base of v lt orange stripped Holocene Bt horizon
STRAT	1765582.02	1614407.24	7507.25	top of v dk brn orange to choc brn clay-rich unit; base of black organic-rich deposit
STRAT	1765582.02	1614407.24	7508.15	base of unit grading from v dk gray to dk orange silt
STRAT	1765582.02	1614407.24	7509.55	base of v lt orange silty Holocene Bt horizon
STRAT	1765565.36	1614517.38	7505.88	top of v dk brn orange to choc brn clay-rich unit; base of black organic-rich deposit
STRAT	1765565.36	1614517.38	7507.38	base of unit grading from v dk gray to dk orange silt
STRAT	1765565.36	1614517.38	7508.58	base of v lt gray silty competent loess
STRAT	1765553.57	1614616.79	7506.75	base of unit with silt to f sand matrix and 15–25% gravel—large dacite and tuff clasts up to 15 cm (6 in)
STRAT	1765553.57	1614616.79	7507.75	base of massive choc brn v clayey unit with 10% gravel [clasts up to 15 cm (6 in) on long axis]
STRAT	1765553.57	1614616.79	7508.05	base of porous lt brn silty loess with cobbles up to 7.6 cm (3 in) long

Table C-1 Continued. TA-9 Trench Total Station Survey Data (notes on page 94)

Mapped Contact*	Coordinates†			Comments‡
	Northing (ft)	Easting (ft)	Elevation (ft)	
STRAT	1765553.57	1614616.79	7508.55	base of fill
STRAT	1765469.73	1615248.26	7507.90	top of mottled lt orange to orange massive silt with med-coarse sand; base of lt orange silt
STRAT	1765469.73	1615248.26	7508.30	base of brownish orange massive clay-rich porous silt with 2–3% sand with roots; pinches out to the W
STRAT	1765469.73	1615248.26	7509.40	base of lt orange massive eolian silt
STRAT	1765469.73	1615248.26	7509.80	base of grayish orange platy silt
STRAT	1765483.36	1615285.36	7508.95	top of brn orange massive clayey porous unit; base of massive lt orange eolian silt
STRAT	1765483.36	1615285.36	7509.25	base of greyish orange platy silt
STRAT	1765516.58	1615373.10	7503.88	top of pumice-rich lt orange–med brn unit with 50% pumice (same stratigraphic position as white ashy); base is massive
STRAT	1765516.58	1615373.10	7503.88	top of massive dk brn base to lt orange top silty sandy 5–10% pumice; base of lt orange eolian silt
STRAT	1765516.58	1615373.10	7503.88	base of lt brn platy silt
STRAT	1765538.05	1615415.07	7504.53	base of sandy unit with 10–30% clayey matrix
STRAT	1765538.05	1615415.07	7504.93	base of red-brn clayey-silty mottled unit
T-C	1765942.91	1612817.33	7543.08	
T-C	1765938.59	1612825.02	7543.22	
T-C	1765937.60	1612825.88	7543.66	
T-C	1765938.59	1612827.02	7542.72	
T-C	1765927.61	1612845.13	7544.16	
T-C	1765916.54	1612867.14	7544.38	
T-C	1765909.05	1612884.52	7542.95	
T-C	1765905.81	1612890.47	7544.29	
T-C	1765893.27	1612915.60	7542.15	
T-C	1765884.34	1612932.69	7544.08	organic-rich sediments 24 cm (9.6 in) thick over tuff
T-C	1765882.09	1612938.91	7543.24	
T-C	1765867.64	1612964.54	7544.35	
T-C	1765860.84	1612977.50	7544.53	
T-C	1765853.49	1612990.68	7545.62	
T-C	1765851.92	1612994.00	7543.51	
T-C	1765849.69	1612998.28	7542.56	
T-C	1765847.05	1613004.04	7545.56	

Table C-1 Continued. TA-9 Trench Total Station Survey Data (notes on page 94)

Mapped Contact*	Coordinates†			Comments‡
	Northing (ft)	Easting (ft)	Elevation (ft)	
T-C	1765845.56	1613006.08	7545.33	alluvium 0.3 m (1 ft) thick over tuff in brecciated zone with slabby tuff in orange matrix
T-C	1765825.43	1613046.55	7543.60	alluvium 0.76 m (2.5 ft) thick over tuff
T-C	1765816.26	1613065.02	7543.43	
T-C	1765796.63	1613101.84	7542.63	alluvium 0.9 m (3 ft) thick over tuff
T-C	1765777.42	1613210.81	7540.18	
T-C	1765769.76	1613265.71	7539.13	
T-C	1765768.87	1613270.55	7538.62	
T-C	1765747.31	1613399.42	7535.95	clay-rich alluvium over tuff
T-C	1765553.57	1614616.79	7505.95	base of lt orange to med orange v coarse sand with 5–10% pumice and 90–95% crystals; v porous
T-C	1765548.00	1614624.97	7506.90	
T-C	1765547.26	1614631.00	7507.77	
T-C	1765550.17	1614637.16	7508.65	
T-C	1765545.36	1614642.33	7509.31	
T-C	1765545.01	1614644.26	7509.45	
T-C	1765547.94	1614653.27	7509.12	
T-C	1765543.18	1614656.53	7509.65	
T-C	1765543.06	1614657.20	7509.01	
T-C	1765542.37	1614661.04	7509.69	
T-C	1765540.85	1614669.74	7510.19	
T-C	1765543.02	1614674.01	7510.56	
T-C	1765542.23	1614674.82	7510.13	
T-C	1765539.12	1614679.79	7510.36	vertical fracture
T-C	1765538.71	1614682.07	7510.14	
T-C	1765538.59	1614682.73	7509.20	
T-C	1765538.58	1614683.39	7510.24	
T-C	1765536.40	1614696.40	7510.16	
T-C	1765534.13	1614709.70	7510.90	
T-C	1765533.41	1614713.69	7510.68	
T-C	1765533.34	1614714.49	7510.16	
T-C	1765533.14	1614715.63	7510.85	
T-C	1765532.81	1614718.55	7511.01	
T-C	1765532.41	1614719.54	7510.47	
T-C	1765531.97	1614722.54	7510.77	
T-C	1765531.06	1614729.28	7509.98	
T-C	1765530.86	1614729.62	7509.62	fissure 9.1 cm (3.6 in) wide

Table C-1 Continued. TA-9 Trench Total Station Survey Data (notes on page 94)

Mapped Contact*	Coordinates†			Comments‡
	Northing (ft)	Easting (ft)	Elevation (ft)	
T-C	1765530.78	1614730.08	7509.43	fissure 9.1 cm (3.6 in) wide
T-C	1765529.38	1614737.95	7510.61	
T-C	1765529.38	1614738.42	7511.11	fault?; rubble zone in tuff
T-C	1765528.53	1614744.22	7511.46	
T-C	1765529.72	1614748.27	7511.29	
T-C	1765529.54	1614749.47	7511.60	
T-C	1765529.17	1614751.47	7511.46	
T-C	1765528.63	1614754.30	7511.03	
T-C	1765526.32	1614755.87	7511.11	
T-C	1765528.13	1614757.86	7511.11	tuff is brecciated in 0.6-m (2-ft) wide crushed zone
T-C	1765527.68	1614759.32	7510.79	W side brecciated zone
T-C	1765527.63	1614760.84	7510.84	E side brecciated zone
T-C	1765527.64	1614761.09	7511.26	E side brecciated zone
T-C	1765527.12	1614764.57	7511.27	
T-C	1765524.69	1614767.26	7510.83	
T-C	1765523.18	1614776.72	7511.54	alluvium 20 cm (7.9 in) thick over tuff
T-C	1765522.65	1614779.50	7511.31	
T-C	1765522.06	1614783.20	7510.84	alluvium 0.46 m (1.5 ft) thick over tuff
T-C	1765521.74	1614785.46	7509.97	
T-C	1765521.54	1614786.55	7511.06	
T-C	1765522.97	1614790.06	7511.97	
T-C	1765521.48	1614799.06	7511.98	
T-C	1765521.12	1614800.45	7511.09	
T-C	1765520.93	1614801.53	7510.46	
T-C	1765520.71	1614802.38	7509.61	
T-C	1765520.70	1614802.78	7510.90	
T-C	1765520.73	1614804.38	7512.15	
T-C	1765520.28	1614806.87	7511.89	fissure
T-C	1765519.20	1614813.73	7512.15	fissure
T-C	1765518.79	1614815.15	7511.91	
T-C	1765518.76	1614815.67	7511.71	
T-C	1765518.46	1614819.01	7512.62	
T-C	1765516.54	1614829.20	7512.54	
T-C	1765515.51	1614838.50	7512.11	
T-C	1765502.69	1614908.89	7512.37	
T-C	1765500.01	1614926.15	7511.37	tuff overlain by rubbly Holocene colluvium
T-C	1765496.66	1614935.01	7509.95	bottom of channel incised into tuff

Table C-1 Continued. TA-9 Trench Total Station Survey Data (notes on page 94)

Mapped Contact*	Coordinates†			Comments‡
	Northing (ft)	Easting (ft)	Elevation (ft)	
T-C	1765498.27	1614938.16	7510.28	
T-C	1765497.78	1614942.17	7510.98	
T-C	1765496.94	1614946.75	7511.11	
T-C	1765496.74	1614948.35	7511.68	W edge of zone of subhorizontal fractures that create slabby tuff
T-C	1765496.27	1614951.92	7512.14	
T-C	1765495.34	1614956.43	7511.92	
T-C	1765494.84	1614959.05	7512.06	
T-C	1765493.99	1614962.92	7511.58	
T-C	1765493.53	1614965.54	7511.48	
T-C	1765492.68	1614971.09	7511.47	
T-C	1765491.91	1614976.08	7511.33	
T-C	1765491.30	1614980.48	7511.29	
T-C	1765490.39	1614984.81	7512.08	
T-C	1765490.01	1614987.40	7511.93	
T-C	1765489.42	1614991.07	7511.30	silt 18 cm (7 in) thick overlain by Holocene colluvium
T-C	1765488.39	1614997.92	7512.06	
T-C	1765479.44	1615051.36	7510.84	
T-C	1765477.22	1615065.22	7511.05	
T-C	1765476.70	1615067.80	7510.39	
T-C	1765475.89	1615074.33	7510.02	
T-C	1765474.97	1615079.00	7510.54	
T-C	1765459.56	1615185.50	7508.52	domino blocks and clay-filled fractures N10W 44SW and N15E 50NW
T-C	1765459.56	1615217.73	7507.29	T-C disappears under base of trench
T-C	1765534.45	1615406.28	7503.30	tuff appears at base of trench
T-C	1765538.05	1615415.07	7504.13	base angular to subangular cobbles up to 0.6 m (2 ft) long in silty-clayey matrix
T-C	1765544.29	1615431.54	7505.45	
T-C	1765554.32	1615464.55	7503.09	base of trench
T-C	1765557.41	1615472.61	7504.15	
T-C	1765561.85	1615483.27	7504.11	
T-C	1765567.15	1615495.91	7503.77	tuff overlain by cobbly colluvium with blocks up to 0.51 m (1.7 ft) long imbricated towards west
T-C	1765572.94	1615510.01	7504.04	
T-C	1765576.45	1615518.54	7504.36	blocks of tuff up to 0.85 m (2.8 ft) long in colluvium over tuff

Table C-1 Continued. TA-9 Trench Total Station Survey Data (notes on page 94)

Mapped Contact*	Coordinates†			Comments‡
	Northing (ft)	Easting (ft)	Elevation (ft)	
T-C	1765597.17	1615574.15	7503.16	colluvium 1.1 m (3.5 ft) thick on S side and 0.57 m (1.9 ft) thick on N side
T-C	1765601.46	1615584.10	7502.54	colluvium 1.2 m (3.9 ft) thick
T-C	1765618.71	1615619.79	7504.81	
T-C	1765623.32	1615638.67	7501.57	colluvium 0.98 m (3.2 ft) thick on S side of trench, 0.54 m (1.8 ft) on N side; blocks up to 0.79 m (2.6 ft) long
T-C	1765631.99	1615655.73	7502.58	possible low angle fault N50W 25SW; clay layer and colluvium on top on S side, tuff blk on N side
T-C	1765635.61	1615671.36	7501.06	colluvium 0.7 m (2.3 ft) thick with blocks of tuff up to 1.2 m (3.8 ft) long
T-C	1765645.10	1615690.97	7500.47	colluvium 0.73 m (2.4 ft) thick on N side, 0.98 m (3.2 ft) thick on S side
T-C	1765659.17	1615725.08	7500.64	
T-C	1765662.45	1615733.03	7500.21	N32W 74NE; rare clay-filled fracture
T-C	1765668.79	1615749.02	7500.81	middle of 3-m (10-ft) wide zone of massive structureless tuff
T-C	1765676.97	1615769.16	7499.62	N61W 25SW and N27E 28SE; clay-filled fractures
T-C	1765686.71	1615795.57	7500.55	colluvium < 9.1 cm (3.6 in) thick
T-C	1765692.49	1615811.71	7499.70	N48W 60NE; fracture
T-C	1765697.49	1615823.05	7500.23	colluvium 0.3–0.5 m (1–1.5 ft) thick
T-C	1765704.73	1615840.09	7499.84	colluvium 0.33 m (1.1 ft) thick on N, 0.49 m (1.6 ft) thick on S
T-C-F	1765546.86	1614633.30	7507.99	
T-C-F	1765546.96	1614633.65	7508.23	
T-C-F	1765544.60	1614647.33	7507.90	clay-filled fissure 24.4 cm (9.6 in) wide
T-C-F	1765544.48	1614648.54	7509.41	clay-filled fissure 24.4 cm (9.6 in) wide
T-C-F	1765543.78	1614651.55	7509.55	
T-C-F	1765543.75	1614652.19	7509.02	
T-C-F	1765541.64	1614665.05	7510.21	
T-C-F	1765541.73	1614665.45	7509.74	
T-C-F	1765540.26	1614673.43	7509.64	
T-C-F	1765540.17	1614673.98	7510.06	
T-C-F	1765539.73	1614676.67	7510.47	
T-C-F	1765539.50	1614677.64	7510.18	
T-C-F	1765537.57	1614689.01	7510.94	

Table C-1 Continued. TA-9 Trench Total Station Survey Data (notes on page 94)

Mapped Contact*	Coordinates†			Comments‡
	Northing (ft)	Easting (ft)	Elevation (ft)	
T-C-F	1765537.49	1614689.97	7510.23	
T-C-F	1765536.32	1614696.83	7509.70	
T-C-F	1765535.84	1614699.25	7510.05	
T-C-F	1765535.50	1614701.76	7510.37	
T-C-F	1765525.36	1614761.87	7511.32	
T-C-F	1765524.69	1614766.90	7510.36	
T-C-F	1765524.01	1614772.23	7510.18	
T-C-F	1765523.80	1614772.84	7510.62	alluvium (?) 0.42 m (1.4 ft) thick over tuff
T-C-F	1765522.81	1614778.68	7511.23	N60E 66NW; clay-filled fracture 0.46 m (1.5 ft) wide
T-C-F	1765522.24	1614782.08	7510.76	
T-C-F	1765522.66	1614791.69	7511.74	
T-C-F	1765522.44	1614792.31	7511.41	
T-C-F	1765522.14	1614794.35	7510.36	
T-C-F	1765517.73	1614822.25	7512.55	N38E 55SE; fracture
T-C-F	1765517.61	1614822.85	7511.76	N38E 55SE; fracture
T-C-F	1765517.19	1614825.75	7512.22	
T-C-F	1765516.89	1614826.33	7511.93	
T-C-F	1765516.75	1614827.89	7511.81	N5E 68SE; fault
T-C-F	1765501.03	1614919.19	7511.86	
T-C-F	1765500.95	1614919.87	7512.36	
T-C-F	1765491.56	1614978.09	7510.82	
TTR	1766795.15	1611654.02	7575.04	alluvium > 1.2 m (4 ft) thick
TTR	1766773.81	1611691.38	7574.71	alluvium > 1.2 m (4 ft) thick
TTR	1766722.11	1611737.76	7573.21	alluvium > 1.2 m (4 ft) thick
TTR	1766643.46	1611817.41	7572.09	sediments 1.1 m (3.7 ft) thick; pumice-rich gravel at 0.6 m (1.7 ft) depth
TTR	1766605.59	1611853.14	7571.47	alluvium 1.1 m (3.6 ft) thick
TTR	1766516.14	1611939.65	7565.94	pumice with prominent Bt lamellae at 0.54-m (2.2-ft) depth to base of trench; truncated just E of point
TTR	1766490.17	1611967.64	7564.33	
TTR	1766470.51	1611990.49	7563.42	top 0.67 m (2.2 ft) is reworked pumice with prominent Bt lamellae
TTR	1766381.11	1612090.21	7558.95	massive red clayey sediment; 0.54-m (1.8-ft) thick pumice deposit with Bt lamellae
TTR	1766322.50	1612155.77	7556.94	center of coarse gravel with Tschicoma dacite gravels > 0.3-m (1-ft) diameter; 0.9 m (3 ft) thick

Table C-1 Continued. TA-9 Trench Total Station Survey Data (notes on page 94)

Mapped Contact*	Coordinates†			Comments‡
	Northing (ft)	Easting (ft)	Elevation (ft)	
TTR	1766284.09	1612198.29	7555.54	white ashy unit in bottom 0.3 m (1 ft); pinches out W but thickens E
TTR	1766271.19	1612211.51	7555.13	white ashy unit is 0.76 m (2.5 ft) thick; gravel is thinner
TTR	1766248.10	1612238.27	7554.90	white ashy unit is 2 cm (5 in) thick and pinches out E; overlain by clay-rich matrix gravels
TTR	1766229.80	1612262.10	7554.83	0.98-m (3.2-ft) clay-rich matrix gravels
TTR	1766184.69	1612348.54	7554.76	gravels with orange sandy matrix; cobbles 0.46-m (1.5-ft) long Tschicoma dacite and Qbt
TTR	1766149.45	1612418.28	7554.14	extremely clay-rich deposit with sparse cobbles [< 9.1-cm (3.6-in) diameter]; bottom 0.6 m (2 ft) is more cobbly
TTR	1766129.87	1612456.33	7553.70	center of 3-m (10-ft) wide pocket of coarse cobbles in bottom 0.76 m (2.5 ft) of trench; cobbles are maximum 0.3-m (1-ft) diameter Tschicoma and more Qbt
TTR	1766122.07	1612470.06	7553.48	center of pocket of coarse cobbles in bottom 0.7 m (2.3 ft) [average 0.5 m (1.6 ft) thick]; maximum 0.3-m (1-ft) diameter Tschicoma and more Qbt
TTR	1766109.54	1612494.43	7553.05	bottom 0.49 m (1.6 ft) is clayey cobble-rich deposit
TTR	1766098.11	1612517.31	7552.64	cobble-rich layer is 0.18 m (0.6 ft) from bottom and pinches out to E
TTR	1766034.92	1612640.95	7550.43	
TTR	1765978.38	1612750.07	7547.96	sample of pumice from pebbly unit
TTR	1765958.96	1612786.97	7547.16	
TTR	1765942.91	1612817.33	7546.38	
TTR	1765909.05	1612884.52	7544.95	
TTR	1765884.34	1612932.69	7544.88	organic-rich sediment 24-cm (10-in) thick over tuff
TTR	1765867.64	1612964.54	7546.05	W margin of channel; alluvium 0.5 m (1.7 ft) thick over tuff; alluvium > 0.9 m (3 ft) thick in center of channel
TTR	1765780.98	1613162.72	7544.06	
TTR	1765754.96	1613330.45	7538.22	
TTR	1765747.31	1613399.42	7537.95	clay-rich alluvium 0.6 m (2 ft) thick
TTR	1765741.14	1613411.18	7538.25	N30E 10SE; bedding
TTR	1765740.32	1613414.55	7538.26	
TTR	1765743.14	1613428.00	7538.38	alluvium > 1.2 m (4-ft) thick

Table C-1 Continued. TA-9 Trench Total Station Survey Data (notes on page 94)

Mapped Contact*	Coordinates† Northing (ft)	Easting (ft)	Elevation (ft)	Comments‡
TTR	1765736.53	1613468.86	7539.01	
TTR	1765732.88	1613491.74	7539.06	
TTR	1765724.10	1613545.76	7537.98	
TTR	1765714.64	1613605.49	7536.80	
TTR	1765696.92	1613662.59	7535.89	
TTR	1765699.88	1613692.29	7533.74	
TTR	1765685.30	1613750.20	7531.93	
TTR	1765680.60	1613782.60	7531.01	
TTR	1765671.28	1613833.09	7529.81	
TTR	1765660.07	1613906.07	7527.57	
TTR	1765656.66	1613920.19	7527.01	
TTR	1765649.18	1613999.39	7523.25	
TTR	1765643.98	1614003.95	7523.65	
TTR	1765630.51	1614088.56	7520.45	
TTR	1765634.95	1614090.61	7520.22	
TTR	1765617.80	1614172.38	7517.76	
TTR	1765616.97	1614173.39	7517.59	
TTR	1765604.57	1614257.85	7514.90	
TTR	1765598.83	1614296.40	7513.59	
TTR	1765596.81	1614336.61	7511.98	
TTR	1765590.76	1614343.18	7511.87	
TTR	1765582.02	1614407.24	7510.05	
TTR	1765578.41	1614429.94	7509.59	
TTR	1765565.36	1614517.38	7509.08	
TTR	1765558.58	1614562.65	7507.80	east edge of organic-rich deposit; ~ 0.3 m (1 ft) thick but top is disturbed
TTR	1765560.01	1614579.66	7507.43	orange colluvium with pumice and organics
TTR	1765551.73	1614592.84	7508.40	
TTR	1765551.84	1614608.29	7508.73	
TTR	1765553.57	1614616.79	7509.15	
TTR	1765546.90	1614625.21	7509.61	
TTR	1765550.17	1614637.16	7510.15	colluvium 0.46 m (1.5 ft) thick; clay-filled fracture N15E 85SE; tuff surface dips 10° W
TTR	1765538.71	1614682.07	7510.94	
TTR	1765538.59	1614682.73	7511.10	
TTR	1765538.58	1614683.39	7511.14	
TTR	1765536.40	1614696.40	7511.26	
TTR	1765535.50	1614701.76	7511.47	

Table C-1 Continued. TA-9 Trench Total Station Survey Data (notes on page 94)

Mapped Contact*	Coordinates†			Comments‡
	Northing (ft)	Easting (ft)	Elevation (ft)	
TTR	1765534.13	1614709.70	7511.40	
TTR	1765532.46	1614714.23	7511.51	
TTR	1765533.34	1614714.49	7511.46	
TTR	1765533.14	1614715.63	7511.55	
TTR	1765529.38	1614738.42	7512.41	
TTR	1765528.63	1614754.30	7511.93	
TTR	1765526.32	1614755.87	7512.11	
TTR	1765527.63	1614760.84	7512.04	
TTR	1765527.12	1614764.57	7512.07	
TTR	1765524.69	1614766.90	7512.16	
TTR	1765495.90	1614934.16	7513.15	
TTR	1765499.17	1614936.94	7512.99	axis of channel
TTR	1765495.27	1614959.94	7513.08	
TTR	1765489.24	1614998.08	7513.19	
TTR	1765487.75	1615005.52	7513.30	axis of channel trending S35E; 2 m (6.6 ft) wide at T-C contact filled with sandy gravel > 1.2 m (4 ft) deep
TTR	1765477.41	1615067.96	7512.01	
TTR	1765476.81	1615071.74	7512.06	
TTR	1765459.56	1615185.50	7510.92	
TTR	1765459.49	1615210.88	7510.17	tuff overlain by 0.5-cm (0.2-in) thick white powder overlain by mottled unit
TTR	1765459.56	1615212.73	7510.29	
TTR	1765469.73	1615248.26	7510.30	
TTR	1765483.36	1615285.36	7509.75	
TTR	1765516.58	1615373.10	7507.88	
TTR	1765534.45	1615406.28	7507.20	
TTR	1765538.05	1615415.07	7507.03	
TTR	1765550.89	1615457.03	7507.22	colluvium 0.85 m (2.8 ft) thick over tuff, above N75W 50NE clay-filled fracture 6.1 cm (2.4 in) wide
TTR	1765557.89	1615475.75	7507.11	
TTR	1765557.84	1615475.79	7507.15	
TTR	1765584.50	1615531.44	7507.18	
TTR	1765609.83	1615597.37	7506.00	
TTR	1765641.07	1615676.84	7503.48	
TTR	1765659.84	1615724.98	7502.38	colluvium 0.54 m (1.8 ft) thick with blocks up to 1.3 (4.2 ft) long

Table C-1 Continued. TA-9 Trench Total Station Survey Data (notes below)

Mapped Contact*	Coordinates†			Comments‡
	Northing (ft)	Easting (ft)	Elevation (ft)	
TTR	1765671.23	1615752.68	7501.27	
TTR	1765693.09	1615811.62	7500.65	
TTR	1765694.48	1615815.36	7500.57	Holocene colluvium 0.46 m (1.5 ft) thick
TTR	1765700.12	1615828.77	7500.04	
TTR	1765731.01	1615907.17	7499.36	
TTR	1765757.73	1615976.02	7496.76	
TTR	1765758.22	1615976.84	7496.68	
TTR	1765763.47	1615990.01	7494.43	
TTR	1765778.88	1616029.53	7483.92	colluvium to base of trench
TTR	1765786.68	1616052.60	7476.27	
TTR	1765796.64	1616081.90	7467.16	
TTR	1765805.83	1616107.78	7461.16	
TTR	1765823.03	1616151.86	7453.89	tuff overlain by eolian silt
TTR	1765824.38	1616155.56	7453.46	
TTR	1765842.45	1616204.41	7448.29	

*Explanation of Mapped Contact codes:

BTR = Bottom of trench
F = Fracture, fissure, or fault
G = Gasline
S = Sample; S4 = Within Unit 4 surge
STRAT = Stratigraphic contact
T-C = Tuff-colluvium contact
T-C-F = Tuff-colluvium contact cut by fracture
TTR = Top of trench
"Fissures" in many cases may be merely topography at the surface of the tuff produced by erosional plucking of fracture-bounded tuff blocks.
Field descriptions included in the table do not necessarily match the stratigraphic units shown in Fig. 6.

†Contacts surveyed by LANL Seismic Hazards Program (see text for details).

‡Explanantion of Comments codes:

brn = brown (as in "red-brown")
Bt = soil horizon with silicate clay either formed in situ or translocated within or into the horizon
choc = chocolate (as in "chocolate-brown")
dk = dark
f = fine
ft = feet
lam'd = laminated
lt = light
v = very

Table C-2. MDA P Total Station Survey Data (notes on page 98)

Mapped Contact*	Coordinates†			Comments
	Northing (ft)	Easting (ft)	Elevation (ft)‡	
3T	1764476	1615778	7413	
4	1764469	1615784	7415	
3T-4	1764477	1615794	7414	
3T-4	1764480	1615808	7415	
3T-4	1764483	1615819	7415	
3T-4	1764482	1615835	7415	
3T-4	1764485	1615859	7414	
3T-4	1764504	1615893	7412	
3T-4	1764512	1615908	7410	
3T-4	1764511	1615929	7411	
3T-4	1764515	1615958	7411	
3T-4	1764517	1615994	7411	
3	1764584	1615944	7388	
3-3T	1764572	1615922	7390	
3-3T	1764566	1615894	7390	
3-3T	1764559	1615875	7391	
3-3T	1764539	1615834	7395	
3-3T	1764548	1615851	7393	
3-3T	1764517	1615783	7397	
F1	1764500	1615759	7396	
F1	1764550	1615740	7365	
F1	1764536	1615751	7375	
3-3T	1764494	1615756	7397	
F1	1764527	1615753	7381	
F1	1764519	1615758	7386	
F1-2	1764516	1615760	7387	
F2	1764504	1615761	7396	
F2	1764495	1615762	7398	
F1	1764511	1615764	7391	
F2	1764482	1615762	7403	
F1	1764507	1615765	7394	
F1	1764498	1615776	7402	
F1	1764487	1615784	7408	
F1	1764479	1615790	7414	
3-3T	1764462	1615725	7399	
3-3T	1764475	1615735	7395	
F1	1764473	1615794	7415	
F	1764458	1615698	7399	N70E

Table C-2 Continued. MDA P Total Station Survey Data (notes on page 98)

Mapped Contact*	Coordinates†			Comments
	Northing (ft)	Easting (ft)	Elevation (ft)‡	
3T-4	1764483	1615816	7415	
3T-4	1764478	1615799	7415	
3T-4	1764476	1615790	7414	
3T-4	1764466	1615776	7415	
3T-4	1764449	1615753	7417	
3T-4	1764432	1615723	7419	
3T-4	1764414	1615694	7419	
3T-4	1764400	1615663	7420	
3T-4	1764394	1615639	7420	
3-3T	1764449	1615692	7401	
F	1764462	1615713	7399	
3-3T	1764448	1615679	7400	
F3	1764512	1615765	7391	
F3	1764508	1615762	7392	
3	1764434	1615640	7400	
3-3T	1764492	1615758	7398	
3-3T	1764507	1615780	7399	
3-3T	1764498	1615764	7399	
3	1764465	1615719	7399	
F	1764497	1615700	7375	N70E
3T	1764463	1615713	7399	
F4	1764465	1615711	7398	
F4	1764457	1615730	7402	
F	1764490	1615734	7390	
F	1764485	1615730	7390	
F	1764501	1615714	7376	fault N50W 90
F	1764470	1615716	7396	
F	1764497	1615748	7391	N85E 90
F	1764496	1615755	7395	
F	1764500	1615747	7391	N60W 90
F	1764496	1615756	7397	
F5	1764511	1615745	7383	
F5	1764522	1615718	7371	N70W 85NE
F5	1764530	1615705	7361	
3WB	1764542	1615729	7367	
3WB	1764561	1615762	7367	
3WB	1764570	1615774	7366	

Table C-2 Continued. MDA P Total Station Survey Data (notes on page 98)

Mapped Contact*	Coordinates† Northing (ft)	Easting (ft)	Elevation (ft)‡	Comments
F5	1764555	1615761	7371	N27W
3WB	1764581	1615801	7366	
3WB	1764591	1615840	7363	
3WB	1764600	1615876	7368	
3WB	1764607	1615901	7367	
3WB	1764615	1615921	7368	
3WB	1764628	1615950	7363	
BH 557	1764475	1615848	7415	
F	1764704	1615684	7372	fault N17E 85SE with grooves
F	1764727	1615694	7383	fault N17E 85SE with grooves
3WB	1764730	1615744	7370	
F	1764725	1615714	7373	
F	1764730	1615735	7371	
F	1764767	1615736	7398	fault zone with fissures
F	1764764	1615718	7401	N5E 87NW
TG	1764811	1615891	7363	
F	1764921	1615898	7396	fault N7W 90
3-3T	1764870	1615858	7400	
3-3T	1764838	1615817	7399	
3-3T	1764790	1615762	7400	
F	1764817	1615732	7417	
3-3T	1764768	1615750	7395	
3T-4	1764819	1615724	7418	
3-3T	1764741	1615689	7397	
3T-4	1764800	1615689	7420	
3-3T	1764706	1615651	7398	
3T-4	1764778	1615649	7419	
3-3T	1764689	1615600	7396	
3T-4	1764742	1615599	7419	
3-3T	1764675	1615572	7398	
3T-4	1764722	1615562	7420	
3-3T	1764655	1615521	7397	
3T-4	1764706	1615518	7420	
3-3T	1764635	1615496	7393	
3T	1764696	1615468	7425	
3-3T	1764614	1615400	7400	
3-3T	1764591	1615330	7401	

Table C-2 Continued. MDA P Total Station Survey Data (notes below)

Mapped Contact*	Coordinates† Northing (ft)	Easting (ft)	Elevation (ft)‡	Comments
3T	1764640	1615315	7428	
4	1764699	1615466	7426	

*Explanation of Mapped Contact codes

3T = Within Unit 3T
3 = Within Unit 3
3WB = Welding break within Unit 3
4 = Within Unit 4
3-3T = Unit 3-Unit 3T contact
3T-4 = Unit 3T-Unit 4 contact
F*n* = Fault *n* (*n* = 1–5)
F1-2 = Intersection of faults 1 and 2
F = Fissure (unless designated otherwise in "Comments")
BH = Borehole
TG = Terrace gravel

†Contacts surveyed by LANL Seismic Hazards Program with a Total Station; data points are referenced to the MDA P grid surveyed by the LANL ER Project.

‡Contacts are located with an accuracy better than ± 3 ft in elevation.

Los Alamos NM 87545